ANALYSIS OF RESIDUAL STRESSES IN PARTS CREATED BY THE STEREOLITHOGRAPHY PROCESS

Thesis

Submitted to

Graduate Engineering & Research
School of Engineering

UNIVERSITY OF DAYTON

In Partial Fulfillment of the Requirements for

The Degree

Master of Science in Materials Engineering

by

Brett Andrew Bolan

UNIVERSITY OF DAYTON

Dayton, Ohio

December 1991

ANALYSIS OF RESIDUAL STRESSES IN PARTS CREATED BY THE STEREOLITHOGRAPHY PROCESS

APPROVED BY:

Richard P. Chartoff, PhD.
Advisory Committee Chairman

Franklin E. Eastep, PhD.
Interim Associate Dean/Director
Graduate Engineering and Research
School of Engineering

Patrick J. Sweeney, PhD.
Interim Dean
School of Engineering

ABSTRACT

ANAYLSIS OF RESIDUAL STRESSES IN PARTS CREATED BY THE STEREOLITHOGRAPHY PROCESS

Name: Bolan, Brett, Andrew
University of Dayton, 1991

Advisor: Dr. R. P. Chartoff

Several techniques were explored in an effort to quantify the residual stresses present in single strands of a photoreactive epoxy-acrylate based resin (Ciba-Giegy's XB5081-1) cured by the stereolithography process. The "Annealing-Straining" technique was found to be the most successful in this effort. This technique involved annealing a specimen above its T_g, determining the strain in the specimen as a result of the annealing allowing residual stresses to be relaxed (i.e. the specimen shrinks), and then straining this specimen the amount it had shrunk, while measuring the force required to do so. The measured stress equated to that which was initially present in the specimen (before annealing) as residual stress. For the XB5081-1 based resin, the residual stress level measured was 3.93 MPa. Modifying the XB5081-1 resin with 10.81 pph CTBN, keeping all other conditions identical, resulted in a 12 percent reduction in residual stress levels (i.e. 3.47 MPa). Water loss by the specimens during the annealing cycle accounted for some of the specimen's observed change in length and hence for some of the measured residual stress. Assuming linear elastic behavior for the specimens, the residual stress levels calculated from the storage modulus and strain were within 10 percent of the measured residual stress levels. This greatly simplifies the utilization of this technique, making it a viable screening method for determining which resin will have the

tendency to develop less residual stresses in parts during the manufacturing process.

ACKNOWLEDGEMENTS

My sincere appreciation to Dr. Larry Flach, Dr. James Snide, Dr. Shwn-Meei Linden, and Dr. Richard Chartoff for their guidance and support given on this thesis.

I would also like to express my thanks to the following individuals for their aid, expertise and patience in teaching me to operate much of the instrumentation utilized throughout this thesis; Pete Weissman, Mary Galaska, Brad Pinnell, Tom Dusz and John Murphy. Special thanks go to Rich Striebick of the Environmental Sciences Group at the University of Dayton Research Institute who conducted the crucial experiment with the GC/MS.

In conclusion I would like to thank my wife and children for all their patience, support, and constant encouragement.

TABLE OF CONTENTS

LIST OF TABLES

LIST OF FIGURES

LIST OF NOMENCLATURE

UV	Ultra Violet
NC	Numerically Controlled
CAD	Computer Aided Design
N	fringe number; number of fringes measured at a particular point on the specimen
f_σ	material fringe value; the material's optical response to a stress field and corresponds to psi per fringe
SLA	Stereolithography Apparatus
VP	Vinyl Pyrroldinone, a diluent and crosslinking agent
CTBN	Carboxyl Terminated Butadiene Acrylonitrile
SEM	Scanning Electron Microscope
MMA	Methyl Methacrylate
PMMA	Polymethyl Methacrylate
HDDA	Hexanediol Diacrylate
DMA	Dynamic Mechanical Analysis
RSA II	Rheometrics Solid Analyzer II
LVDT	Linearly Variable Differential Transformer
TGA	Thermogravimetric Analysis
DSC	Differential Scanning Calorimetry
GC/MS	Gas Chromatograph/Mass Spectrometer
T_g	glass transition temperature
Pa	Pascals
MPa	1×10^6 Pa

CHAPTER I

INTRODUCTION

Stereolithography is a technique for rapidly producing three dimensional parts. The process utilizes a three dimensional (3-D) generated Computer Aided Design (CAD) model, which has been horizontally sliced into discrete layers, to guide a focused Ultra-Violet (UV) laser on the surface of a vat of UV photosensitive liquid resin. The laser draws one horizontal layer of the part on the surface of the liquid resin causing it to undergo a photo-polymerization reaction which results in the layer becoming solidified. The first layer is attached via this photopolymerization reaction to a moveable elevator platform in the vat. The platform is then lowered one layer thickness (e.g. 10 mils) at which time the laser traces the image of the next layer on the surface of the resin. This results in the second layer becoming solidified and attached to the pre-existing layer. This process is repeated until the complete part has been generated.

The goal of stereolithography is to not only rapidly produce a solid object from the computer representation of a 3-D form, but also to produce an accurate representation of the object. Any deviations in the built part's dimensions from that of the computer model tends to limit the utility of the part. Currently this technology cannot achieve a high level of dimensional accuracy. This has limited the prime use of this technology to producing prototype parts for "show and tell"[1,2], i.e. solid objects which represent a blueprint or CAD design. Although this "show and tell" application serves a very important purpose for industry, in order for Stereolithography to reach its full potential dimensional accuracy rivaling that of

Numerically Controlled (NC) machines must be obtained so that production quality parts can be manufactured.

The ability to obtain and maintain dimensional accuracy can be related to several factors[1,2]. There is laser beam width, shape of the beam spot on the resin surface, slice layer overcure, and shrinkage. Dimensional accuracy is reduced as a result of the laser beam being centered on the edge of the surface boundary of a part. This causes the outer surface to be overbuilt by approximately half the beam width or 0.005 inches. There are existing software programs built to solve this problem but they create others.

The shape of the beam spot on the surface of the resin, which is different at different locations in the vat, has a direct impact on the dimensional accuracy of a part as well. As a consequence of the Stereolithography Apparatus (SLA) directing the movement of the laser beam spot on the surface of the resin with a rapidly positionable computer controlled mirror centered approximately 2.5 feet above the top surface of the vat, the shape of the spot changes from being circular at the center of the vat to elliptical at the sides. This change in shape of the beam spot on the surface of the resin impacts on the dimensional accuracy of the part and is obviously of more concern with a large part and/or part segments built near the edge of the vat.

Slice layer overcure can also result in the loss of dimensional accuracy of the part. This overcure, although necessary to insure adhesion between layers, can result in the loss of dimensional accuracy in the Z or depth direction. Nominally, a depth of cure set equal to 0.006 inches beyond the current slice layer thickness is programmed into the SLA. This overcure therefore results in the bottom layer being approximately 0.006 inches greater than specified.

By far, the most significant factor affecting dimensional accuracy is shrinkage. It has been found to be a function of several

parameters[1], including the part geometry, process control variables (e.g. cross hatch pattern spacing), post curing, and resin properties. Shrinkage of parts as they are being made in the vat can be partially compensated for by selecting the appropriate "shrink factor"[1] for the resin. Unfortunately being in error by as little as 0.1% makes holding a 0.005 inch tolerance on a five inch part difficult. Selecting this "shrink factor" requires part building experience and/or an expensive trial and error process of inputting different values until the correct part dimensions are obtained.

Shrinkage also causes the parts to warp, a much more obvious cause for dimensional inaccuracies. This warpage is probably due to different internal stress levels at different locations within the part which in turn results in differential amounts of shrinkage. This differential can be developed while creating the part in the vat as well as through post curing operations. The varying amounts of shrinkage causes differential internal stress levels in the parts, which when allowed to relax can cause severe warpage. When these stresses are not allowed to relax, due either to part geometry and/or external constraints (e.g. adhering the part via the support structure to the elevator platform), significant amounts of non-uniform internal or rather, residual stresses can develop both before and after post curing. Although initially the restrained parts may hold dimensional tolerances, with aging, the residual stresses can be relieved resulting in warpage. In severe cases the residual stresses can be so high as to cause the part to fragment.

Another negative side to residual stresses is that they reduce the ability of an already brittle part (due to the nature of the epoxy acrylate resin system typically utilized) to tolerate low energy impacts. Consequently the parts tend to fracture more readily thereby further limiting the parts to the "show and tell" application and not production quality parts.

The primary purpose of this study was to develop a method to measure the residual stresses that develop in parts created by the stereolithography process. This was accomplished through the "Annealing-Straining Analysis" technique, after two other techniques, namely Photoelastic Analysis and "Constant Strain", failed to yield measurable values of residual stress. A secondary purpose of this study was to minimize or reduce the residual stress levels through resin formulation manipulation.

CHAPTER II

PHOTOELASTIC ANALYSIS

A. Summary and Chronology of Experimental Procedures

This is a summary and chronology of the experimental procedures initially proposed for this study. The complete procedure was never followed due to problems associated with the material, the details of which will be explained in the "Results and Discussion" section of the photoelastic technique. It is included here for completeness.

1. Make the specimens - use the same light intensity for all samples

   i. Five 1/2 inch diameter disks of 1.0mm thickness for photoelastic analysis

   ii. Two rectangular beams (~50x12x1mm) for Dynamic Mechanical Analysis (DMA) determination of T_g

2. Photoelastic Analysis - measure stress field at the center of the disks as a function of f_σ(material fringe value)

3. Determine T_g of disks - use DMA of a rectangular specimen in a 3 pt flexural fixture

4. Determine f_σ of the disks

   i. Place disk in a compression loading frame with known load and then place in an oven and hold at previously determined T_g value. Slowly cool disk back to room temperature. This freezes in fringe pattern due to the load.

ii. Place specimen in field of circular polariscope to determine f_σ

iii. Use f_σ determined above, to back calculate absolute values of stress fields determined in step 2

5. Repeat Steps 1-4 for each resin formulation being tested

B. Introduction to Photoelasticity

The first task defined as part of this study was to develop a method to measure the residual stresses present in parts created by the stereolithography process. It was decided, for a number of reasons (see Master Thesis Proposal, Appendix A), to take advantage of a transparent polymer's tendency to exhibit a phenomenon known as "birefringence" or "double refraction" to aid in this study of residual stresses. This effect occurs when light (see Figure 1[3]), which is plane polarized and normal to the surface of a stressed transparent polymeric material, passes through the material and is broken up into two components (waves) which are normal to each other. These waves, which are in phase initially, are out of phase when they emerge from the material. This is due to the fact that they travel different path lengths as a result of the stresses in the material at that point. When the waves of light are recombined into the same plane, an interference pattern is developed. The pattern obtained is characteristic of the stresses within the material and the material's optical properties.

Figure 2[3] depicts a typical stress pattern for a disk in diametral compression when exposed to monochromatic light. Each of the dark lines, called fringes, represent a locus of points where the relative retardation between the two waves is an integral number of wavelengths. Analyses taking advantage of this birefringence phenomenon are called photoelastic studies. These have been conducted on various structures exposed to external loads to verify mechanical analysis, such as models of bridges, for well over fifty years. This technique was also used to confirm the stress intensity factors present around circular holes. A description of the theory of photoelasticity can be found in Appendix A.

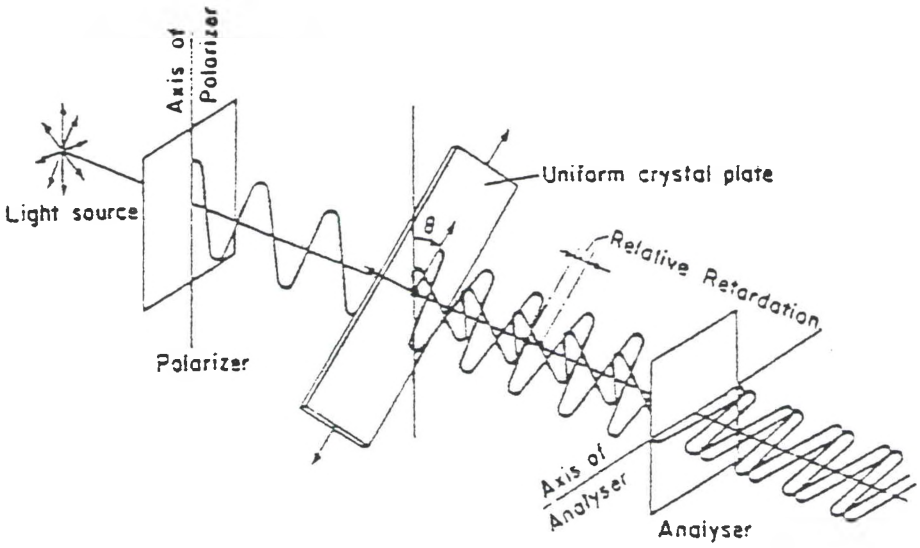

Figure 1. Uniform Crystal Plate in the Plane Polariscope.

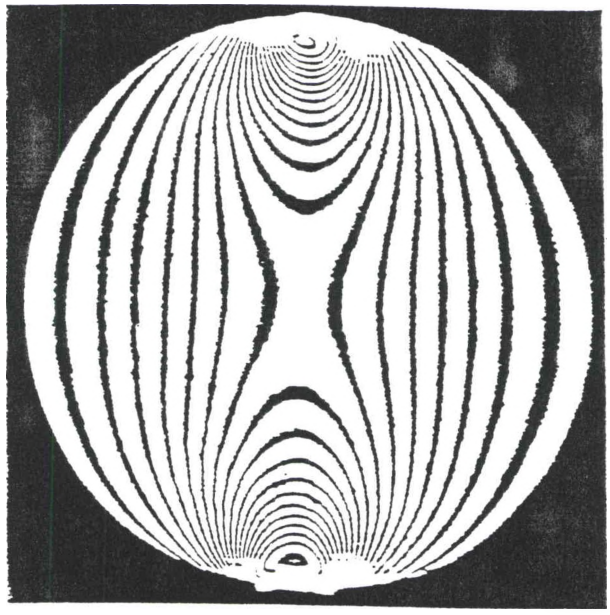

Figure 2. Fringe Pattern in a Disk Under Diametral Compression.

C. Experimental Methods

1. Sample Preparation

The procedure utilized in making the disk specimens for study in the crossed circular polariscope is detailed in this section. The choice of a disk shape for the specimens was made because of the relative ease in loading a disk in pure diametral compression verses a specimen in tension. This could have been an important factor in determining the material fringe value, f_σ, (a material's optical response to a stress field) of the disk.

The SLA-250 was not utilized in making the disk specimens because at the time this work was completed it typically only polymerized a relatively small volume of material, leaving liquid resin trapped in triangular hatches to be polymerized in a post curing oven. This leads to a sample with two significantly different crosslink densities which violates a key assumption necessary for photoelastic analysis of the specimens, i.e. the specimen under study must be a homogeneous material. This stems from the fact that materials with more than one crosslink density have more than one f_σ. This, along with other considerations (e.g. ease of experimenting with different resin systems), lead to the utilization of a bench top arrangement consisting of a Spectra Physics Model 2130 Argon-Ion laser operating in the UV at a wavelength of between 350 to 360nm.

The beam of this laser was manipulated so as to expand it into a large circular spot (i.e. one inch in diameter), the central portion of which was nearly uniform in intensity. Figure 3 shows the arrangement of the apparatus used to achieve this end. The laser beam was focused to a very small point, with a 5X microscope objective lens, just above the top surface of a 25 micron pin hole spatial filter. This filter only allowed the beam which was focused to pass through. All other parts of the beam (e.g. scattering due to

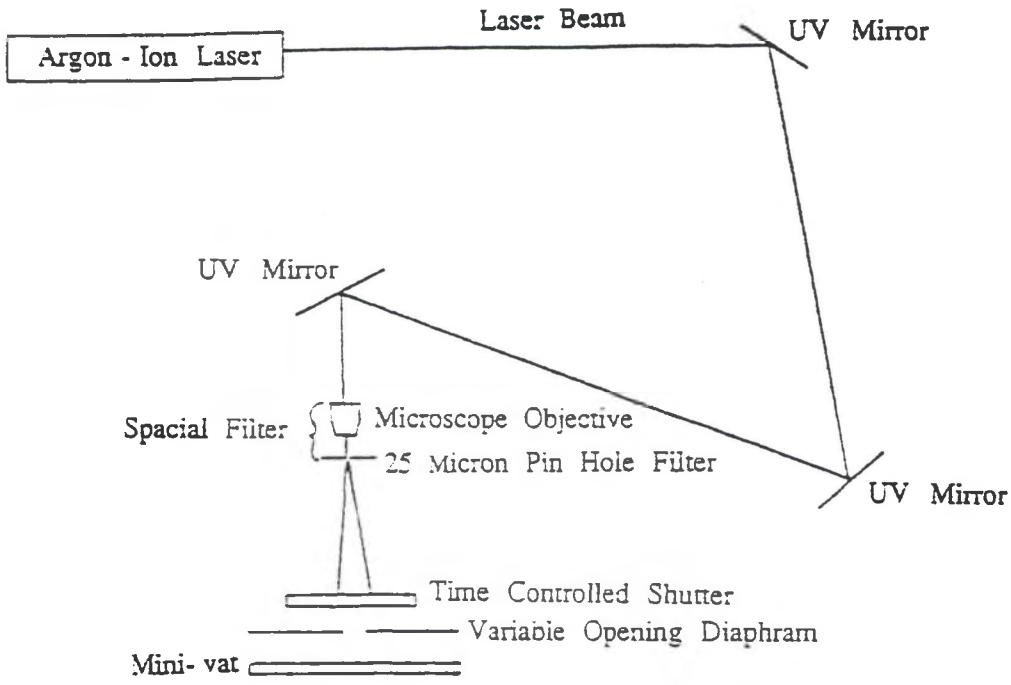

Figure 3. Table Top Laser and Optics Arrangement.

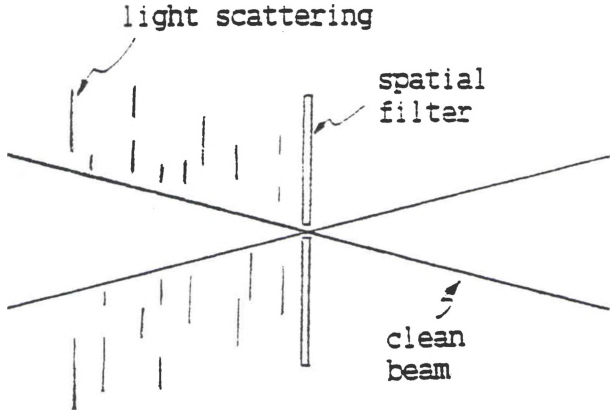

Figure 4. Laser Beam Focused Through Spatial Filter, Cross-Sectional View.

imperfections in the mirrors, dust in the path of the beam, or lens aberrations) were blocked out by this spatial filter (see Figure 4). The beam then expanded, as depicted in Figure 3, as it moved further from the spatial filter. When expanded sufficiently, the central portion of this circular spot (i.e. approximately 0.5 inches in diameter) became almost uniform in intensity.

The uniformity of this beam at the center was measured with the arrangement shown in Figure 5. The pieces of equipment included a one square centimeter silicon detector, sensitive to energy in the UV, and a fast memory oscilloscope. The detector had a 0.3mm by 0.5mm slit mask mounted on it and was placed on a single axis micron-steppable platform oriented so that as the detector was displaced by the platform the width of the slit would traverse the beam's diameter (see Figure 6). As the detector moved across the beam, the oscilloscope measured the beam's intensity. The detector was not calibrated against a reference and hence was only able to give qualitative values. This was suitable for this study. It was found that the beam's intensity was uniform to within -6% of maximum.

The disks were made by a lithographic process. This involved utilizing a variable iris with an opening of 0.5 inches placed over the top of a mini-vat with a glass plate as its bottom surface (see Figure 7). This vat, which has a depth of approximately 1.08mm, was placed under a time controlled shutter in the path of the expanded beam as depicted in Figure 5. The shutter was opened for 5 seconds duration to expose and cure the resin. With the energy density of UV light being utilized, 3.37 mW/mm^2 the resin was cured through the depth of the mini-vat and adhered to the top of the glass plate. The polymerized sample was then removed from the mini-vat, cleaned in isopropyl alcohol and then polished first with 150, followed by 220, 320, 400, and 600 grit sand paper. The samples were further polished with 15 micron, 6 micron and then given a final polish with 0.3 micron alumina compound. Extreme care was exercised at this stage so as to keep the two surfaces as nearly parallel as possible.

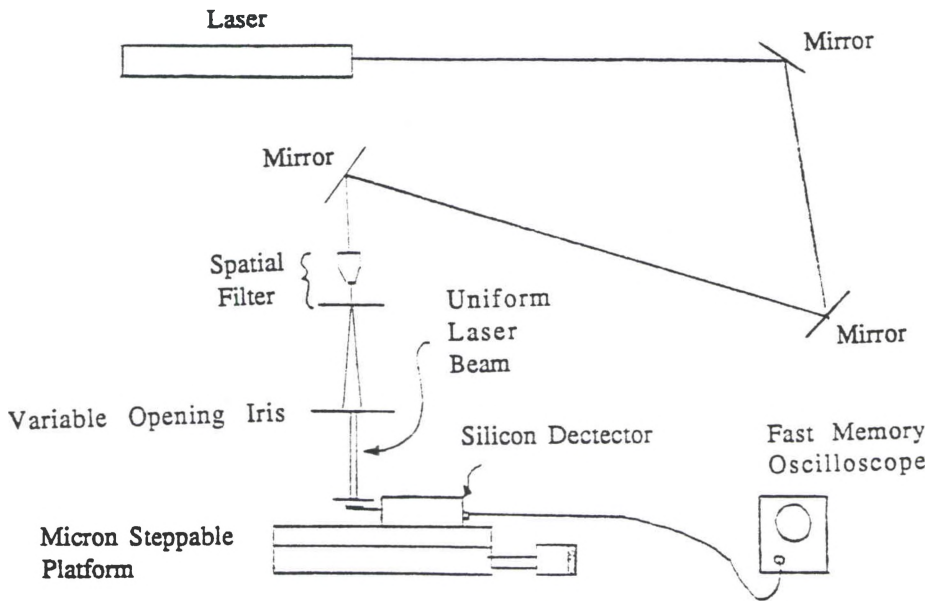

Figure 5. Schematic of Apparatus Utilized to Measure Uniformity of Beam.

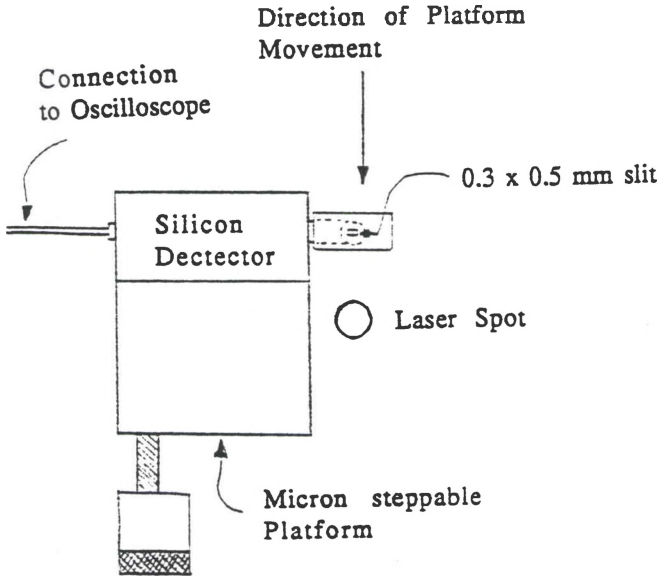

Figure 6. Silicon Detector Traversing Beam's Diameter.

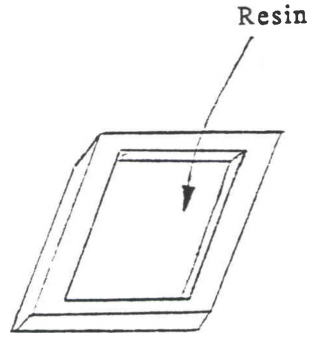

Figure 7. Mini-vat.

Deviations from parallel as a result of polishing could have caused errors in the fringe order measurements, N, since the determination of the fringe order assumes the polarized light is normal to the surface of the specimen.

The rationale behind using the mini-vat in the lithographic process was that it mimicked the SLA process in two functions. First, the excess resin in the mini-vat acted as a large heat sink which may turn out to account for some of the residual stress in parts made in the SLA. This excess resin could have caused a possible rapid cool down of over 30°C/min, as calculated in Flach's[4] modeling of a Hexanediol Diacrylate (HDDA) resin undergoing photopolymerization, resulting in the cured resin transitioning so rapidly from T_g to ambient temperature that not all thermal and curing shrinkage was allowed to occur. This would result in frozen-in stresses, or rather residual stresses. Second, the adherence of the resin to the top surface of the glass plate was similar to a succeeding layer adhering to the previous layer.

2. Instrumentation and Their Function for Photoelastic Analysis

The instrumentation that was utilized in studying the parts photoelasticly was a crossed circular polariscope as schematically depicted in Figure 8[3]. It consisted of a white light source with a monochromatic filter (green, λ=5461 Å) , a polarizer, a quarter-wave plate, a frame that held the specimen, a Babinet-Soleil compensator (the theory of operation of this instrument can be found in Appendix B) which could be moved in and out of the light path, and another quarter-wave plate followed by another polarizer (called an analyzer).

The theory behind the operation of the crossed circular polariscope is detailed in this paragraph. The first polarizer makes the incoming monochromatic light plane polarized, whereas the first quarter-wave plate's function is to make the incoming plane polarized light circular. Circularizing the light eliminates the effect that the sample's orientation has on the intensity of light transmitted thereby allowing one to observe only isochromatic fringe patterns (i.e. locus of points at which the principal stress difference, σ_1-σ_2, is constant) rather than both isochromatics and isoclinics (locus of points at which a principal stress direction coincides with the direction of polarization). When the light emerges from the sample (a disk shape in these experiments) it is broken up into two components, plane polarized and at right angles to each other. The retardation between these two components is due to the specimen plus a quarter-wave length attributed to the first quarter-wave plate. At this point, in general, the light is elliptically polarized. When the light passes through the second quarter-wave plate its path is reduced by a quarter-wave length. This elliptical wave is then resolved into its two plane polarized components in the same plane with the analyzer, resulting in an interference pattern. From the

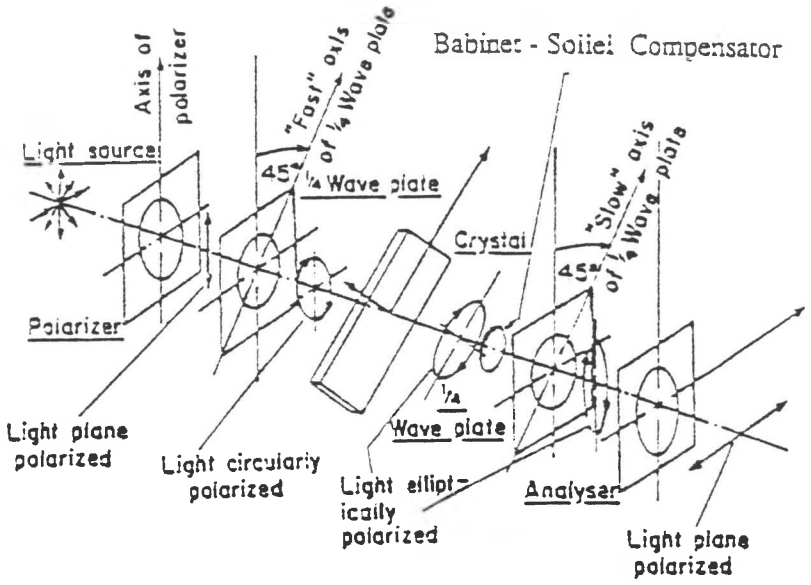

Figure 8. Crossed Circular Polariscope.

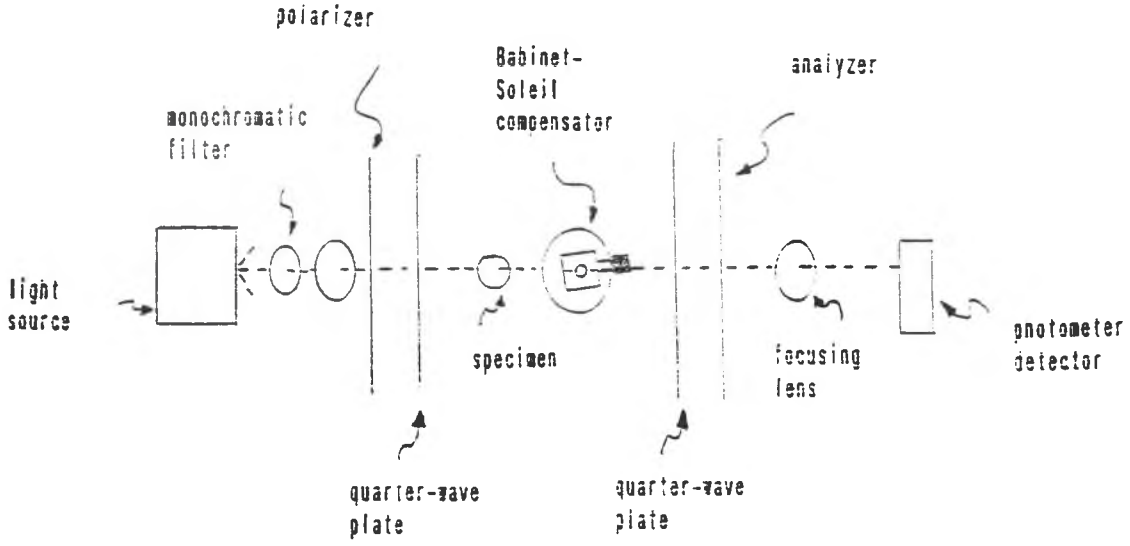

Figure 9. Schematic of Photoelastic Apparatus.

interference pattern obtained, it is possible to determine the stresses at each point within a homogeneous specimen.

The manner in which stresses are determined relates directly to the stress optic law (see Appendix A):

$$\sigma = Nf_{\sigma}/h$$

The crossed circular polariscope, as mentioned above, gives the isochromatic fringe pattern in the specimen. In order to determine stresses in this specimen, there must be an apparatus to measure the isochromatic fringe order, N, of the specimen at different locations. This is made possible with a photometric device placed at the desired location of the focused image of the specimen and a Babinet-Soleil compensator placed between the specimen and the second quarter-wave plate (see Figure 9). The photometric device is sensitive to slight variations in light intensity (1/10,000 of a candle light) and as such, in conjunction with the Babinet-Soleil compensator, can measure the fraction of a fringe order at a given point. This is done by adjusting the thickness of the compensator with the micrometer drum until the relative retardation of the specimen in the direction of the principal stress, σ_1, is nullified. The reading of the drum can then be related to the fringe order, N, at the point of concern through the calibration equation of the compensator.

It has been found that the specimens studied were not homogeneous thereby violating the key assumption necessary in evaluating material photoelasticly. An interpretable interference pattern was not therefore obtained. For specific details of analysis by the photoelastic technique the reader is referred to several references on the topic area (ref. 5-9).

3. Materials

The base line photosensitive resin that was utilized throughout this study was Ciba-Geigy's Cibatool XB5081-1 formulation. This is primarily an acrylate ester epoxy resin (see Figure 10 for typical chemical structure) with a diacrylate and triacrylate crosslinking agent, a photoinitiator and a diluent or viscosity reducing agent. The approximate composition of the resin is shown below[10]:

Acrylate ester of bisphenol A epoxy resin	~ 50%
Ethoxylated bisphenol A dimethacrylate	~ 20%
Timethylolpropane triacrylate (TMPA)	~ 10%
1-hydroxylcyclohexyl phenyl ketone (Irgacure 184)	~ 10%
1-vinyl pyrrolidinone (VP) (diluent)	~ 10%

This resin was chosen as the base line material due primarily to its use as the predominate photosensitive resin in the stereolithography industry.

The XB5081-1 acrylate-epoxy resin was modified with 10.81 part per hundred (pph) weight of Carboxyl Terminated Butadiene Acrylonitrile (CTBN) rubber to determine the effect that this addition has on residual stress values. This was B.F. Goodrich's X1300 CTBN with 26% acrylonitrile content. The high acrylonitrile content CTBN was utilized so as to maximize the compatibility between the rubber modifier and the acrylate-epoxy resin. The CTBN was vigorously mechanically mixed into the XB5081-1 resin and then vacuum degassed for about 30 minutes at approximately 45 °C to remove all air bubbles. The resultant mixture was macroscopically homogeneous in appearance.

Epoxy/Acrylate

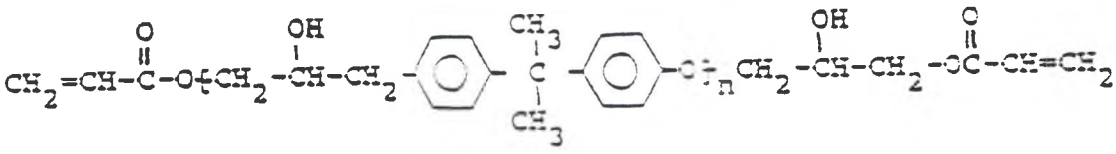

Figure 10. Typical Chemical Structure of Acrylate Ester Epoxy Resin portion of XB5081-1.

D. Results and Discussion

Several disk specimens were made with the expanded laser beam arrangement as described in the previous section. These specimens were to be placed in the crossed circular polariscope to determine the fringe order, N, at the center of the disks. The first step in finding this value of N though, required that the direction of the principal stresses, σ_1 and σ_2, be found so that the Babinet-Soleil compensator could be aligned with the direction of the σ_2 stress. This was a necessity as the compensator's axis must be aligned with this principal stress direction if it is to exactly compensate for the retardation of the specimen and hence be able to measure the fringe order in the specimen at this location (see Appendix B for more details on the workings of a Babinet-Soleil compensator).

The process of determining the direction of the principal stresses, σ_1 and σ_2, in the specimen involved simultaneous rotation (in the same direction), of the crossed polarizing elements of the plane polariscope (Figure 7 but with the quarter-wave plates removed) in discrete steps, i.e. 5 degrees, while the light intensity at the photometer was monitored.

In theory, when the polarizing element located before the specimen, was aligned with the direction of one of the principal stress axes (the analyzer is therefore crossed or at a 90 degree angle to the polarizing element) the photometer should have given a reading of zero intensity. That this should be the case can be seen from eq (a1) in Appendix A, where whenever θ is equal to 0 or 90 degrees (i.e. direction of polarization of the incident beam is in alignment with a polarizing axis in the specimen) the light being transmitted should be completely blocked by the analyzer.

In actuality, the light intensity at the photometer never becomes zero as there are slight imperfections in the polarizing elements that cause light to be transmitted even when they are crossed. Fortunately, because of this, it becomes possible to distinguish which rotation corresponds to σ_1 and σ_2. Since σ_1 is by definition larger than σ_2, when its axis is aligned with the first polarizing element the specimen transmits more light to the analyzer and hence, because of imperfections in the polarizing elements, more light will reach the photometer. This results in a larger minimum than for the alignment of the polarizer with the σ_2 direction and is the way in which the principal stresses can be separated from each other.

Not only must the directional axes σ_1 and σ_2 correspond to two minimums in light intensity, the phenomenon of birefringence dictates that the directions of these principal stresses must be perpendicular to each other, i.e. the incoming plane polarized light is broken up into two waves which are normal to each other.

When each of the disk specimens was placed into the field of the crossed polariscope (with quarter wave plates removed) the directions of the principal stresses at the center were determined by looking for two local minimums which were 90 degrees apart. In every case, two minimums could be found but the angle between them ranged anywhere from 50 degrees to 170 degrees with none being closer than $\pm$ 15 degrees of perpendicular. These results were perplexing and lead to a further investigation of two of the disk specimens.

As a check to verify that the directions (although not 90 degrees apart) determined for σ_1 and σ_2 were genuine and not something associated with the material, each disk was rotated in the plane slightly so as to keep the image of the center of the disk centered on the photometer. This rotation should have had no effect on the angle between the principal stress directions. This was not the case at all which meant that what was being measured was either the fringe

order, N, at a different spot on the specimen or there was some sort of problem with the material itself. The effect of measuring N at a different location of the specimen should have had on the angle between the principal stress directions was determined to minimal. This was due to the fact the even taking into consideration that the center of the disk was not exactly maintained on the photometer as a result of the rotation, because the magnification of the image of the disk at the photometer, a maximum error of 0.5mm off center would have occurred. Any non-uniformity in crosslink density due to non-uniformity of the laser beam intensity profile would therefore have to be great in order for it to effect the measurements as much as what was being observed. As previously stated, the measurements of the laser light intensity profile across the specimen did not show a great variance (i.e. less than -6% across the whole specimen; less the closer one was towards the center) and hence it was believed at the time that the results obtained for the angle between the principal stress directions were a function of the material.

This lead to an in-depth micro-examination of the disks. An optical microscope at 40X was utilized to study the disk specimen composed of cured XB5081-1 resin. One of the disks of XB5081-1, which had been placed in the polariscope, was polished to a 0.3 micrometer finish and then viewed with a transmitted light microscope with an analyzer and polarizer element. Figure 11 shows a slightly off center non-polarized 40X view of the disk. The microscope was focused on the top surface of the disk. The dark edges at the top of the photomicrograph was a result of the camera tube attached to the microscope and not the edge of the disk. It can be seen from this Figure, that the disk did not appear to be homogeneous as there were numerous optical distortions in the material. Upon viewing this same disk under crossed polarized light, see Figure 12, the non-uniformity became readily apparent. In this photomicrograph, one can also see that there appeared to be directionality to the nonuniformity with the pattern radiating outwards from the center of the disk.

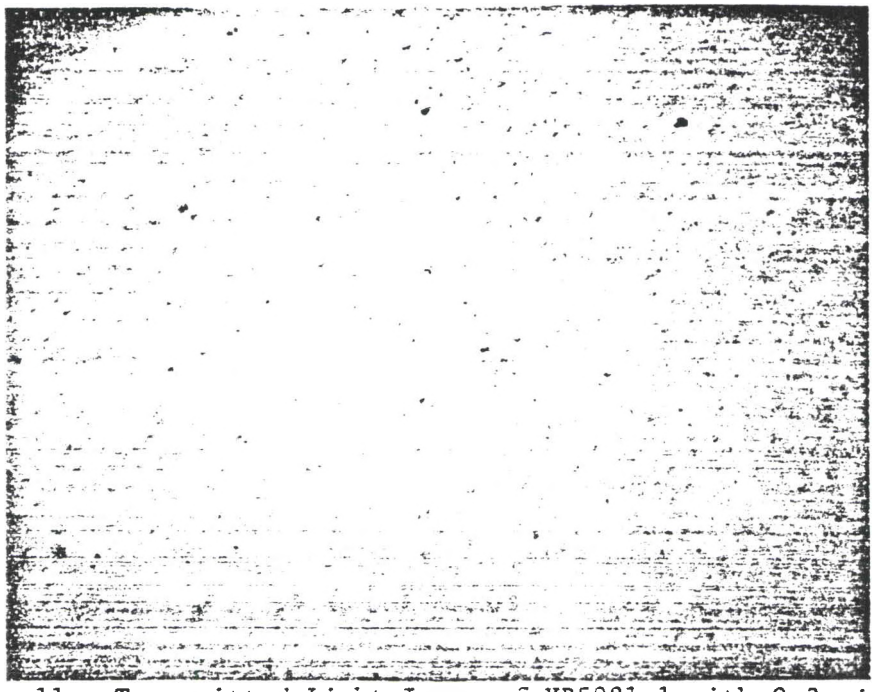

Figure 11. Transmitted Light Image of XB5081-1 with 0.3 micron finish, 40X.

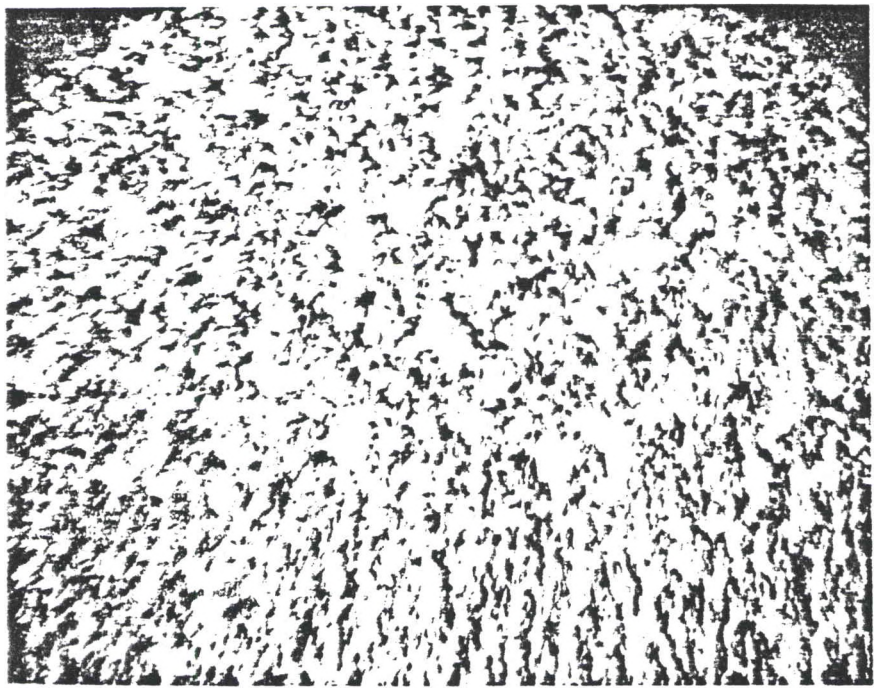

Figure 12. Interference Pattern of Same Disk as in Figure 11, Under Crossed Polarized Light, 40X.

This disk specimen was then coated with a thin gold layer, using a Common Wealth Scientific Mini-Coater, to allow high magnification viewing, with reflectance type microscopes, of the coated polished surface. Figure 13 shows a 13.5X plane polarized view of the disk taken with a stereomicroscope. The dark side of the disk was a result of the physical arrangement of this microscope and its lighting mechanism. It has no implications for the material. What is apparent from this photomicrograph is that the surface was full of what appears to be pock-marks. Higher magnifications of the same area were taken with a Zeiss Model Axiovert 10 reflectance microscope and are shown in Figures 14 and 15. From these pictures it appears that these marks were voids, but it required further investigation with a Scanning Electron Microscope (SEM) to be conclusive. Figure 16, which is a SEM photomicrograph of the specimen, shows that in fact the dark spots were voids with the size of the vast majority of them being approximately 10 microns in diameter.

In order to be sure that these voids existed throughout the specimen and not just at a surface, the disk was cleaved in two with a scalpel. Figure 17 shows the photomicrograph of one of the fractured surfaces. From this, it can be seen that these voids were prevalent throughout the thickness as well. Figures 18 and 19 represent higher magnifications of the fractured surface.

It is believed that two phases were present throughout the specimen resulting in a nonhomogeneous material. This belief is based upon research conducted by Weissman et al[11] which identified the possibility that an XB5081-1 resin systems, cured only with a laser, formed two discrete, dispersed phases. These two phases are believed to be a gelled resin swollen with residual monomer and a higher crosslinked resin. These different regions of crosslink density constitute two materials with different indexes of refraction and hence can account for part of the complex interference observed.

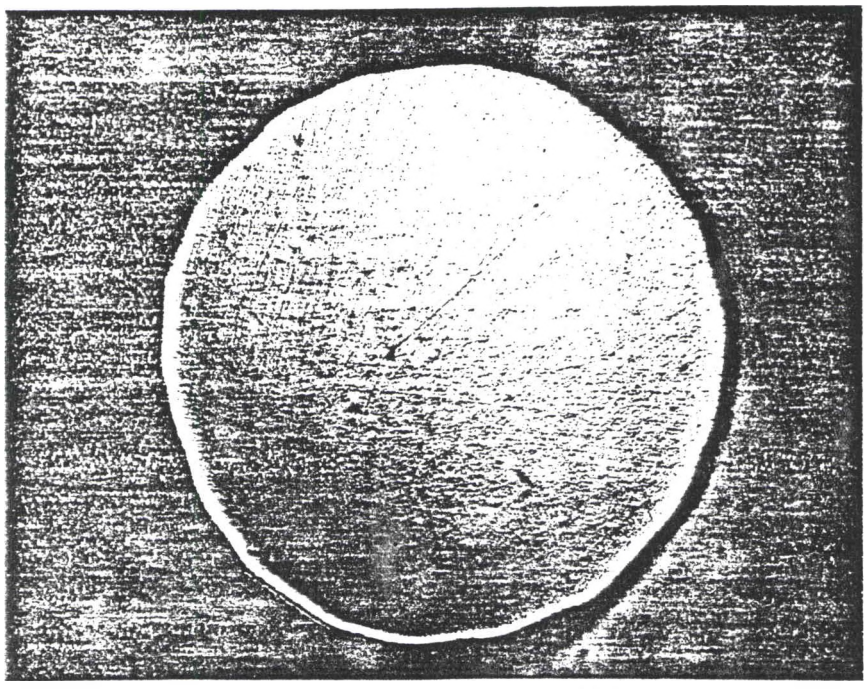

Figure 13. Image of Gold Coated Surface (0.3 micron finish) of XB5081-1 Disk Under Plane Polarized Light, 13.5X.

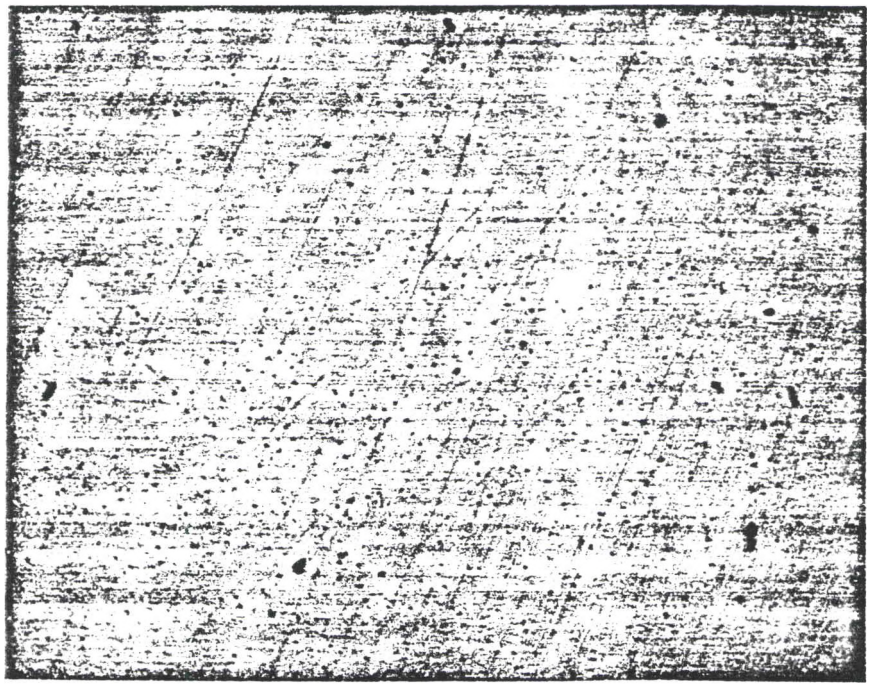

Figure 14. Image of an XB5081-1 Polished Disk Surface Disk Surface, 50X.

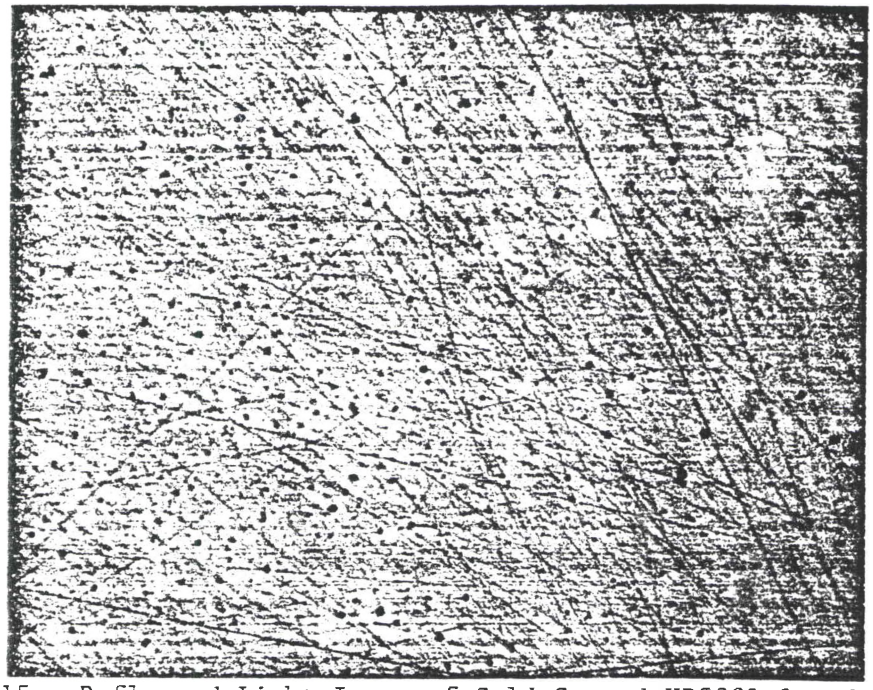

Figure 15. Reflected Light Image of Gold Coated XB5081-1 Polished Disk Surface, 100X.

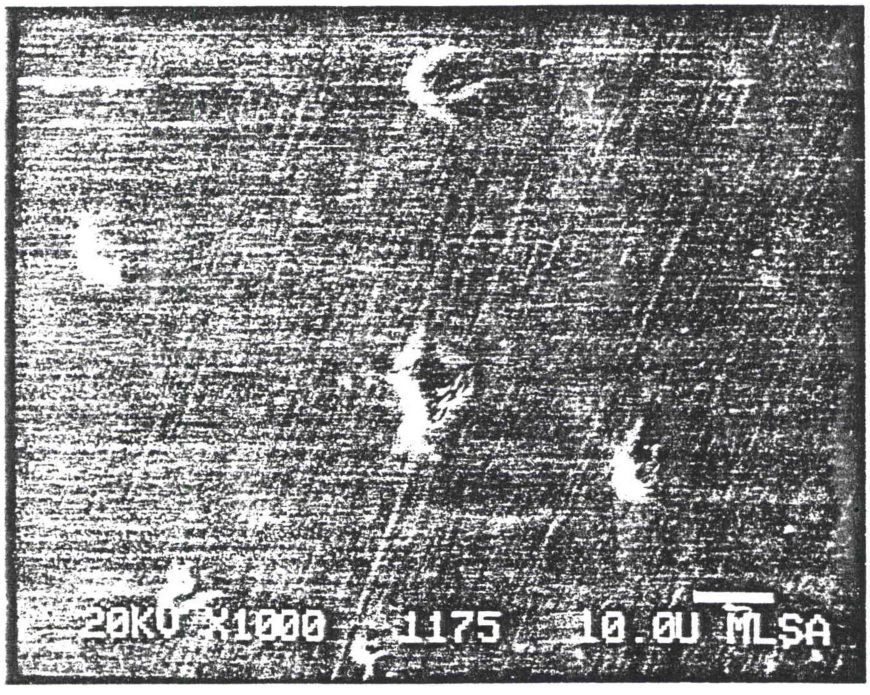

Figure 16. SEM Image of XB5081-1 Polished Disk Surface, 1000X.

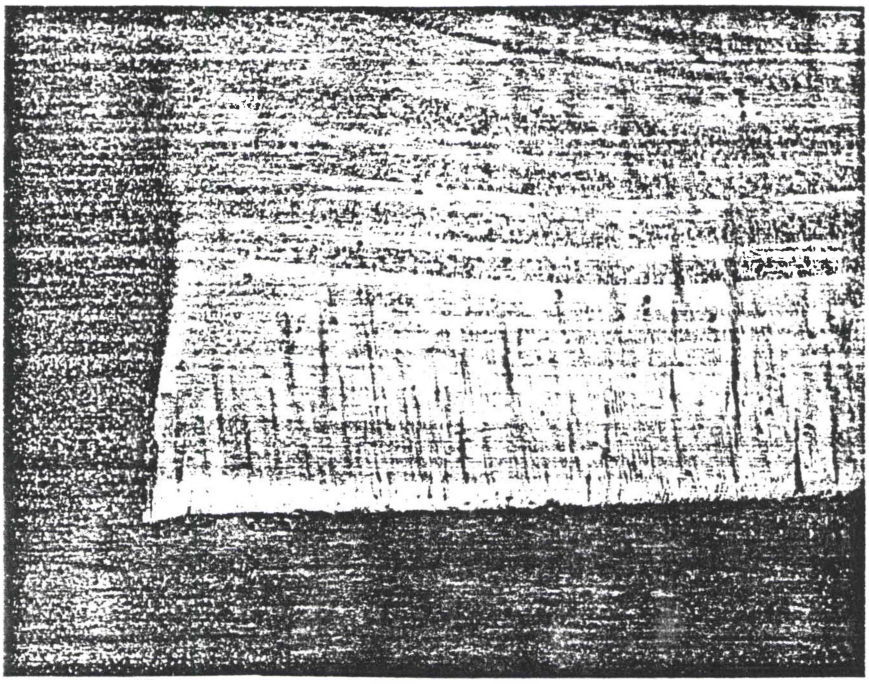

Figure 17. Through-the-Thickness Image of a Fractured Surface of a XB5081-1 Disk, 50X.

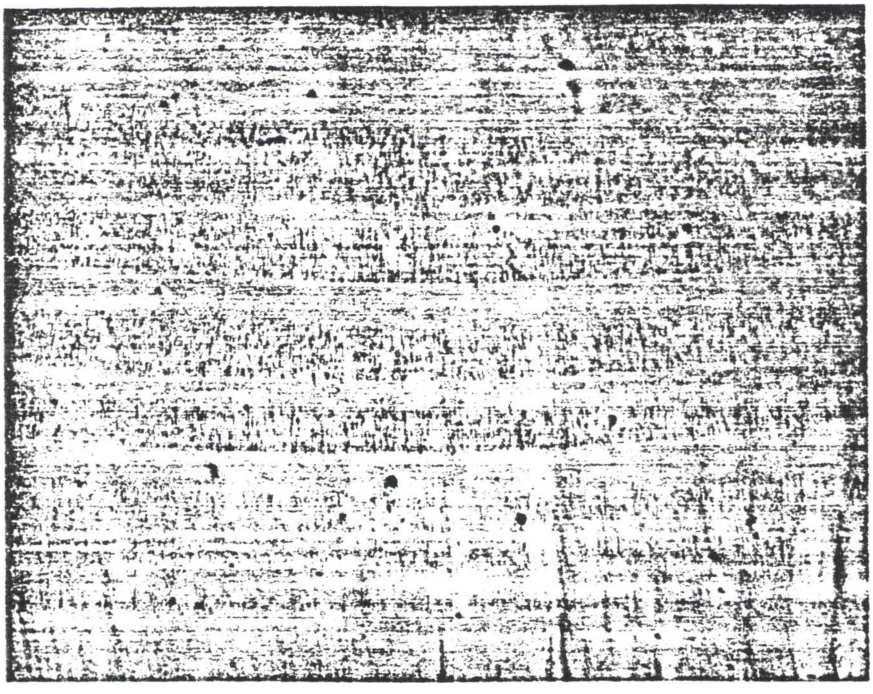

Figure 18. Higher Magnification of Surface Shown in Fig. 17, 100X.

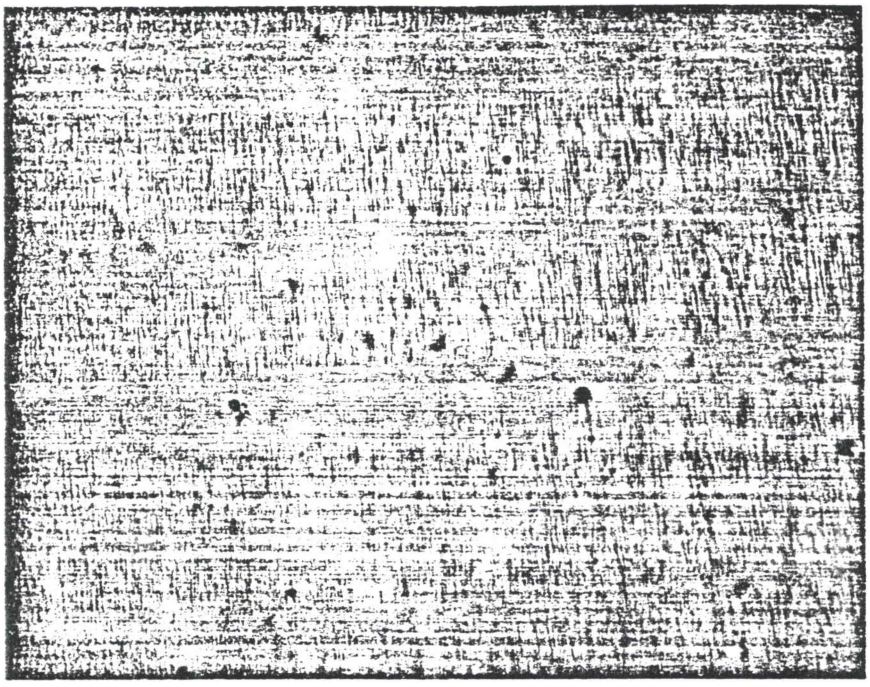

Figure 19. Higher Magnification of Surface Shown in Fig. 17, 200X.

It is believed that the multi-component nature of the resin system was partly responsible for the inhomogeneity through possible microphase separation. Liu and Armeniades[12] showed this to exist in a Methyl Methacrylate (MMA) resin containing 30% by weight Polymethyl Methacrylate (PMMA) modified with a thermoplastic as a method in which to control shrinkage without loss of strength. They found that their system contained microdomains rich in MMA near the PMMA chains and microdomains rich in thermoplastic near the MMA due to the thermoplastic monomer not being completely miscible with the pre-existing polymer. The fast thermal reaction, (completely cured in 5 minutes or less), they proposed, did not allow diffusion of the remaining monomer species to their equilibrium levels thereby resulting in MMA and thermoplastic rich cured microdomains i.e. phase separation. The photomicrograph of this system under polarized light looks somewhat similar to that for the XB5081-1 resin although the PMMA/MMA/thermoplastic system has a finer interference pattern. It is also noted that Liu and Armeniades found that their system exhibited a radial growth direction to the microdomains, which was also similar to that observed for the XB5081-1 specimens.

As a result of the possibility of the complex interference pattern being due to a multi-component system, it was decided to try to use a single component (not including the photoinitiator) photopolymerizable resin system for further study. The system tried was Hexanediol Diacrylate (HDDA) with 3.66% by weight Irgacure 184 photoinitiator (this is the approximate percent by weight of Irgacure 184 used in the XB5081-1 resin formulation, as determined by the University of Dayton Research Institute personnel). The same laser arrangement was utilized as with the XB5081-1 samples but the energy density was increased to insure the specimens were at least as thick as the XB5081-1 samples with approximately the same exposure times.

After the samples were made they were polished following the same procedure as for the XB5081 and then placed in the field of view

of an optical microscope equipped with a crossed polarizing elements attachment. Figure 20 shows a transmitted light (nonpolarized) image at 40X of one of the HDDA specimens. The dark spots represented either inclusions (e.g. impurities) or voids. Figure 21 is the view through crossed polarized elements of the same location of the specimen (orientation is slightly different). From this it can be seen that inhomogeneity still existed. It also shows that the pattern appears to radiate outwards from the center of the specimen. A closer examination of a couple of the inclusions (marked by white arrows) in Figure 21 revealed that there was a white zone that existed starting at the inclusions and running (pointing) in towards the center of the specimen. With the appropriate filter this white zone became colored and it was evident that this zone was a stress field. It is believed that stresses were generated in the material as a result of the inclusions being locked into place by the top layer of the resin as it cured. The layers forming below this top layer, would then have to strain against this immobile inclusion as they cured and subsequently contracted due to the curing process (i.e. shrinkage). This strain resulted in the observed stress pattern or white zone.

The edge of one of the HDDA specimens is shown in Figure 22. This photomicrograph was taken from the vantage point of looking at the bottom surface through to the top surface. From this image it can be seen that discrete layers formed in the process of creating this disk with each successive layer being smaller than the first. It is possible that part of the reason why the succeeding layers were smaller (other than due to absorption of photons by the previous layer) was that they were allowed to shrink to a greater degree as a result of them being less crosslinked. This would account for the stress patterns around the inclusions as discussed in the preceding paragraph.

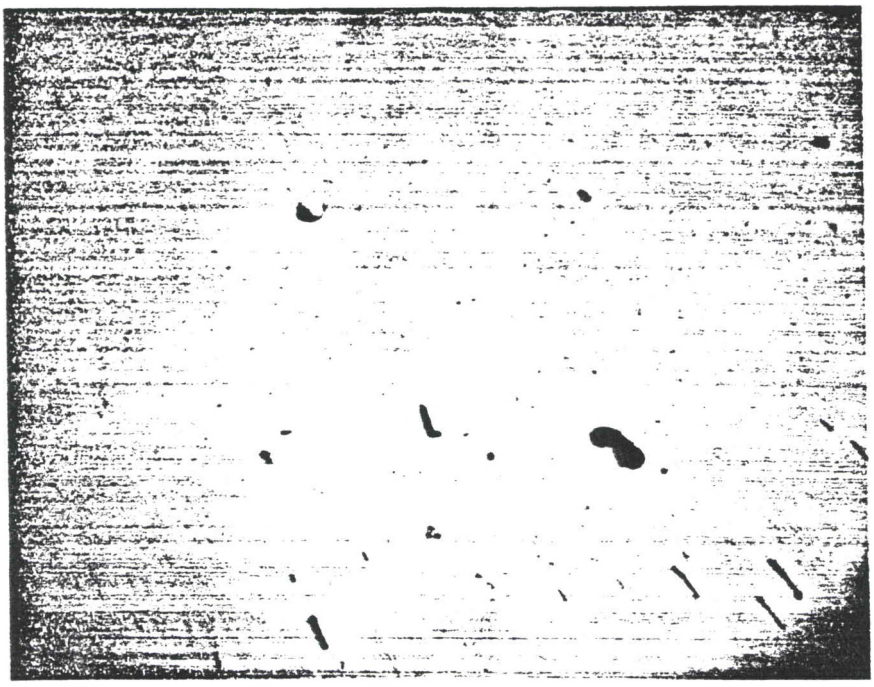

Figure 20. HDDA Polished to 0.3 Micron Finish, 40X.

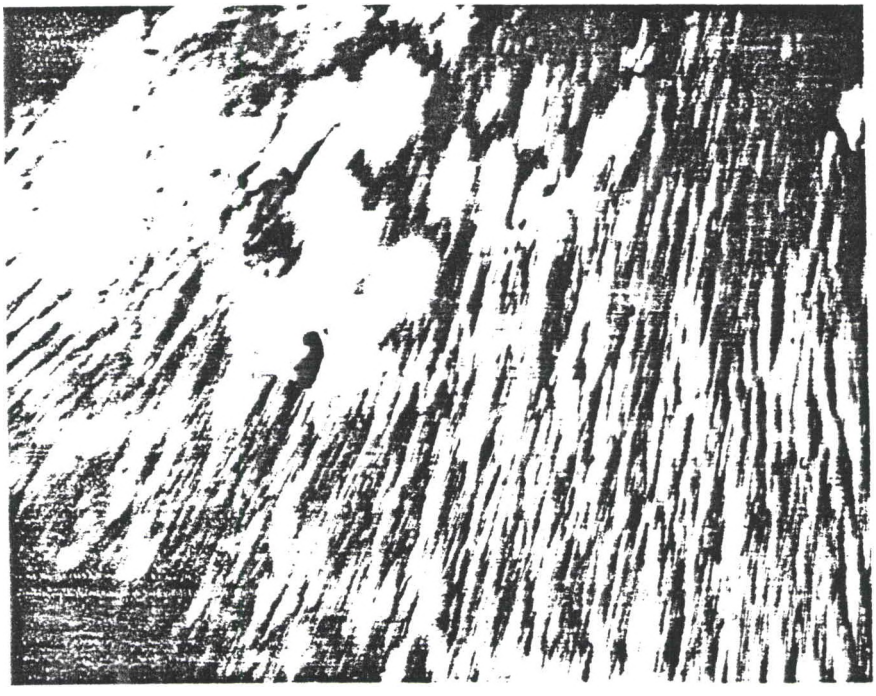

Figure 21. Same as Fig. 20 but Under Crossed Polarized Light, 40X.

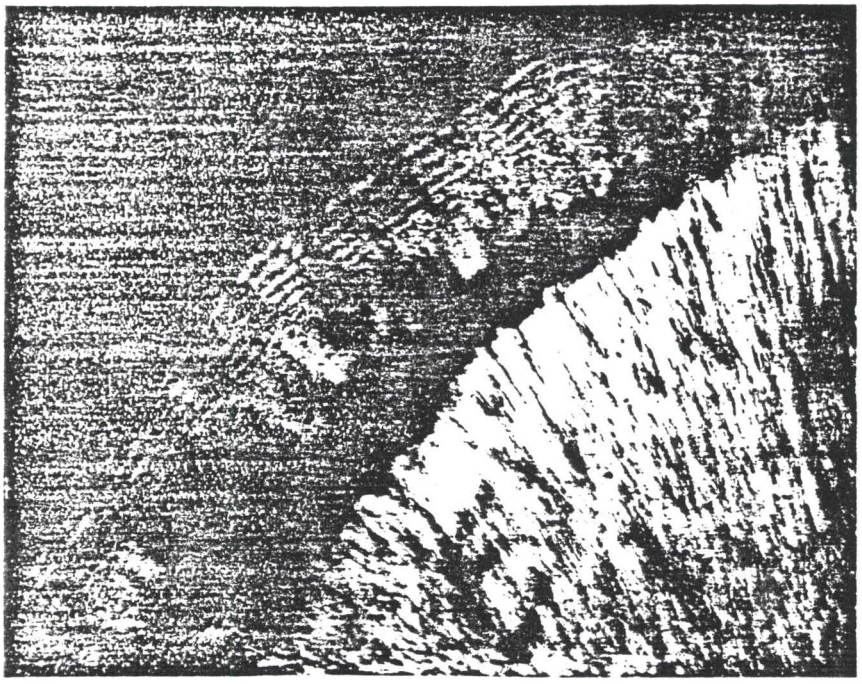

Figure 22. Crossed Polarized View of an Edge of a HDDA Specimen, 40X.

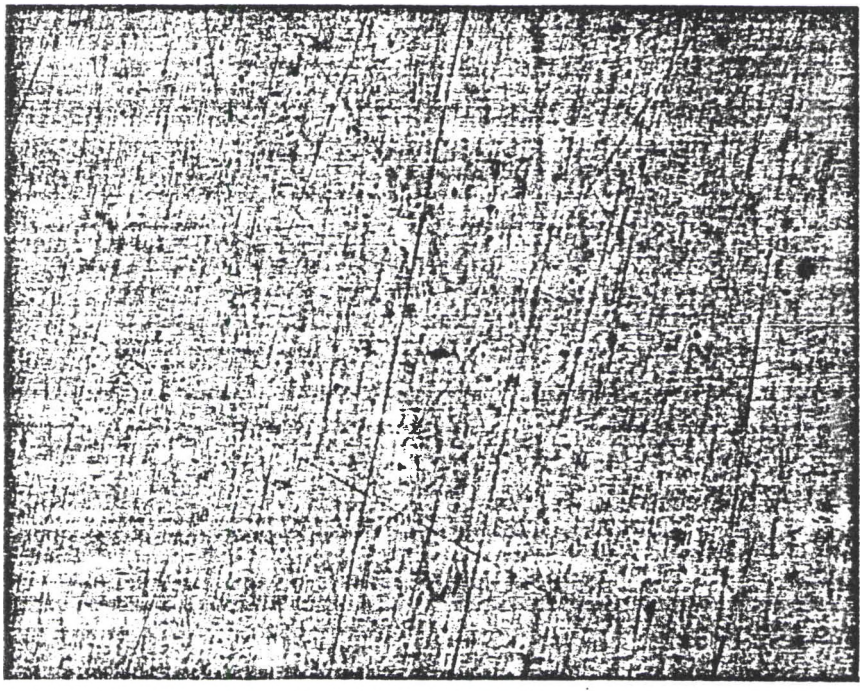

Figure 23. Reflected Light Image of Gold Plated HDDA Disk, Polished to 0.3 Micron Finish, 100X.

Figure 23 shows that the HDDA specimen (coated with a gold film) had a similar pock-marked surface to that of the XB5081-1. A SEM was utilized to try to identify these marks as voids but was unsuccessful as it was impossible to obtain a focused image of the surface. By comparing photomicrographs of the surface of the XB5081-1 and the HDDA specimens (Figures 15 and 23 respectively) it appeared that the XB5081-1 specimen had a larger quantity of voids present than did the HDDA. It is believed that these voids form as the result of the cure shrinkage associated with polymer formation.

Cure shrinkage is inherent to the formation of polymeric materials from monomers since the formation of polymer chains converts the longer secondary bonds between monomeric segments to the shorter primary bonds and hence also reduces the amount of free space swept out by a given molecule due to reduced chain mobility.

In laser cured systems Decker[13] showed that the kinetic rate expression for polymerization was first order not half order as is usual for a low light intensity cure. The polymerization reaction consequently proceeds at an accelerated rate, which as Kloosterboer[14] demonstrated, results in chemical conversion leading shrinkage due to an excess (higher than equilibrium value) of free volume present in the resin system. The higher chemical conversion locks in the structure of the resin system even though equilibrium forces desire it to shrink. This sets up a residual tensile force in the material. It is proposed that void formation occurs as a result of the curing resin system attempting to reduce these residual stresses.

It can only be speculated, since the total energy doses were not identical, that a larger quantity of voids (assuming also a larger volume percent of voids) existed in the XB5081-1 due primarily to its chemical formulation and kinetics verses that of the HDDA system. That is, the XB5081-1 system became more highly crosslinked

than the HDDA system. Since a more crosslinked system exhibits a larger amount of shrinkage, one would also expect it to show a larger amount of void formation.

The multitude of voids present in both the XB5081-1 and HDDA cured systems had similar optical effects on the specimens when looked at under crossed polarized light. This was due to the fact that a void represents an index of refraction change since light would travel through a transparent solid material to air (the void) and then through the solid material again. Any index of refraction change would impact heavily on the interference pattern as the phenomenon of birefringence, as previously explained, is dependent upon the index of refraction change due to a stress field. The voids further complicated the interference pattern by the fact that they were generally circular which would diffract the light in a multitude of directions resulting in a more complex interference pattern. Further complicating the interference pattern was the likelihood that the material at the interface of the voids was stressed, thereby being another source of changing index of refraction. When all these factors became overlapping because of the thickness of the specimen, the pattern became even more complex.

The fact that the disks composed of the single component HDDA resin system showed a similar pattern under crossed polarized light as the XB5081-1 resin system, leads one to the conclusion that either the laser (e.g. distortions in the coherent beam as a result of lens imperfections and dust in the air), the rapidity of the reactions caused by the laser and the subsequent void formation, as well as the probable formation of two discrete phases of different crosslink densities within the specimen[11], were the main contributors to the nonhomogeneous nature of the XB5081-1 disks and hence to the complex interference pattern obtained. It is believed that the multi-component nature of XB5081-1 and the speed of the reactions that occurred as a consequence of utilizing the laser, lead to the

possible formation of component rich areas. These microdomains would have different indexes of refraction and hence would have increased the complexity of the interference pattern obtained. The interference pattern would have also been further complicated due to two discrete phases of different crosslink densities being present. The stresses present as a result of the shrinking of succeeding layers also would have caused increased optical distortions in the disk and hence would have added the complexity of the interference pattern obtained.

All of the above factors resulted in the observation of a very complex microscopic interference pattern for the specimens when placed in the crossed circular polariscope. The end result was that photoelastic analysis of the specimens for determination of residual stresses was not viable since the primary assumption of a homogeneous material was not valid.

CHAPTER III

CONSTANT STRAIN ANALYSIS

A. Test Method 1

1. Introduction to the General Concept

As a consequence of the photoelastic technique not being able to measure the residual stress levels in the disk specimens, another technique was attempted. The technique attempted, which has been termed "constant strain" was originally devised by Weissman[15] and was the proposed simplified technique for determining qualitative differences in residual stress levels as outlined in the thesis proposal. The concept behind this method was to take a partially cured (e.g. 50 to 60%) rectangular film and place it in the grips of a machine capable of maintaining a constant specimen length while measuring the force required to do so. The rectangular specimen would then be subjected to a high intensity UV light source for a specified duration, causing some of the remaining uncured resin to react. This additional chemical conversion would have shrinkage associated with it, but because the specimen's length had been fixed by the grips of the instrument, this shrinkage would be converted to stress in the specimen which would be measured by the instrument. The stress should increase as the duration of exposure increased (i.e. as chemical conversion and therefore shrinkage increase).

The first instrument utilized in attempts to get this method to yield useful results was a Rheometrics Solids Analyzer II operating with thin film fixtures in a modified stress relaxation experiment. This arrangement failed to give any interpretable results, the reasons for which are detailed in the Test Method 1, Results and Discussion section.

2. Experimental Methods

The specimens were made using the same laser set-up as was used for the disks specimens in the photoelastic section with the exception that a rectangular mask (approximately 2.5mm x 1.5mm) was used as opposed to a circular one, and the mini-vat construction was entirely different. For these rectangular specimens the liquid resin was held between two glass plates of approximately 5 inches by 5 inches with spacers keeping them approximately 0.007 inches apart. This resin-plate arrangement was then place on a single axis micron steppable moving platform. The platform was moved at its maximum speed (12mm/min) and then the shutter was opened. As the UV light exposed the resin, it cured. The shutter was closed when an approximately 30mm long rectangle had been formed. The resin-plate arrangement was then moved laterally so as to have about 10mm separation between the existing specimen and the one about to be created. The process of creating subsequent rectangular specimens involved merely repeating the steps followed in making the first.

It had been determined, through the same procedure as utilized for the disks, that the intensity of light comprising the rectangular beam was uniform to within -6% of the maximum value. The energy density at any given location in the path of the beam was calculated by first using a GENTEC broad band energy detector to measure the total energy of the square spot beam, which was found to be 13.0mW. Next the area of the beam spot was determined using the same silicon detector arrangement which was employed to measure intensity variations across the square. This was accomplished by moving the masked silicon detector with the micron steppable platform from one edge of the spot to the other. The oscilloscope was used to detect the edges, i.e. when the scope reading jumped from the base line value to a nominal value for a reading in the rectangle spot, this

was marked as one edge and used as the starting point, or 0.000mm reference point for the platform. The platform was then moved so as to allow the silicon detector to traverse the rectangular spot. When the oscilloscope signal dropped sharply, the detector had reached the opposite side of the rectangle and the reading on the platform signal driver corresponded to the width of the square. From this technique it was found that the area of the rectangle was 7.83mm^2 and therefore the energy density of the spot was 1.66mW/mm^2.

The residence time of the laser illuminating any given spot on the rectangular specimen can be calculated from the length of the rectangular laser spot, 2.57mm, and the platform speed (12mm/min). From the above values the residence time for a 1mm length, was found to be 12.85 seconds.

The total energy received at any given location of the rectangular specimen was then calculated by multiplying the residence time by the energy density. This yielded 21.33mJ/mm^2. This was same order of magnitude as is typically utilized by the SLA operating at 15mW output and a step period of 160 (e.g. 74mJ/mm^2).

The thin rectangular specimens were then removed from the glass plates and cleaned in isopropyl alcohol to remove excess liquid resin. As a result of the cured material acting as a light guide additional resin beyond what was directly illuminated with the UV beam, was cured. At the very edges this material was just at the gel point and when cleaned with isopropyl alcohol the result was a very jagged edged rectangular specimen. This necessitated sanding the edges to remove the notches and make them flat. If the notches had been left in the specimens they would have been stress concentrators and consequently would have had an adverse affect on the stress measurements.

The cleaned specimen's width and thickness were then measured with a vernier caliper and micrometer respectively. It was then

placed in the thin film grips of a Rheometrics Solids Analyzer II machine. This machine was capable of performing a variety of mechanical tests on polymeric materials to determine their viscoelastic and mechanical properties. The distance between the grips was measured and this along with the specimen width and thickness were entered into the Rheometric's computer.

The Rheometrics was operated in its stress relaxation mode. Normally this involves straining a plastic specimen a pre-set amount and then maintaining this strain while monitoring the decrease in force levels as the specimen relaxes. This operating mode was modified so as to measure the increase in stress as a result of additional UV curing. This was done by first straining the material and allowing it to come to a stable stress state (i.e. a flat line region of a plot of stress verses time). This was taken as the base line stress value. A high intensity broad band UV light was then turned on to expose the central portion of the specimen. Care was taken to ensure that only a relatively small central section of the rectangular specimen was exposed to the UV light, to minimize possible end effects at the grips. After one minute the UV source was turned off. The force required to maintain the pre-set strain level was monitored from the beginning of the test, through exposure and for approximately 10 minutes after the UV light was shut off. The difference in stress levels from the initial stable stress state to the stress state 10 minutes after the UV light was shut off should have corresponded to the stress which was a direct result of shrinkage due to additional curing.

Provided that specimens made from different resin formulations were cured (both with the laser and the broad band UV source) and strained under identical conditions, this test method could have proved to have been a good qualitative technique for comparing the tendency for residual stress level build up. It could only have been qualitative as the initial stable stress state would be different for different resin formulations dependent upon the chemistry and

kinetics of the resin, which in turn effect the crosslink density obtained and hence the modulus of the specimens. Differences in modulus between specimens would of course affect the stress values measured.

3. Results and Discussion

A rectangular specimen was tested as described in the Experimental section. The plot of stress verses time is shown in Figure 24. The initial decrease in stress, as previously mentioned, was due to stress relaxation of the specimen after being strained. Point A was the time at which the high intensity UV light source was turned on. Stress in the specimen then began to decrease, which was believed to be due to the specimen heating up and expanding. The stress level then began to increase. This was probably due to additional curing occurring in the specimen creating more crosslinks. After this point, the stress oscillated and continued to do so even after the UV light was turned off (point B). Not until about the 800,000 Pascal (Pa) level did the stress stabilize. It then showed an increasing slope. It was thought that this increasing stress slope was possibly due to dark reactions[16,17] (i.e. additional polymerization occurring, without UV light present, as a result of the remobilization of trapped radicals in the resin) and thermal cooling of the specimens.

At first this stress verses time plot, with the exception of the unstable section, appeared to be logical and explicable. That this was not, in fact the case, became evident when the strain verses time plot was overlaid on the stress verses time plot as shown in Figure 25. The nearly constant initial strain level, obtained as the result of the laser cured specimen relaxing, was less than the pre-set strain level of 0.0005. This was found and later confirmed by phone conversations with the manufacturer of the Rheometrics instrument, to be due to machine compliance. This compliance was noticeable at the initial point when the UV light is turned on and stress decreases. This should have had no effect on the strain if

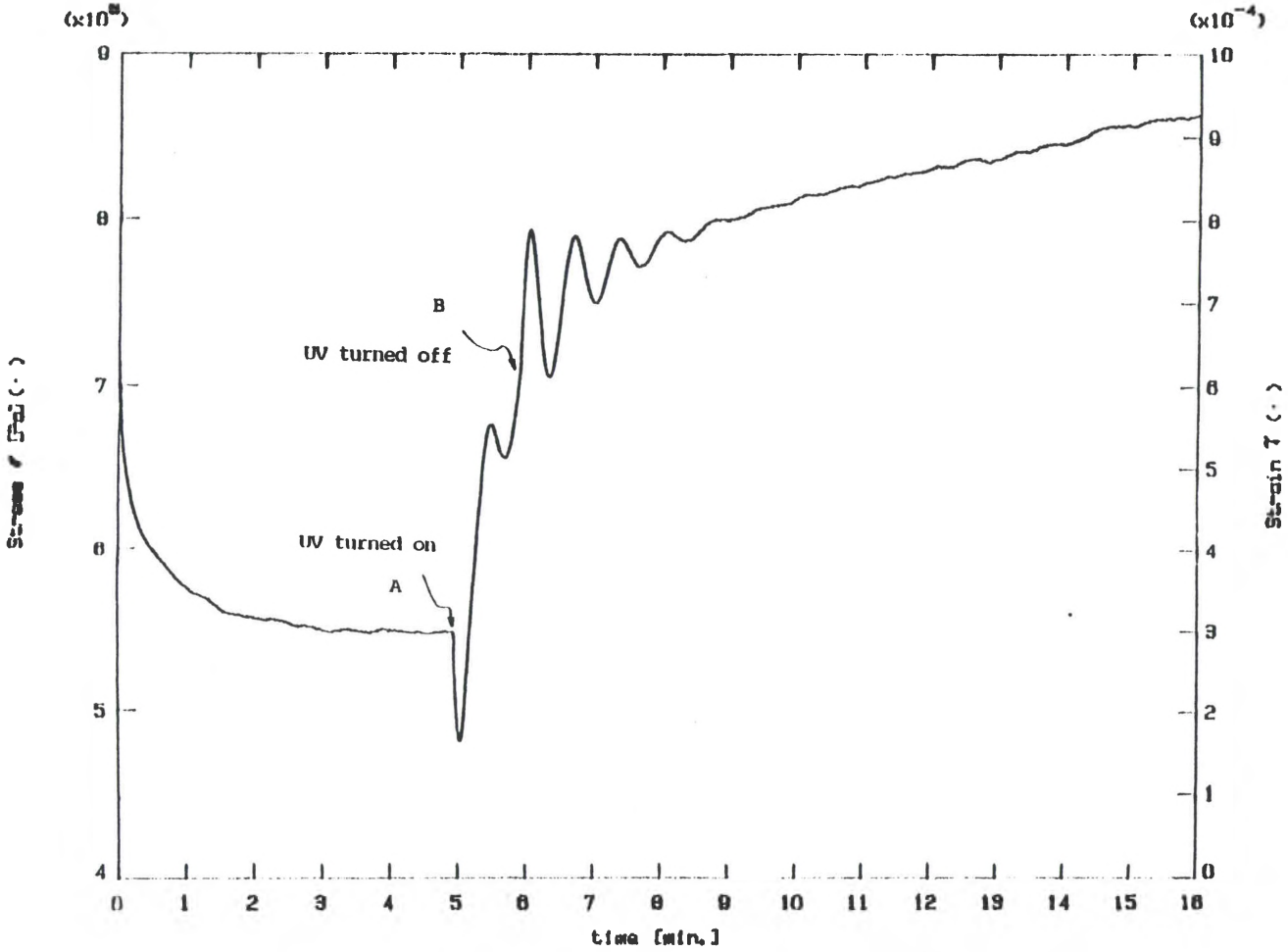

Figure 24. "Constant Strain", Test Method 1. Specimen allowed to relax and then further exposed to UV energy. Plot of stress vs time.

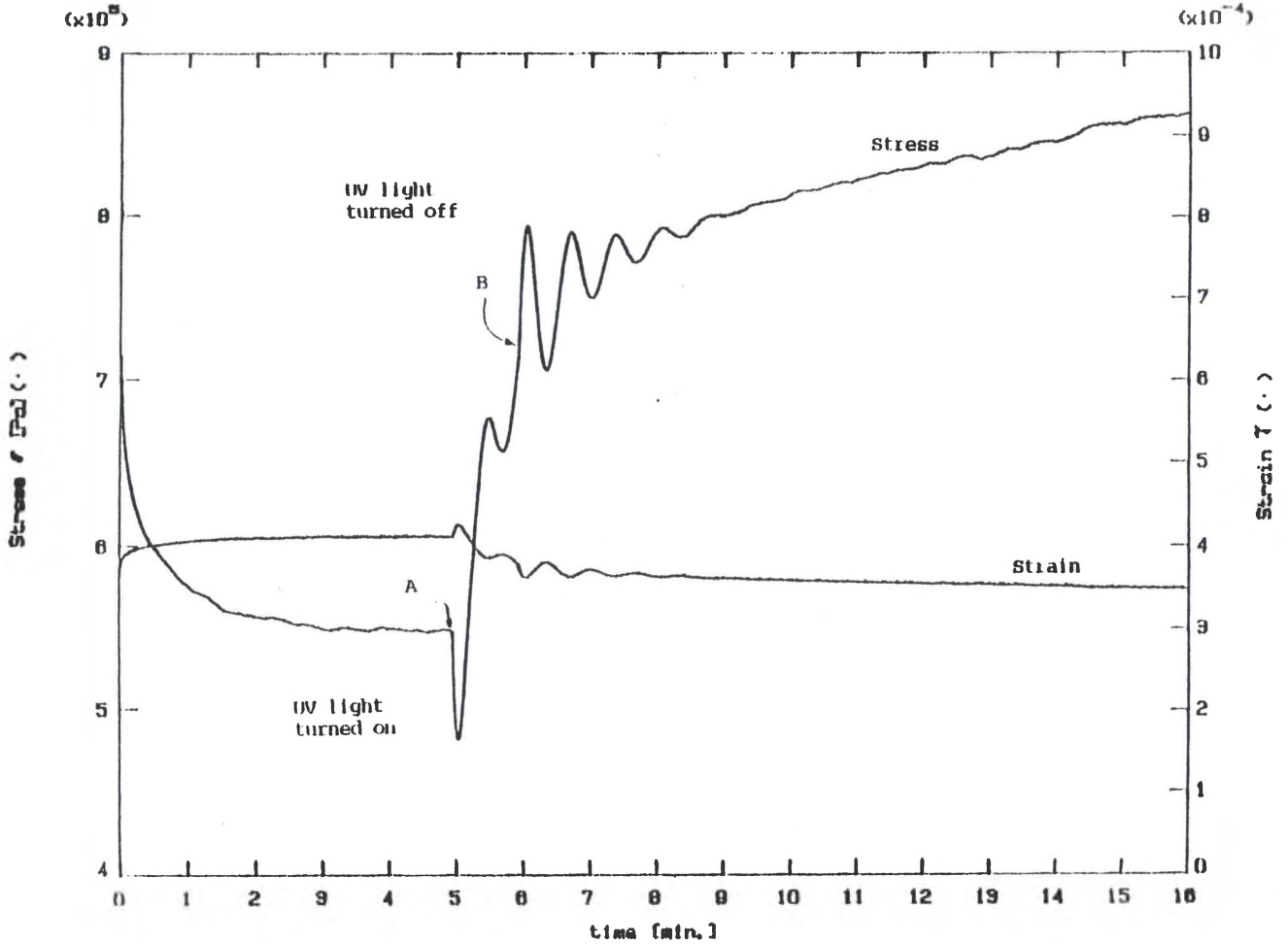

Figure 25. Same plot as in Fig. 24 but with strain vs time overlay.

the machine was maintaining a constant setting. What actually occurred was a strain increase as a result of the machine trying to achieve the pre-set strain level while the stress had been reduced due to heating of the specimen. Curing and its resultant shrinkage then started to overcome the expansion due to heating resulting in a stress increase.

Machine compliance also accounted for the decrease in the strain level seen whenever the stress level increased. As the stress in the specimen increased, the force on the machine increased causing the distance between the grips to shorten (i.e. strain decreased) as a result of the machine bending under the load.

The oscillating segment of the stress vs time curve may be a direct result of the machine trying to compensate for the reduction in strain as stress increased. The stress level eventually started to become linearly increasing after about the 800,000 Pa level while strain continued to decrease slightly. Since the strain level at the time corresponding to a linearly increasing stress level was lower than that of the base line value, the stress level in the specimen must have been actually higher than that represented in Figure 25. Unfortunately it was not possible to readily determine how much more stress would be present if the strain remained constant at its pre-set value as the modulus of the specimen had changed due to additional curing.

Without being able to compensate for machine compliance, either to ensure that initial strain levels in different specimens were identical, or more importantly to maintain a constant strain level throughout the test, even qualitative comparisons between different resin formulations was not possible. Therefore because of its machine compliance, the Rheometrics Solids Analyzer II instrument was not capable of meeting the objectives for this modified stress relaxation experiment.

B. Test method 2

1. Introduction to the General Concept

A DuPont 983 Dynamic Mechanical Analysis (DMA) system was then employed in trying to measure the stress that develops in partially cured thin rectangular specimens exposed to additional UV energy. Although the concept of this experiment was similar to that of the Rheometrics Solids Analyzer II, with the DMA instrument the principles of operation were different which alleviated the problem of machine compliance, thereby giving hope that it would lead to useful information. In both instances, a modified stress relaxation experiment was employed which involved straining a specimen a preset amount, watching the stress decay to a level baseline value, and then exposing the specimen to an additional amount of high intensity UV energy. An increase in stress was expected as additional curing caused shrinkage.

2. Experimental Methods

The physical arrangement of the DMA apparatus is shown in Figure 26[18]. The specimen was clamped between the ends of the two parallel arms, which were mounted on low force flexure pivots allowing motion only in the horizontal plane. An electromagnetic motor attached to one arm displaced the arm an amount selected by the operator. This arm displacement caused the sample to undergo a flexural deformation as depicted schematically in Figure 27[18]. A Linear Variable Differential Transformer (LVDT) mounted on the driven arm measured the sample's response to the displacement and provided feedback to the electromagnetic motor.

In the stress relaxation mode, the arm displacement is kept constant via the LVDT feedback to the electromagnetic motor. The amount of driver energy required to maintain this displacement was recorded and then equated to the stress in the sample via mathematical relationships developed by DuPont[19].

The stress in the sample was allowed to decay to a level base line value, at which time the specimen was exposed to additional UV energy. This was to cause the specimen to undergo further polymerization and hence result in shrinkage. This shrinkage would cause more energy to be utilized by the electromagnetic motor in order to keep the arm displacement constant. An increase in stress level was expected as a result of this action.

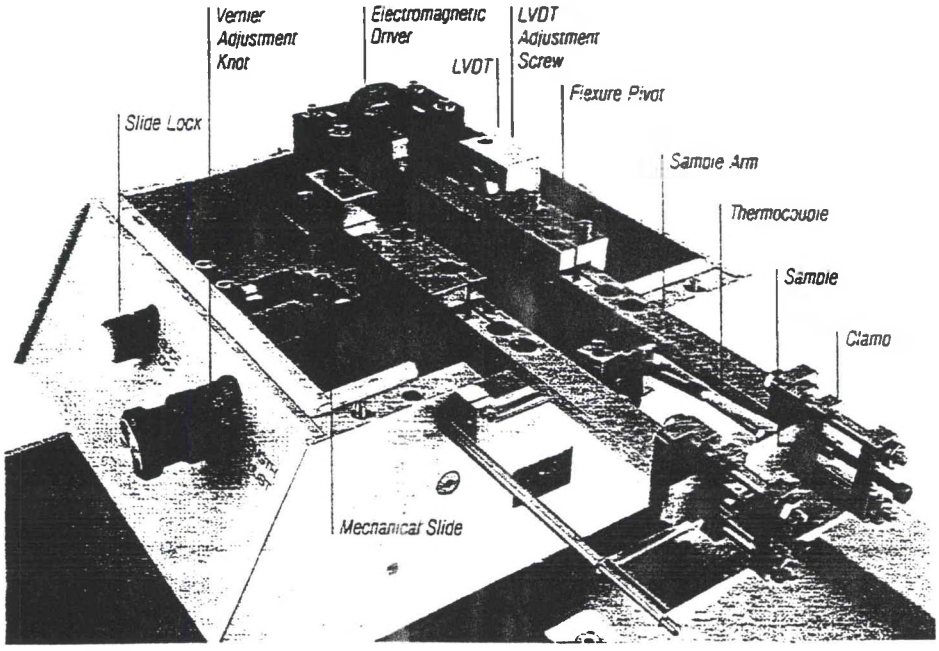

Figure 26. Physical Arrangement of DuPont 983 DMA.

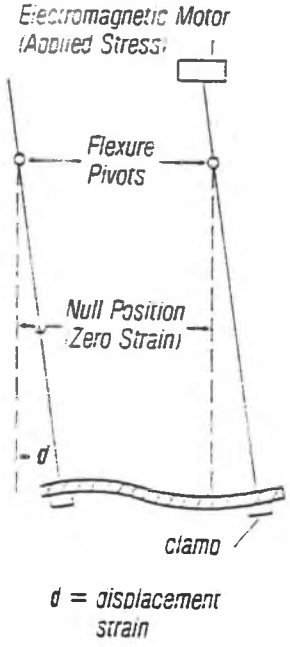

Figure 27. Flexural Deformation of a Specimen in a DuPont 983 DMA.

3. Results and Discussion

The first experiment involving the DuPont DMA 983 utilized a specimen which had been partially cured with the Argon-Ion laser arrangement as previously described. As with all experiments involving the DuPont DMA, the UV energy that the specimen received was not quantified as the purpose of these initial experiments was to verify that this test method could yield measurable values of residual stress.

Figure 28 shows a stress and temperature plot vs time for the first test specimen. The drive arm was initially displaced 0.05mm, thereby stressing the specimen. This stress was allowed to decay to a near level value, due to relaxation of the specimen, at which time the specimen was exposed to a high intensity broad band UV source (i.e. EFOS Ultra Cure 100 machine) for 1 minute. This caused a noticeable jump in the stress level while the specimen was exposed, and a slowly rising stress level after the UV light source was shut off. The initial jump was believed to be due to additional chemical conversion resulting in shrinkage, which in turn would cause an additional amount of energy to be expended in keeping the pivot arms at a constant displacement. The slowly increasing stress levels, after the UV light was shut off, was believed to be due to dark reactions[16,17].

The temperature probe, which was located just beneath the specimen but not in contact with it, recorded a jump in temperature while the UV light was on but then returned to near its base line value when the UV light was shut off. This seemed reasonable as it would be expected that the probe would heat up as it absorbed UV light which had passed through the specimen, as well as the specimen generating some heat upon additional curing reactions occurring.

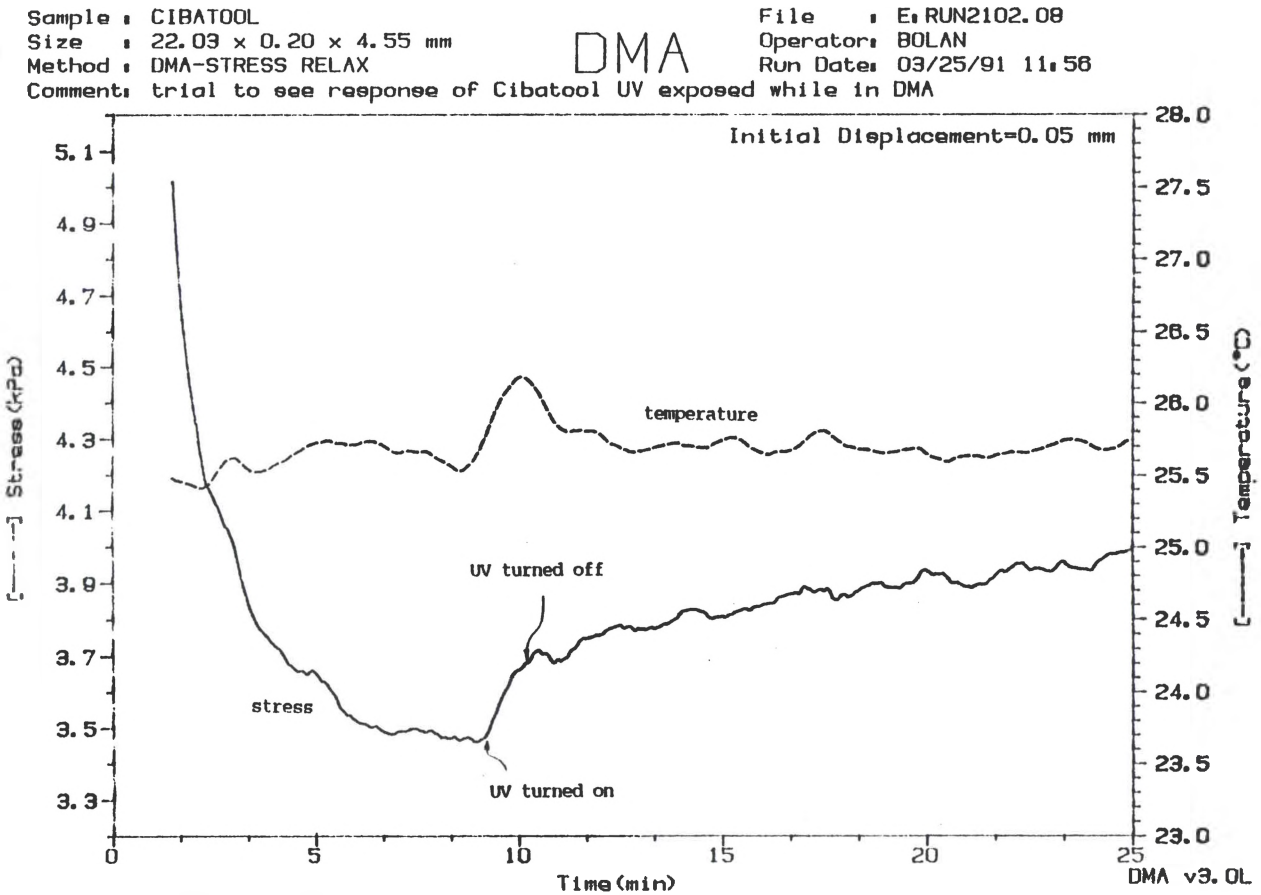

Figure 28. XB5081-1 Specimen Further Exposed to UV Energy While in the DMA.

Another experiment was conducted on a different specimen but this time it received two one minute UV exposures. A plot of stress vs time is shown in Figure 29. It is noticed that the stress vs time curve looks significantly different than that of Figure 28. In this figure the stress curve jumped down when the UV light was turned on and then jumped up slightly when the light was turned off, but then showed a stress state lower than that which was present before the light was turned on. In order to explain this difference it was necessary to examine further the inner workings of the DuPont DMA instrument.

Figure 30a shows the sample, the LVDT, the electromagnetic motor and the pivot arms in their zero position. When the stress relaxation experiments began, the DMA instrument allowed the specimen/pivot arm system to come to equilibrium for one minute prior to displacing the driven arm the preset level. Displacement to the right was positive while to the left it was negative (Figure 30b and 30c show exaggerated displacements).

With regards to Figure 29, the initial displacement was negative, corresponding to Figure 30c. When the UV light was turned on, it was believed that the specimen expanded which would tend to drive the driven arm to the left or more negative. Since the electromagnetic motor was expending energy to drive the system negative anyway, the expansion reduced the amount of energy required to maintain the initial displacement. This showed up as the downward jump in the stress level in the specimen. When the UV light was turned off, the specimen began to cool driving the driven arm in the positive direction, requiring more energy to maintain the initial displacement and hence the stress level increased but not back to the original level. This occurred in both instances that further exposed these specimen to UV light, during this experimental run.

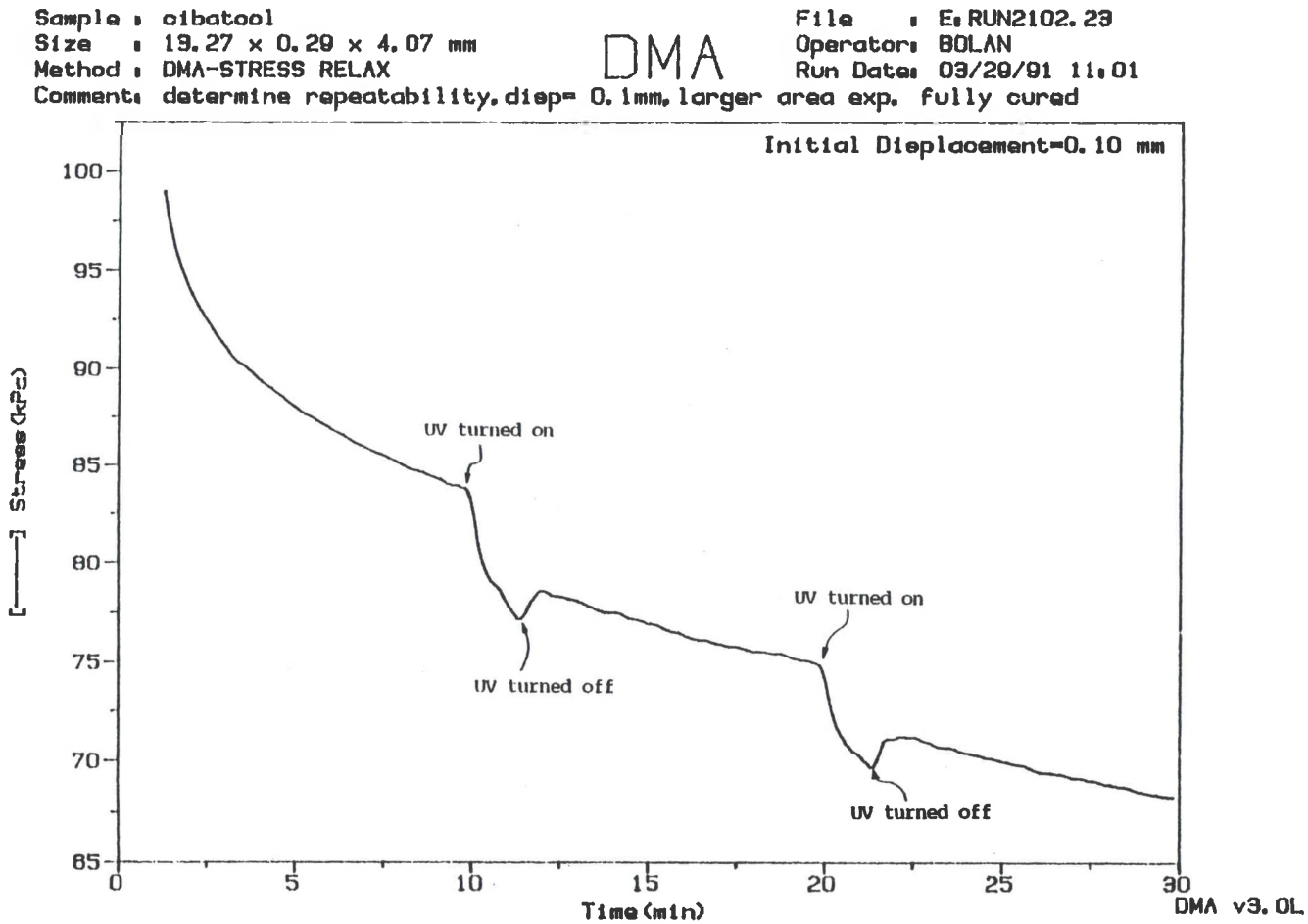

Figure 29. XB5081-1 Specimen Exposed to Additional UV Energy at Two Separate Times.

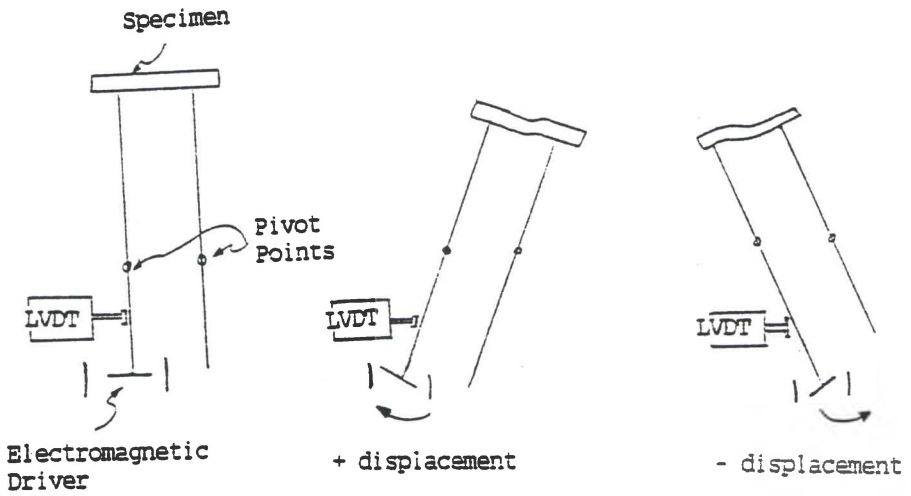

Figure 30. (a) Zero Strain or Null Position, (b) Positive Displacement, (c) Negative Displacement of DuPont 983 DMA Pivot Arms.

A previous experiment with a thin paper specimen confirmed that the initial drop and then increase in stress level could be explained at least in part, by the expansion of the test specimen. Figure 31 shows the plot of stress vs time for that paper specimen. The initial displacement of the arm was in the negative direction which meant that as the specimen expanded the energy required to maintain the initial displacement decreased, indicating less stress in the specimen. Upon shutting the UV light off, the specimen began to return to its normal size (i.e. shrink) and hence stress increased. The difference between Figures 29 and 31, is that in Figure 31 the specimen was non-reactive (i.e. no significant chemical reaction was occurring as the result of the UV light) and therefore it returned to its previous decaying stress level.

Figures 32 through 34, are plots of stress vs time, of the same specimen tested in Figure 29, further exposed to UV light. In all these tests the initial displacement was in the negative direction. In each case, the stress level jumped down when the UV light was turned on and then jumped up when the light was turned off. The level of stress at this point was lower than that which would have been expected if the specimen had not been further exposed to UV light but allowed to continue its stress relaxation uninterrupted. The jump down and then up in stress, corresponding to the UV light being turned on and off is readily explained by the expansion and cooling of the specimens and its consequent effect on the electromagnetic motor driving a pivot arm. The lower stress level, after the UV light had been turned off, is explained by the specimen conforming to the stress state exerted on it. That is the specimen, when exposed to the UV light, was permanently taking on the "s" shape caused by the displacement. This could be occurring through both additional polymerization and/or heating and cooling freezing in the shape. To support this it was found that the specimen that was repeatedly tested, when finally removed from the DMA instrument's thin film grips, remained in an "S" shape. Furthermore, a specimen

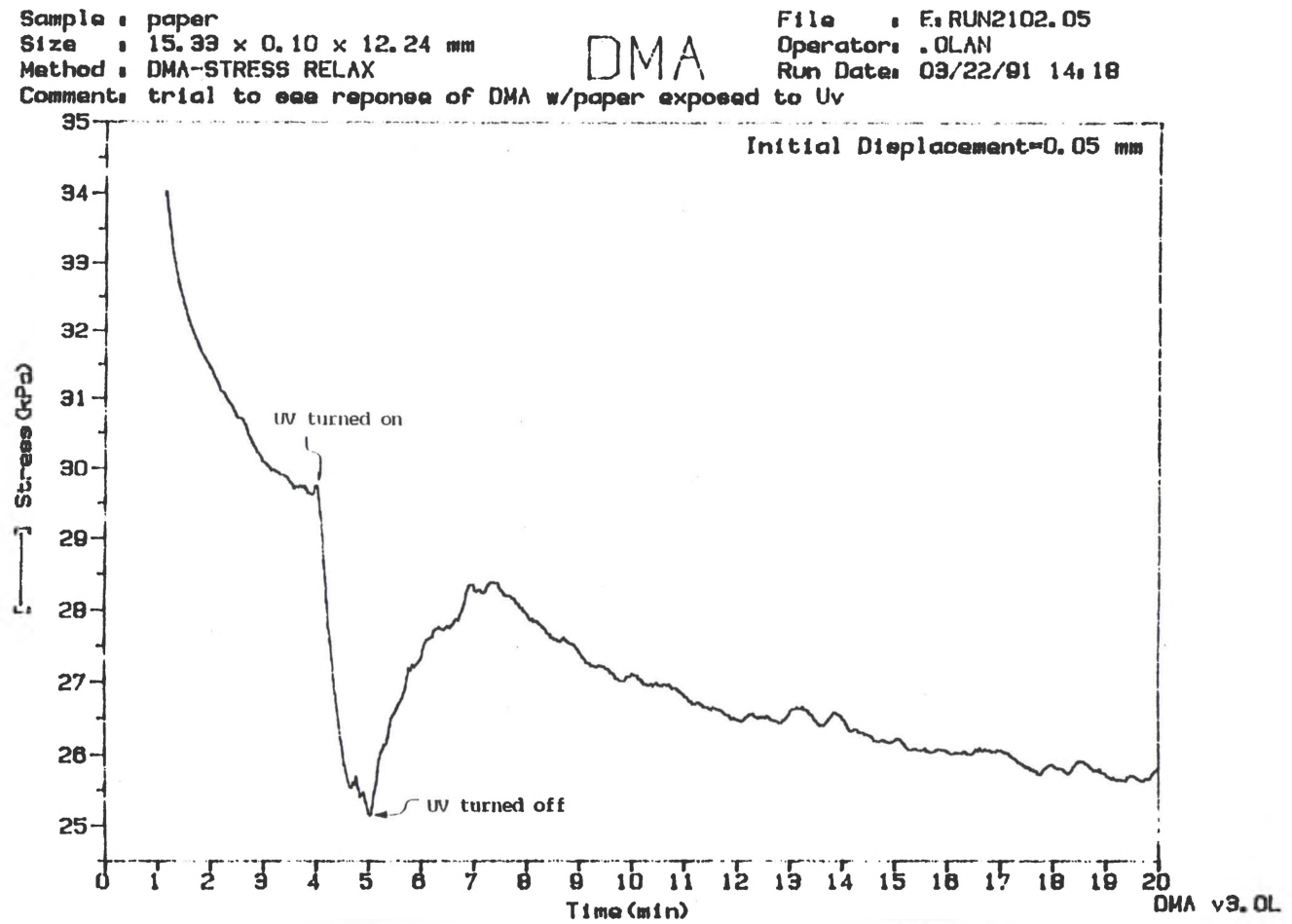

Figure 31. Response of DMA, with Paper in Grips, Exposed to UV.

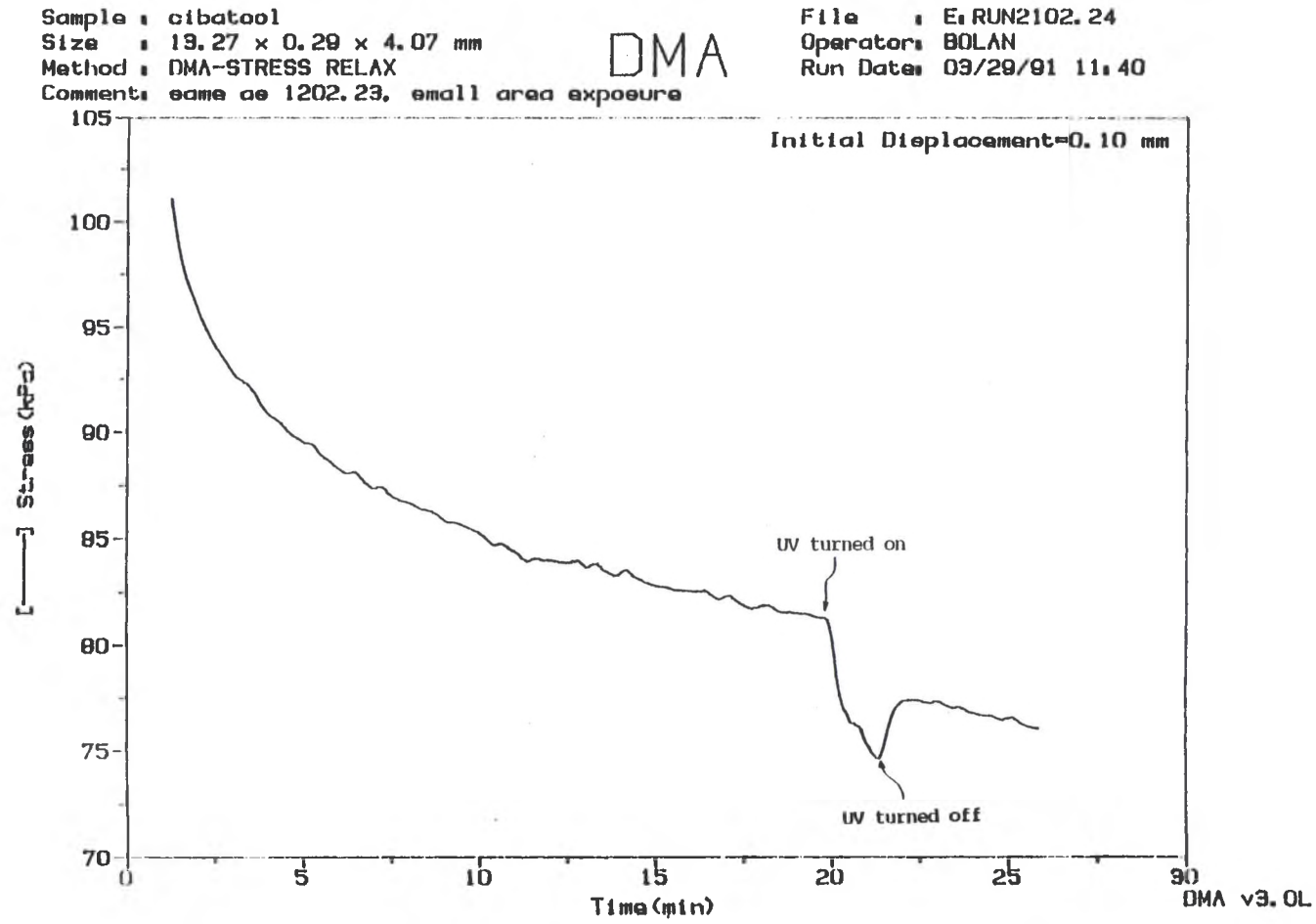

Figure 32. Same XB5081-1 Specimen Utilized in Fig. 29, Further Exposed to UV Energy.

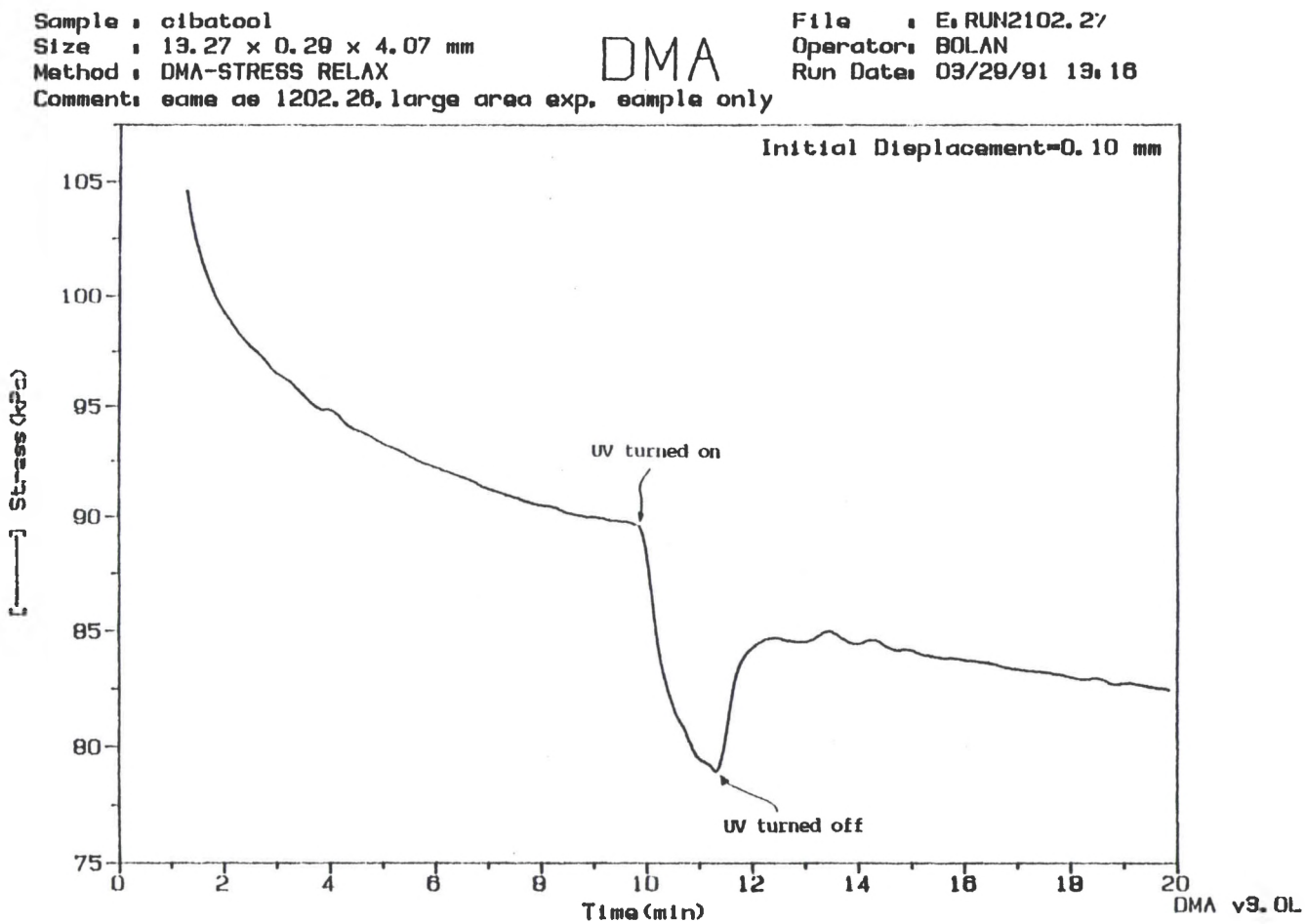

Figure 33. Same XB5081-1 Specimen Utilized in Fig. 32, Further Exposed to UV Energy.

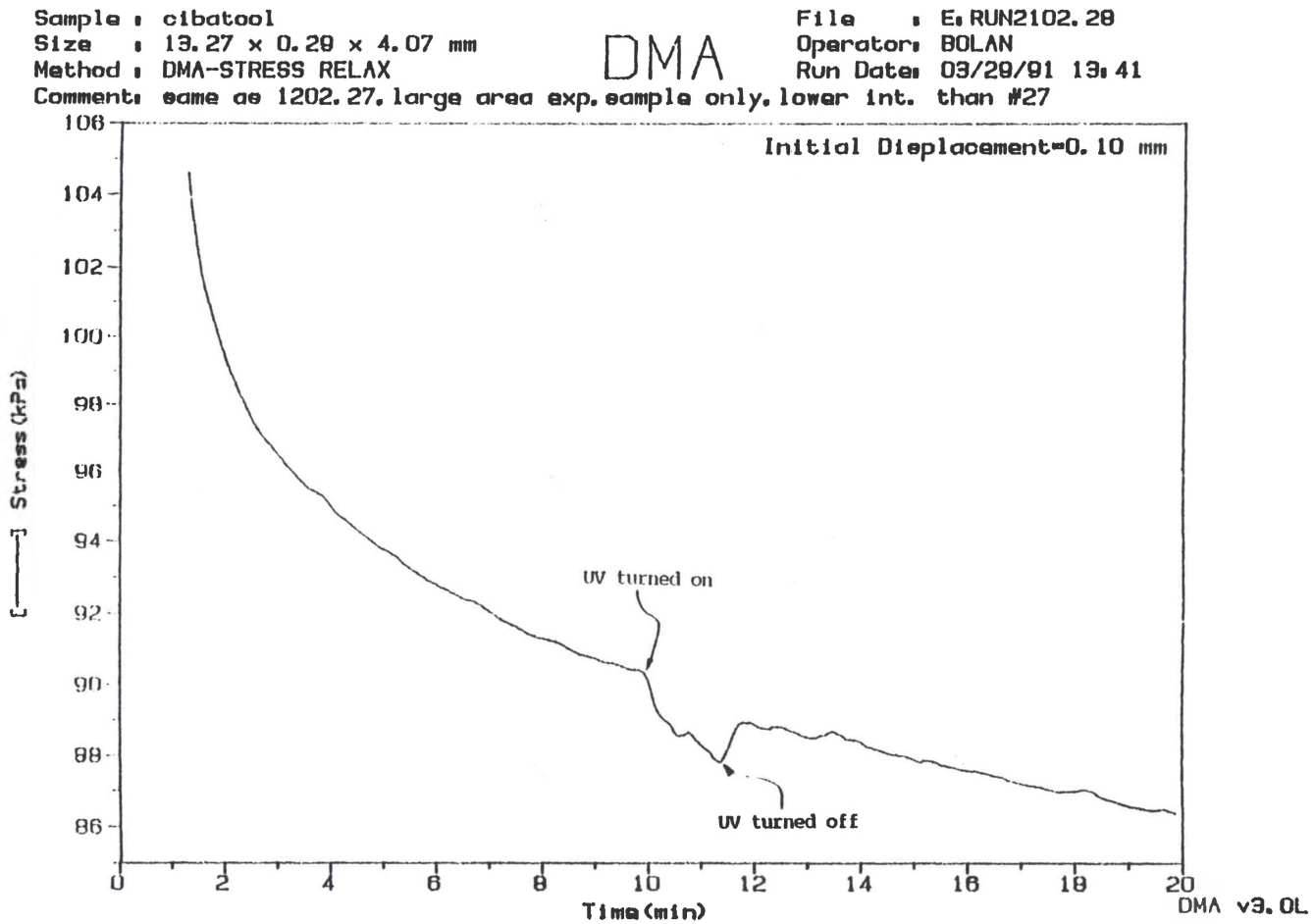

Figure 34. Same XB5081-1 Specimen Utilized in Fig. 33, Further Exposed to UV Energy.

which had been exposed to additional UV light only once while in the grips of the DMA instrument (see Figure 29, the first jump decrease) showed that a lower stress state was reached. It was therefore concluded that a realignment to the stress state was occurring and hence the use of the DMA Constant Strain technique was not a viable method of measuring residual stresses in these specimens.

CHAPTER IV

ANNEALING-STRAINING ANALYSIS

A. Summary and Chronology of Experimental Procedures

1. Making the specimens - use same UV light intensity for all specimens.

   i. Nine rectangular specimens approximately 30mm long by 4mm wide by 0.2mm thick.

      - 5 for stress analysis
      - 1 for percent cure determination via differential scanning calorimetry (DSC)
      - 1 for weight loss determination via thermogravimetric analysis (TGA)
      - 1 for unannealed T_g determination (DMA)
      - 1 for composition of volatiles lost during annealing via gas chromatograph/mass spectrometry (GC/MS)

2. Specimens removed from glass plates, cleaned with isopropyl alcohol, then edges are sanded.

3. Lengths of specimens measured with optical microscope.

4. One specimen tested in Rheometrics Solids Analyzer II for DMA determination of T_g.

5. Five specimens annealed at 3°C above previously determined T_g for approximately 3 minutes.

6. Specimen lengths remeasured. Differences between annealed and initial measurements converted to strain.

7. One specimen tested in DSC to determine percent cure both before and after annealing. Determines if dark reaction is significant.

8. One specimen tested in TGA for determination of percent weight loss during annealing cycle.

9. One specimen placed in GC/MS for determination of composition of volatiles lost.

10. Annealed specimens placed in thin film grips of Rheometrics Solids Analyzer II and strained to the level previously determined. Initial stress at this strain level is that which must have existed in specimen before annealing.

11. Repeat steps 1-10 for different resin formulations.

B. Introduction to the General Concept

The "Annealing-Straining Analysis" technique was the last attempt to measure values of residual stresses in parts created by the stereolithography process. This technique was based upon the fact that when a glassy material is heated above its glass transition temperature (i.e. annealed), any pre-existing residual stresses will be relieved. This is due to the material's molecular chains becoming mobile enough to realign themselves to a lower energy state, i.e. zero stress.

As a result of this molecular realignment the specimen shrinks in size. By measuring this amount of shrinkage, one can determine the strain that was initially present in the specimen before it was annealed. When the annealed specimen is subsequently pulled in tension an amount equal to this strain, the force required to accomplish this can be equated to the original stress present in the specimen. This is true as long as the strain is induced nearly instantaneously in the specimen, since with time the specimen will try to relax(deform) to a zero stress level by elongating.

C. Experimental Methods

The procedures utilized for making the rectangular specimens for this test method were identical to that followed for the "Constant Strain Analysis, Test Method 1". A rectangular shape of approximately 30mm by 4mm by 0.2mm was chosen for the specimens as this gave a large length to width ratio which minimized the Poisson's Ratio effect of shrinkage in the width direction changing the dimensions of the specimen in the length direction. The amount of exposure energy received by any of the specimens was 21.33 mJ/mm^2.

Once cleaned, each end of a specimen was broken at an angle so as to create a sharp edge which would be clearly visible through an optical microscope at 40X (see Figure 35). The points of the sharp edges became the references utilized in measuring the overall lengths of the specimens. This was accomplished with the equipment arrangement shown in Figure 36. The optical microscope was placed above a single axis micron steppable platform oriented such that the table moved parallel to one of the cross-hairs in the microscope lens. A specimen was placed on this platform in the field of view of the microscope and parallel to the direction of motion of the table. One pointed end of the specimen was then made to just touch the intersection of the cross-hairs in the microscope (see Figure 37). The platform was then moved in micron steps to the opposite pointed end with the driving motor recording the distance, in microns, travelled from the referenced (starting) pointed end. This distance was the total length of the specimen. This measurement was made for each specimen shortly after cleaning so as to preclude any annealing (which may be occurring at room temperature) from significantly affecting the data.

One rectangular specimen was tested in a Rheometrics Solid Analyzer II for DMA determination of its T_g. The basic operating principle behind this test[20] was that it subjects a specimen to a

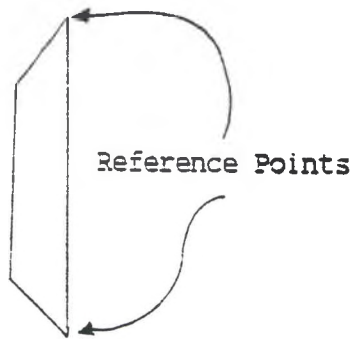

Figure 35. Drawing of a Specimen Showing Reference Points used for Measuring the Length of the Specimen.

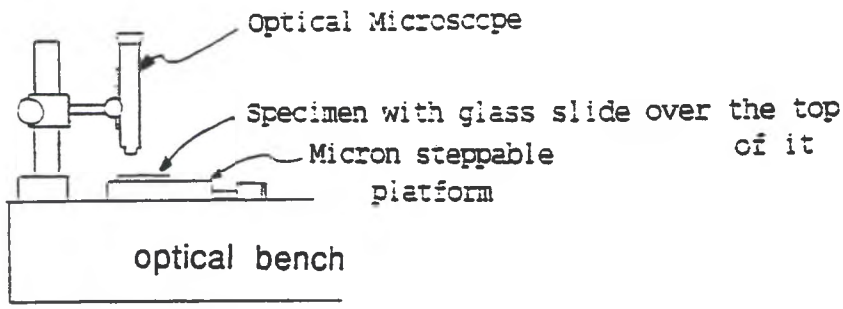

Figure 36. Physical Arrangement of Equipment to Measure the Length of the Specimens.

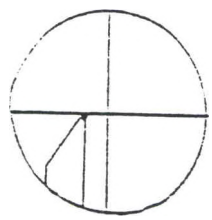

Figure 37. View Through a Microscope Objective Showing Alignment of Horizontal Cross-Hair with Reference Point of a Specimen.

slight amount of initial strain and then oscillates a small additional strain on the specimen (for this experiment, 10 grams) at one hertz. The analyzer then measured the specimen's viscoelastic stress response to this oscillatory strain. The material's viscous or out of phase component (loss modulus) and the elastic or in phase component (storage modulus) were measured by this method. The analyzer then used this data to calculate the ratio between the loss and storage modulus, which has been termed tan delta. A measurement of the in phase and out of phase components of the specimen was taken at 2°C steps (with a one minute hold at temperature to ensure the temperature of the specimen corresponded to that recorded) as the material was heated to 200°C.

Upon initially verifying that annealing did in fact reduce the length of a specimen, it became necessary to develop an annealing cycle which would minimize any volatiles being given off. Thermogravimetric Analysis (TGA) was utilized to quantify the weight loss which occurred during a given annealing cycle. The principle behind this instrument was simple. It merely weighed a sample initially, then placed it in a closed oven and heated at a programmed rate while recording the weight loss via a micro-balance.

It was then necessary to determine whether the observed shrinkage of the annealed specimen could be accounted for by the loss of a given component. A Gas Chromatograph/Mass Spectrometer (GC/MS) accomplished this by subjecting a sample to an annealing cycle. The heat vaporized some of the sample which then traveled through a capillary column in the GC where the gases were separated according to weight[21]. These separated gases were then sent to a MS. This instrument broke the volatiles up into ion fragments and then accelerated these fragments through a strong magnetic field. The difference in the charge to mass ratio of these fragments allowed the magnetic field to separate the different fragments from each other. The computer system of the MS then utilized this information to identify the composition of the original molecule, i.e. the machine

deduced the composition based upon the fact that each molecule fragments in a characteristic pattern.

All the specimens were then annealed according to the annealing cycle developed with the aid of a TGA instrument (see Figure 39 in the proceeding Results and Discussion section). The temperature/time profile was chosen so as to minimize the amount of volatiles lost during the annealing cycle, which could have had a significant effect on the amount of shrinkage attributed to relaxation of residual stresses. The final temperature reached in the oven corresponded to approximately 3°C above the measured T_g value of the respective specimens. After holding at this temperature for a short duration (approximately 2 minutes), the specimens were quickly cooled back to ambient temperature.

The specimen's lengths were then quickly remeasured with the optical microscope. The difference between this value and the initial value was converted to a strain. The Rheometrics Solid Analyzer II was then utilized, with thin film grips, to pull each of the specimens in tension the amount of previously determined strain. The force needed to do this was measured and attributed to the residual stress initially present in the specimen.

A DSC thermograph scan was conducted on an unannealed specimen to determine if any significant dark reaction[16,17] had occurred. A base line thermograph for each resin system was conducted at a heating rate of 40°C/min up to 180°C and then 5°C to near 300°C. This heating profile was followed to minimize the loss of vinyl pyrrolidinone, a reactive diluent, and the most likely component being volatilized based upon 3D Systems' Emission Data[22].

The principle of operation of the DSC instrument involved heating an empty reference cell at the programmed rate while the heat input of the sample pan was regulated to match the heating rate of the reference pan. The heating rate changed as the sample in the pan

experienced an exothermic reaction (less heat required) or an endothermic reaction (more heat required). For the DSC instrument employed, an exotherm was represented by an upward shift in the curve and an endotherm by a downward shift. It should be noted that the use of DSC for determination of T_g was not possible with the materials being studied, as the exothermic dark reaction tended to distort the base line values.

TABLE I

XB5081-1
Stain and Stress Measurements

Specimen	initial length (mm)	length after 14hrs (mm)	length after annealing (mm)	change in length (mm)	percent change in strain	stress psi	stress MPa
1	27.222	27.220	27.114	0.078	0.287	530.12	3.65
2	27.971	not measured	27.902	0.069	0.247	584.69	4.03
3	28.501	28.499	28.447	0.052	0.183	402.60	2.77
4	26.489	not measured	26.427	0.062	0.234	540.45	3.73
5	27.879	27.880	27.800	0.800	0.287	624.72	4.31
Average					0.264	570.00	3.93

Table Ia

Specimen	length (mm)*	width (mm)	thickness (mm)
1	13.01	4.93	0.146
2	13.01	4.93	0.139
3	13.01	4.75	0.164
4	13.01	4.68	0.175
5	13.01	5.30	0.141

*Note: length corresponds to the distance between grips of the instrument

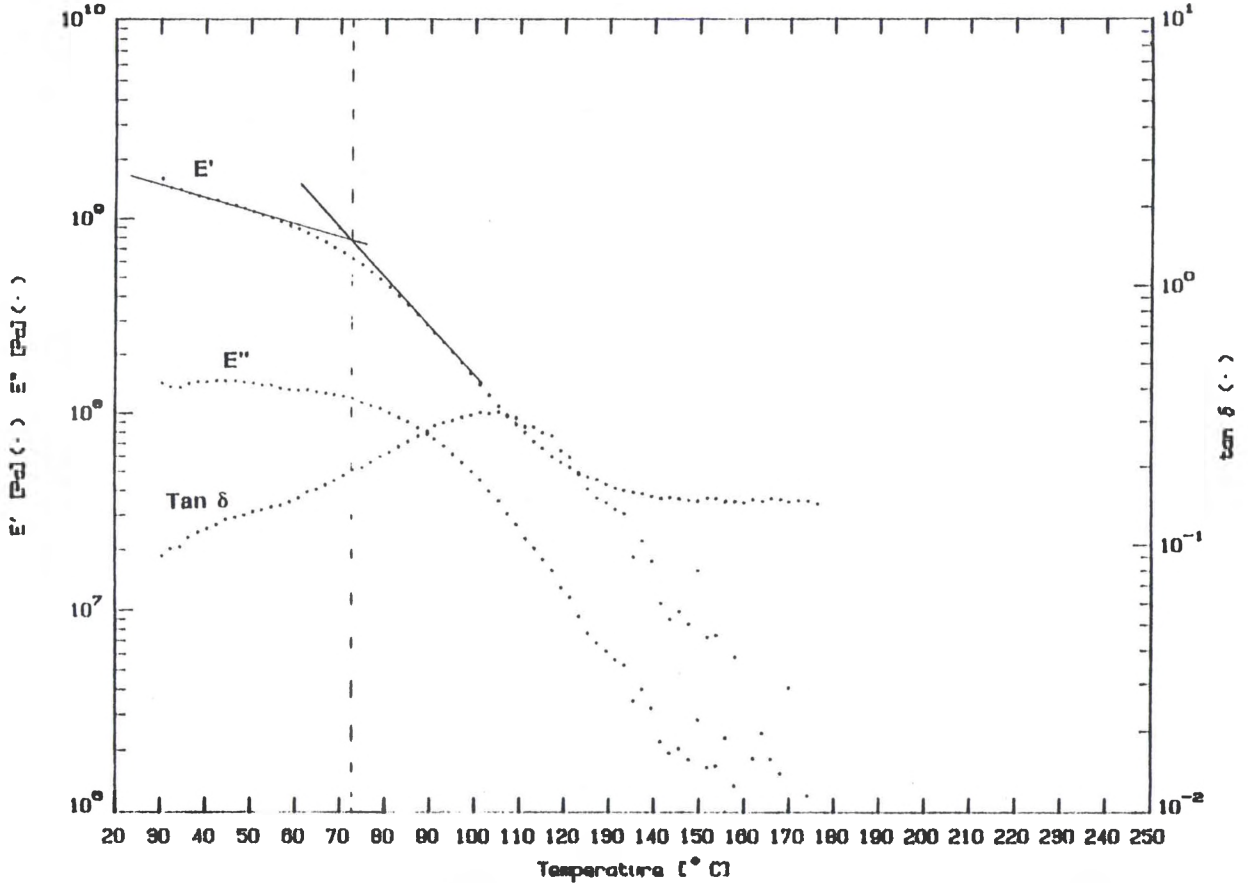

Figure 38. DMA Plot of Storage Modulus (E'), Loss Modulus (E"), and Tan Delta (δ) Versus Temperature for a XB5081-1 Specimen.

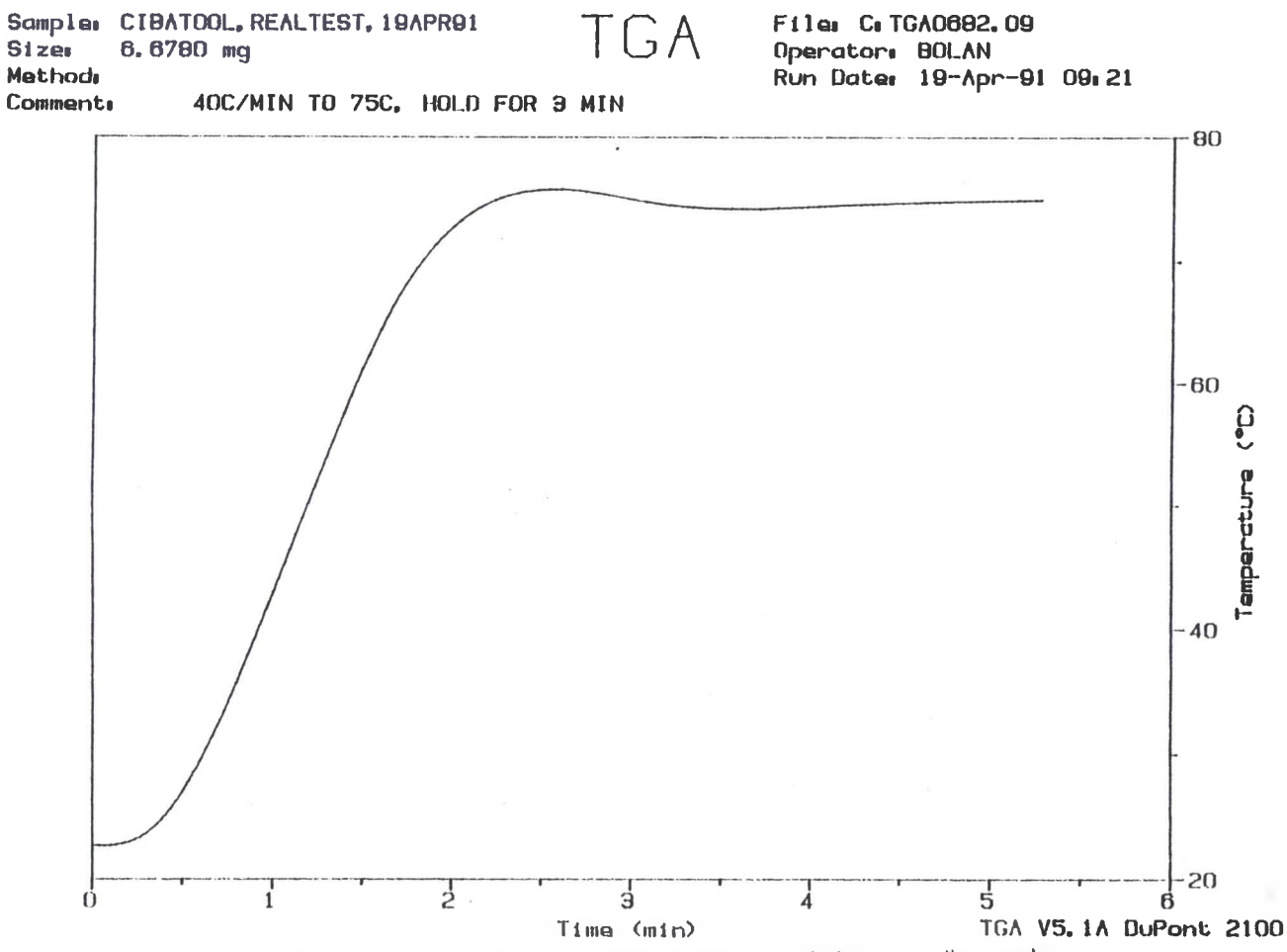

Figure 39. Temperature profile of TGA instrument during annealing cycle

diluent/crosslinking agent, which could reduce the volume of the specimen, could result in a further shrinkage of the specimen. This would have caused higher residual stresses to be measured due to the fact that the specimen would have to be strained a greater amount. The specimen was then held at 3°C above T_g for approximately 2 minutes for annealing (shrinking due to alignment of molecules to the stress field) to occur and then quickly returned to room temperature. It was found that a specimen would loose 1.5 to 2.0 % by weight (Figure 40) due to the volatilizing of components in the specimen.

A GC/MS was then employed to determine the composition of the gas being volatilized from the specimen during the annealing process. A specimen was placed in the programmable oven of the GC/MS and heated according to the temperature versus time profile developed for the annealing cycle. The vapors emitted from the specimen were analyzed by the GC/MS for their composition. The results are shown in Figure 41. As previously mentioned, this was only a qualitative test, and as such it could only determine relative amounts of each substance present. Based upon the 3D Systems Data[22], vinyl pyrrolidinone was specifically searched for with the results being that no detectable amounts of vinyl pyrrolidinone were being volatilized from the specimen (Figure 41). The two most significant components detected were water and isopropyl alcohol (the solution used to initially clean the specimens). The ratio of these two components, obtained from an analysis of the relative areas under the peaks, of five to one suggests that the bulk of the material being volatilized was water. Since water is a relatively small molecule, it was assumed at this point that its loss from the cured specimen would not account for any large amount of dimensional change.

A DSC thermograph scan was conducted on an unannealed specimen to determine if any significant dark reaction (i.e. additional curing) had occurred which might have changed the dimensions of the specimen and its modulus. Any large change in modulus would cause

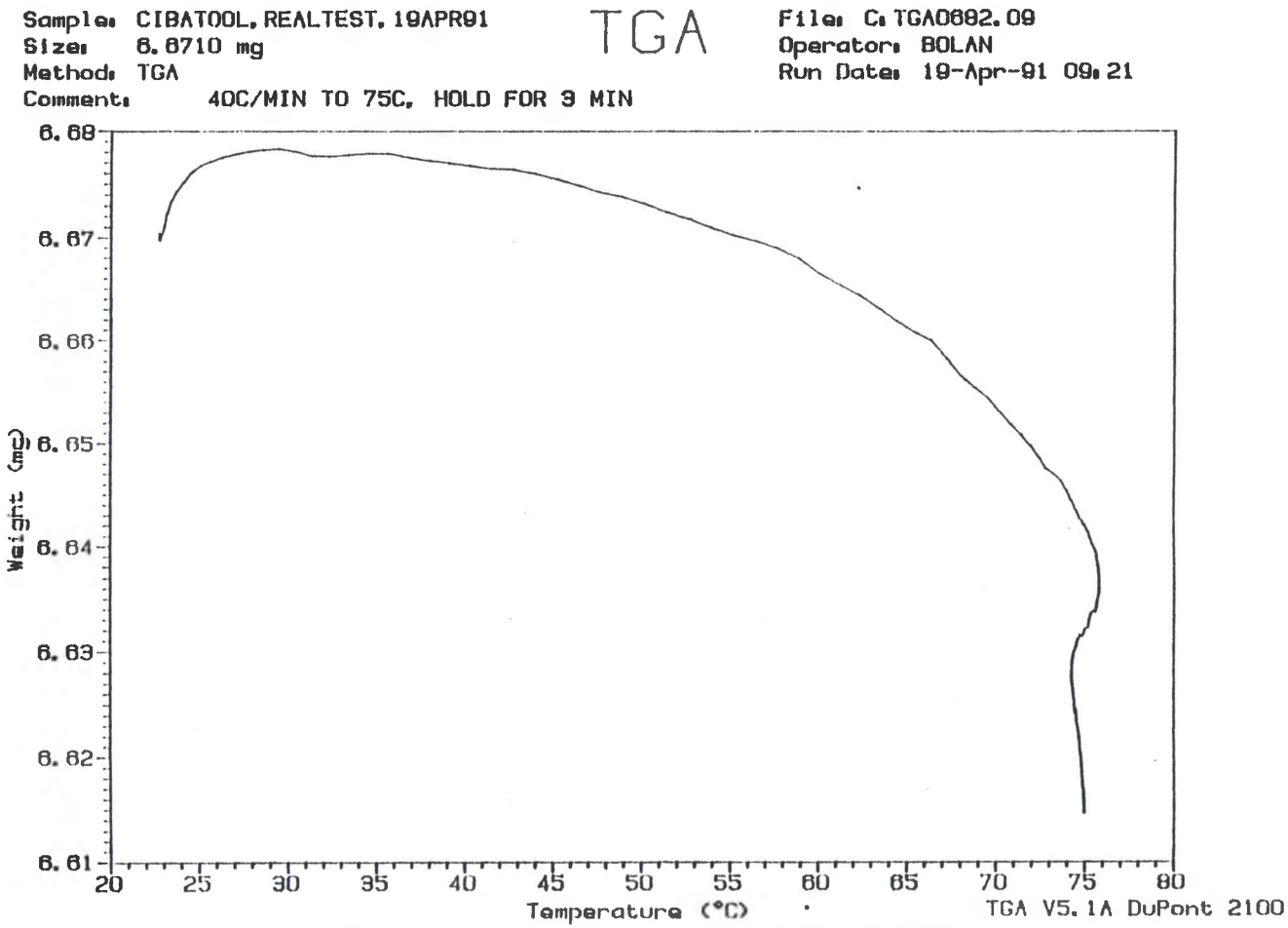

Figure 40. Weight loss occuring while annealing an XB5081-1 specimen

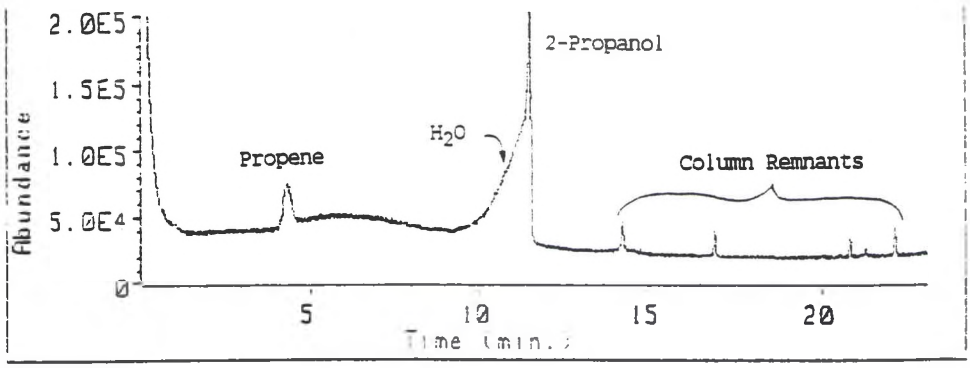

Figure 41. GC scan, with a MS Identification of Gases Emitted from an XB5081-1 Specimen Subjected to an Annealing Cycle.

the value of stress, obtained by straining the specimen after annealing, to be significantly higher than what was present, as the Rheometrics Solids Analyzer II instrument would have had to exert a larger force to strain the specimen. In order for the percent of cure due to dark reaction to be quantified, it was first necessary to determine a base line value of total heat evolved as a result of curing. The same ramp rate as was used for the annealing cycle was employed (i.e. 40°C/min) on a unreacted liquid specimen up to 180°C then 5°C/min up to 300°C. This minimized the loss of VP which could have had the effect of reducing the number of bonds available for reaction (i.e. crosslinking) thereby reducing the amount of energy released as heat. This could have decreased the base line value and hence resulted in an increase in the percentage of dark reaction occurring. The transition temperature of 180°C to go to the 5°C/min ramp rate was based upon earlier work conducted by Weissman[23], which showed thermal curing began around 200°C at a 10°C/min heat up rate.

A plot of heat flow (W/g) vs temperature can be seen in Figure 42. The jump in the curve at 180°C was due to the change in heating rate, establishing a new base line. The large increase in energy released beginning at approximately 210°C was due to polymerization occurring. This continued up till about 280°C at which time the energy released began to drop off to a new base line value. A sigmoidal curve was drawn by the analyzing computer to account for this shift in base line values. The area under the curve bounded by this sigmoidal curve represents the amount of energy released through polymerization. The value obtained was divided by the mass of the sample to yield a value of 246.2 J/g, which represents the amount of energy released as heat for the complete (assumed) polymerization of 1 gram of the material.

To quantify the extent of the dark reaction, which could have occurred as a result of the annealing, a DSC thermograph scan was

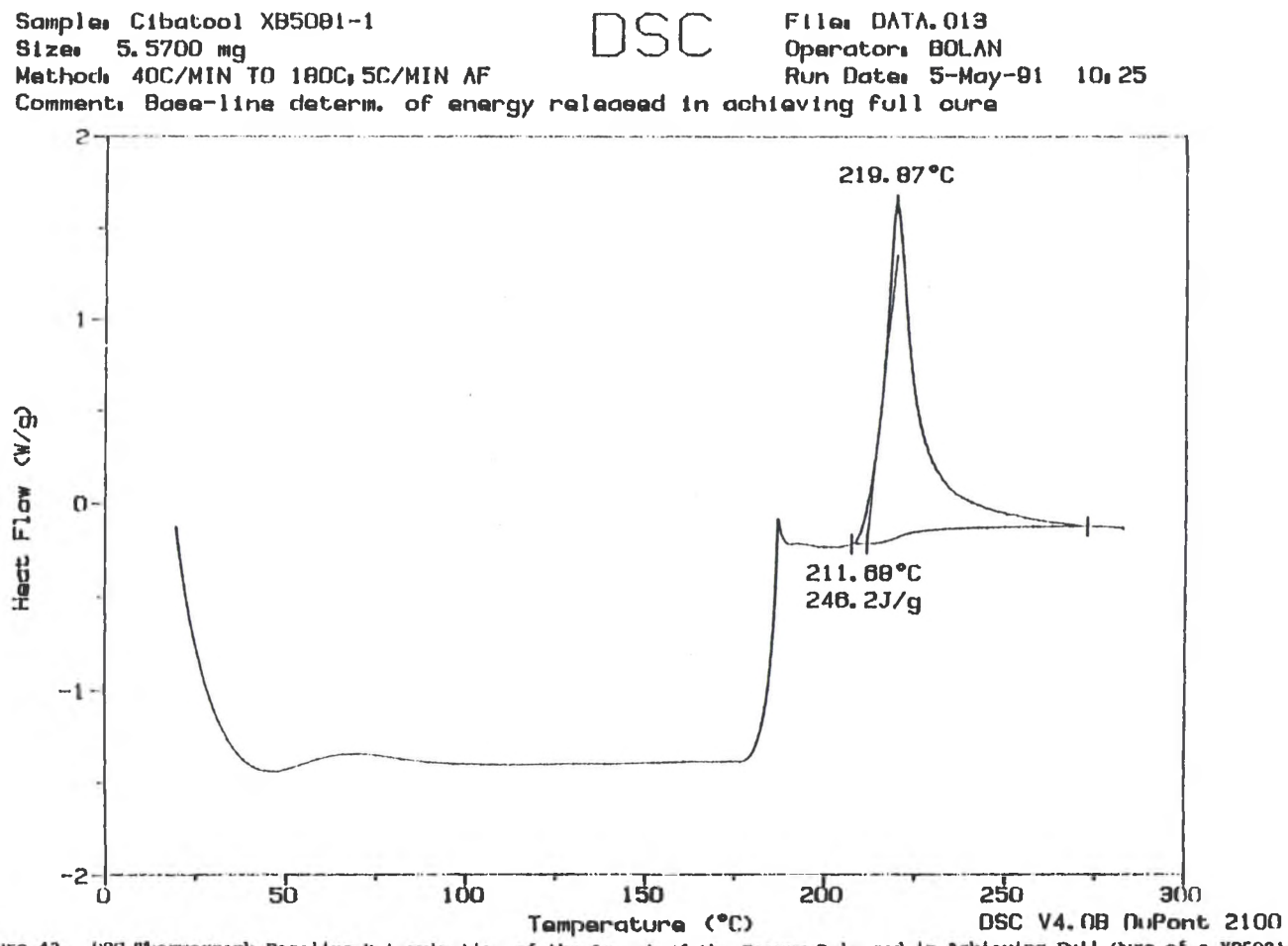

Figure 42. DSC Thermograph Baseline Determination of the Amount of the Energy Released in Achieving Full Cure of a XB5081-1 Resin System. Dual Heating Rate of 40°C/min to 180°C, and then 5°C/min to Full Cure.

conducted on an unannealed sample (Figure 43). A slower temperature ramp of 5°C/min versus 40°C/min, was utilized to ensure sufficient time was allotted for the process of annealing to occur and at the same time preclude over shooting the data. Taking the area under the curve bounded by the line drawn from 56°C to 100°C, yielded a value of 4.534J/g of energy released around the glass transition temperature of the sample (i.e 69°C). It was assumed that this value represented the energy released during the annealing of a sample. Because the DSC base line was changing in this temperature range, the value obtained should represent an overestimation of the energy released. Dividing the 4.534 J/g value by the value for the energy released for a fully cured sample, the amount of additional polymerization attributable to dark reaction (i.e. annealing) becomes about 1.8%. Being even more conservative by using the base line determination of energy released for a fully cured sample based upon a 5°C/min ramp rate (see Figure 44, 213.8 J/g), the percentage of dark reaction still was only about 2.1%. It was assumed that this additional amount of curing would have only a small impact on the results of determining residual stress via a modulus change and a dimensional change (i.e. chemical conversion causing shrinkage).

Quantifying the amount of cure of the specimen involved using the value obtained for the energy released during the DSC scan of the unannealed specimen and dividing this number by the total energy released in obtaining a fully cured state. The total energy released by the unannealed specimen was that obtained after about 200°C (61.71J/g) coupled with the 4.534 J/g estimated for the dark reaction, for a total of 66.24J/g. Dividing this figure by 246.2J/g, yields the value of 26.9 percent of uncured material in the specimen. Therefore the specimen was 73.1 percent cured. If no significant dark reaction was occurring, the specimen would have be approximately 75 percent cured.

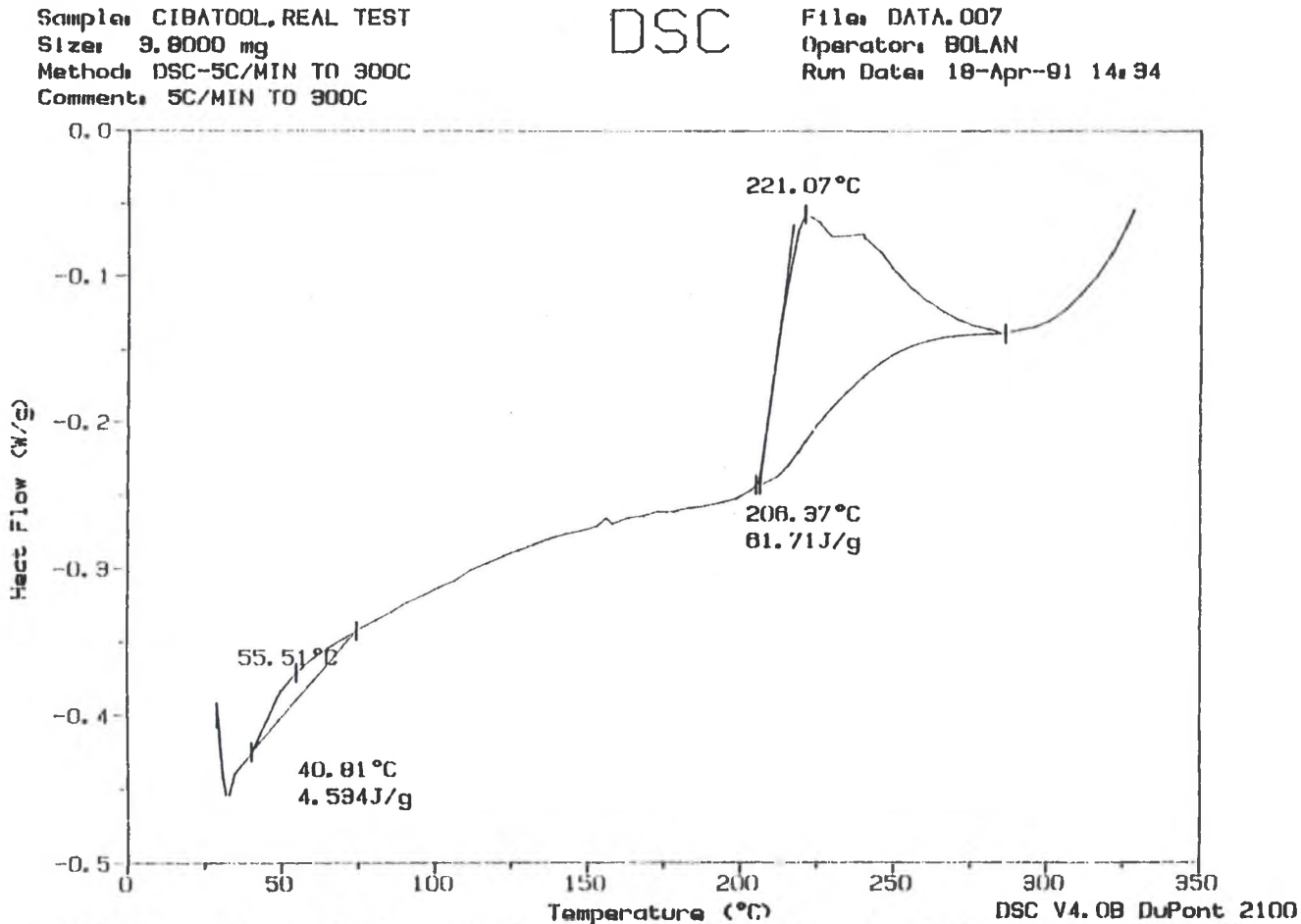

Figure 43. DSC Thermograph Scan of an Unannealed XB5081-1 Specimen, Shows Possible Release of Energy Around Previously Determined T_g.

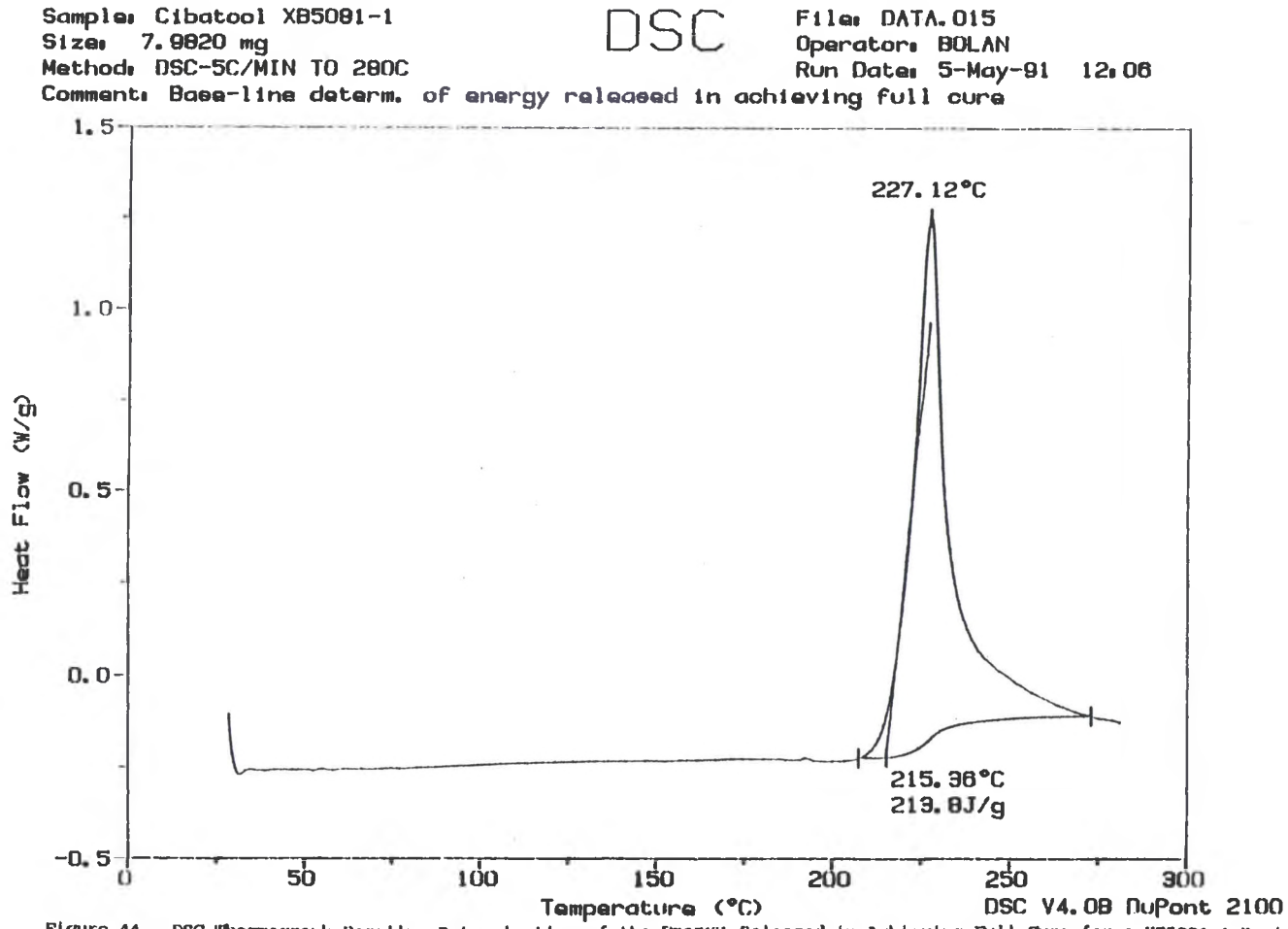

Figure 44. DSC Thermograph Baseline Determination of the Energy Released in Achieving Full Cure for a XB5081-1 Resin System with a Heating Rate of 5°C/min.

Determining the residual stresses present, as previously stated, involved the use of a RSA II operated in a step strain mode. This essentially equated to a stress relaxation test in which the instrument tried to pull the specimen the preset amount of strain while monitoring force and time. A specimen, previously measured for thickness and width, was placed in the instrument's thin film grips. The instrument was adjusted to a zero force/zero strain state at which time the distance between the grips was measured. This became the length of the specimen. Because of the previously mentioned machine compliance problem, the preset strain level was not reached immediately. This was a result of the specimen exerting a force on the grips, which tended to decrease the strain level achieved. Therefore, the task became a trial and error process of inputting a preset strain level into the computer and then observing if the initial strain exerted on the specimen matched the desired strain level. This desired level of strain needed to be reached quickly to preclude the specimen from relaxing. It was found through experimentation that the earliest time at which the RSA II became stable was 0.3125 seconds. It was believed that no significant relaxation was occurring during this time period. The summarized results can be found in Table I. The average value of 570.2 psi (3.93 MPa) of residual stress compares well with the magnitude of residual stress values obtained by Shimbo et al[24] on some thermally cured epoxy (i.e. 2.93 - 6.46 MPa) samples as well as by Kamarchik and Jurczak[25] on some UV cured polyesters (i.e. 2 - 4 MPa). The residual stress present equated to 12.5% of the green material's (i.e. resin which has only undergone laser curing) ultimate tensile strength (i.e. approximately 4550 psi[26]) and about 5% of the fully cured material's ultimate tensile strength (i.e. approximately 11600 psi[26]).

2. XB5081-1 Resin Modified with CTBN

As with the XB5081-1 formulation, five specimens of XB5081-1 with 10.81 pph CTBN were tested for residual stress in the manner outlined in the Experimental Methods Section. The summarized results can be found in Table II and Table IIa.

The glass transition temperature was determined in the identical manner as was done for the XB5081-1. The T_g thus obtained was 66°C (see Figure 45) which was 6°C lower than that for XB5081-1. This lower T_g was not unexpected as it has been demonstrated that the addition of a rubber modifier to an epoxy based resin often reduces the resin's glass transition value as well as its modulus.

A TGA was also conducted on a CTBN modified specimen with an annealing cycle similar to that for the XB5081-1. This annealing cycle had a 40°C/min ramp rate to 3°C above the T_g (i.e. 69°C) of the specimen. The weight loss which occurred during the annealing cycle was similar to that obtained for the unmodified XB5081-1 resin. This was not unexpected as CTBN is a relatively high molecular weight component which does not easily vaporize at low temperatures. Since there was no significant difference in weight loss, a GC/MS analysis was not conducted on a CTBN modified specimen. It was assumed that the composition of the volatiles being emitted from the rubber modified specimen would have yielded similar results as for the pure resin system, i.e. water was the major component being volatilized.

A DSC thermograph scan was conducted on an unannealed specimen to determine the percentage of dark reaction which occurred as a result of the annealing process. Again, as was the case for the pure XB5081-1 resin system, a base line needed to be determined. This was accomplished with a dual heating rate (i.e. 40°C/min up to 180°C the 5°C/min up to 280°C) and employing the same analysis techniques as

TABLE II

XB5081-1 with 10.81 pph CTBN
Stain and Stress Measurements

Specimen	initial length (mm)	length after 19hrs (mm)	length after annealing (mm)	change in length (mm)	percent change in strain	stress psi	stress MPa
1	30.607	30.607	30.536	0.071	0.232	525.76	3.62
2	28.782	not measured	28.718	0.064	0.222	490.52	3.38
3	30.490	30.491	30.424	0.066	0.217	475.43	3.28
4	31.085	not measured	31.013	0.072	0.232	511.35	3.53
5	23.748	not measured	23.696	0.052	0.219	510.97	3.52
Average					0.224	502.81	3.47

Table IIa

Specimen	length (mm)*	width (mm)	thickness (mm)
1	14.53	3.59	0.195
2	14.53	3.59	0.206
3	14.53	3.80	0.195
4	14.53	3.64	0.229
5	14.53	3.97	0.136

*Note: length corresponds to the distance between grips of the instrument

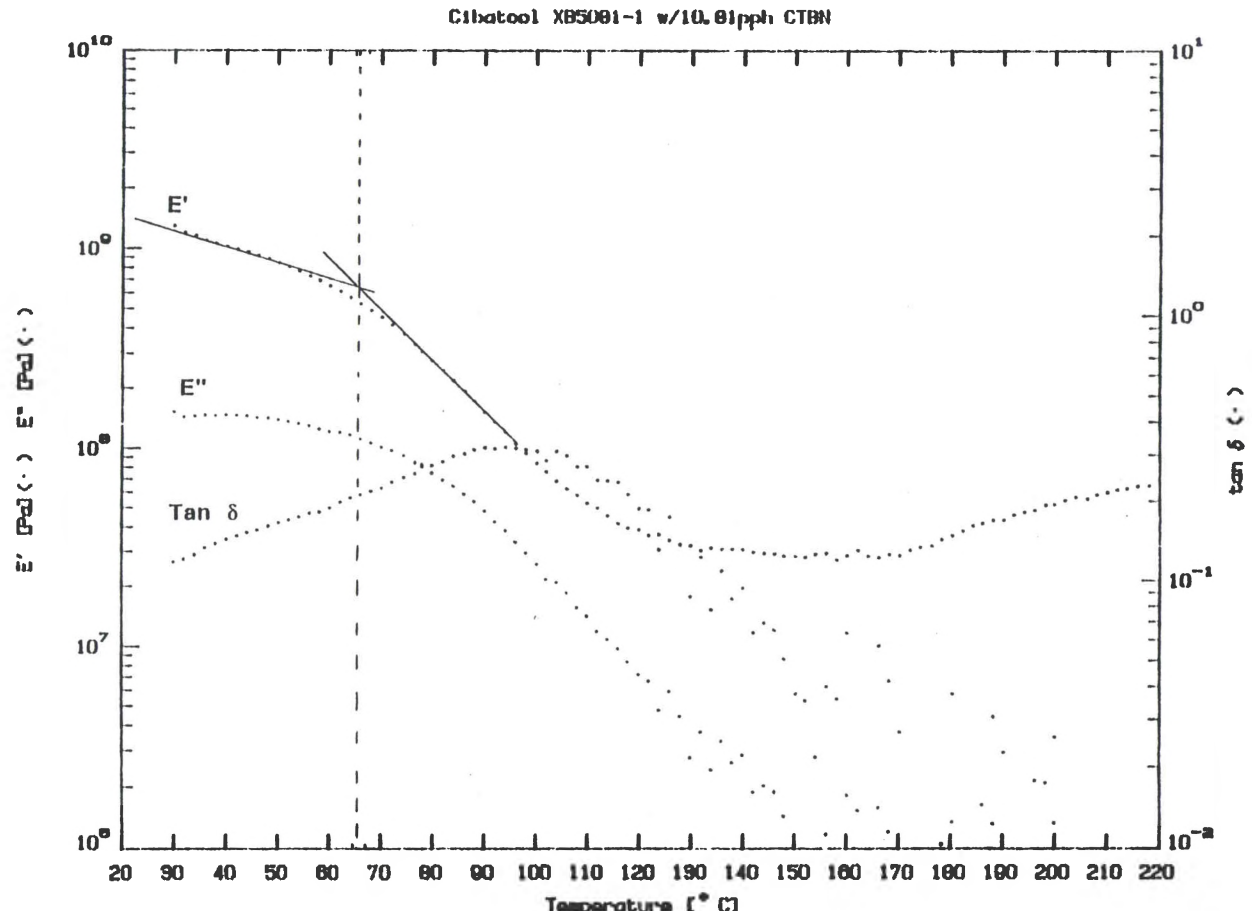

Figure 45. DMA Plot of Storage Modulus (E'), Loss Modulus (E"), and Tan Delta (δ) Versus Temperature for a XB5081-1 Resin Modified with 10.81 pph CTBN.

was utilized for the XB5081-1 specimen. The plot of Figure 46 yielded a base line value of 197.8 J/g for the complete polymerization of the sample. From Figure 47, again also taking the same approach as for the pure XB5081-1 resin system, the amount of energy released around the T_g was about 5 J/g. Therefore the percentage of additional polymerization occurring as the direct result of annealing equated to around two percent. As before, this was assumed to have only a small impact on the values obtained for residual stress.

Following the same procedure as for the XB5081-1 specimens, the percentage of cure of the CTBN modified specimens was found to be approximately 65 percent accounting for the dark reaction, and 67 percent assuming no significant dark reaction.

Determining the residual stresses present involved the same process as was utilized for the XB5081-1 specimens. The average value of 502.81 psi (3.47 MPa) of residual stress (see Table II), was 67.19 psi (0.46MPa) lower than that obtained for the pure XB5081-1 resin. This shows that an addition of approximately ten percent by weight of a rubber modifier can decrease the amount of residual stress present by about 12 percent. This still leaves several questions unanswered prior to actually using this modified resin system in product development. These include; what effect does the modifier have on the viscosity of the resin and how does this impact on the part building process? Obviously the rubber addition will increase viscosity, but at which point does this increase significantly impact on part building time and quality of the part? Another question pertains to the hardened material's impact properties, i.e. will they be significantly enhanced by the rubber addition? If the rubber phase separated during the curing process a significant increase in impact resistance may be noticed. At a minimum an increase in impact resistance is expected through the CTBN either plasticizing the matrix or increasing the distance between

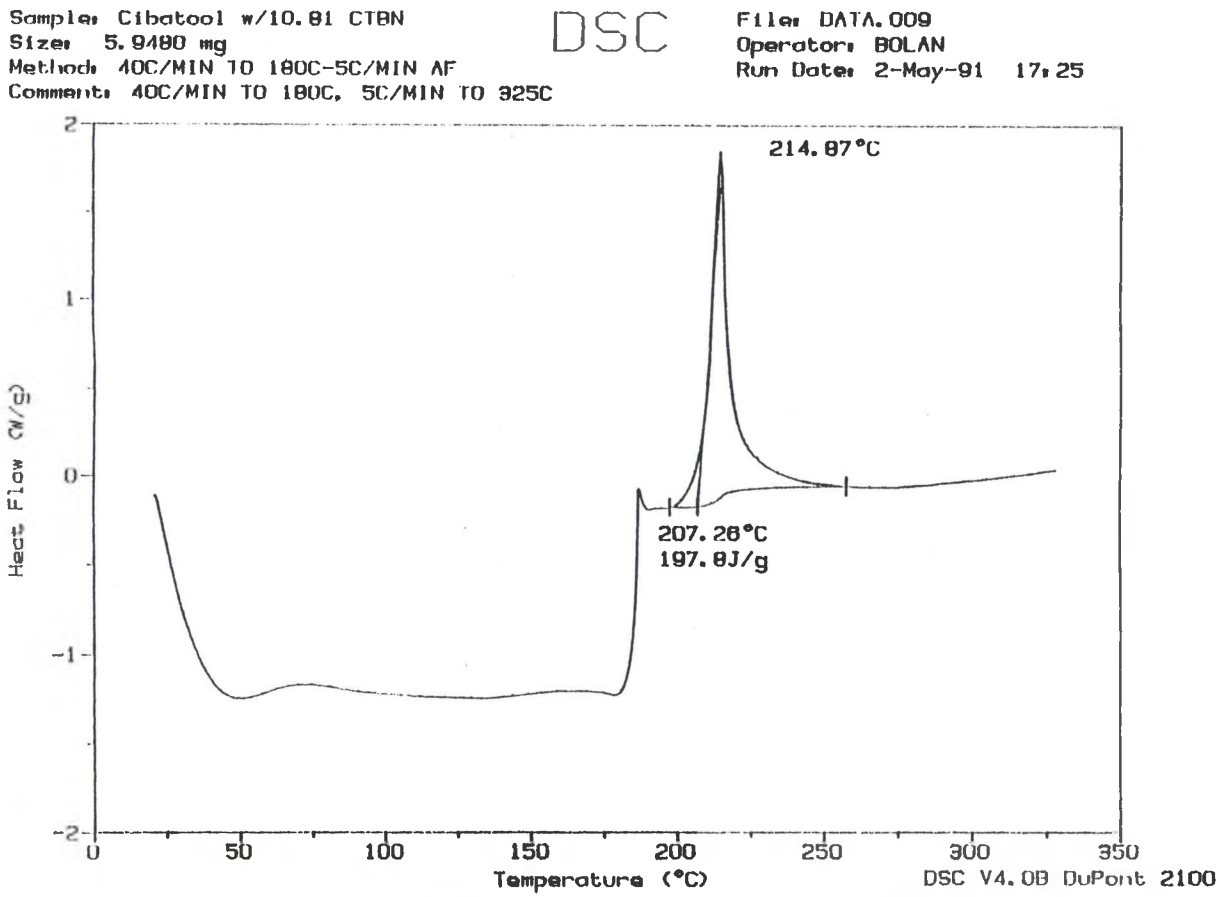

Figure 46. DSC Baseline Determination of the Energy Released in Achieving Full Cure for a XB5081-1 Resin Modified with 10.81 pph CTBN. Dual Heating Rate of 40°C/min to 180°C, and then 5°C/min to Full Cure.

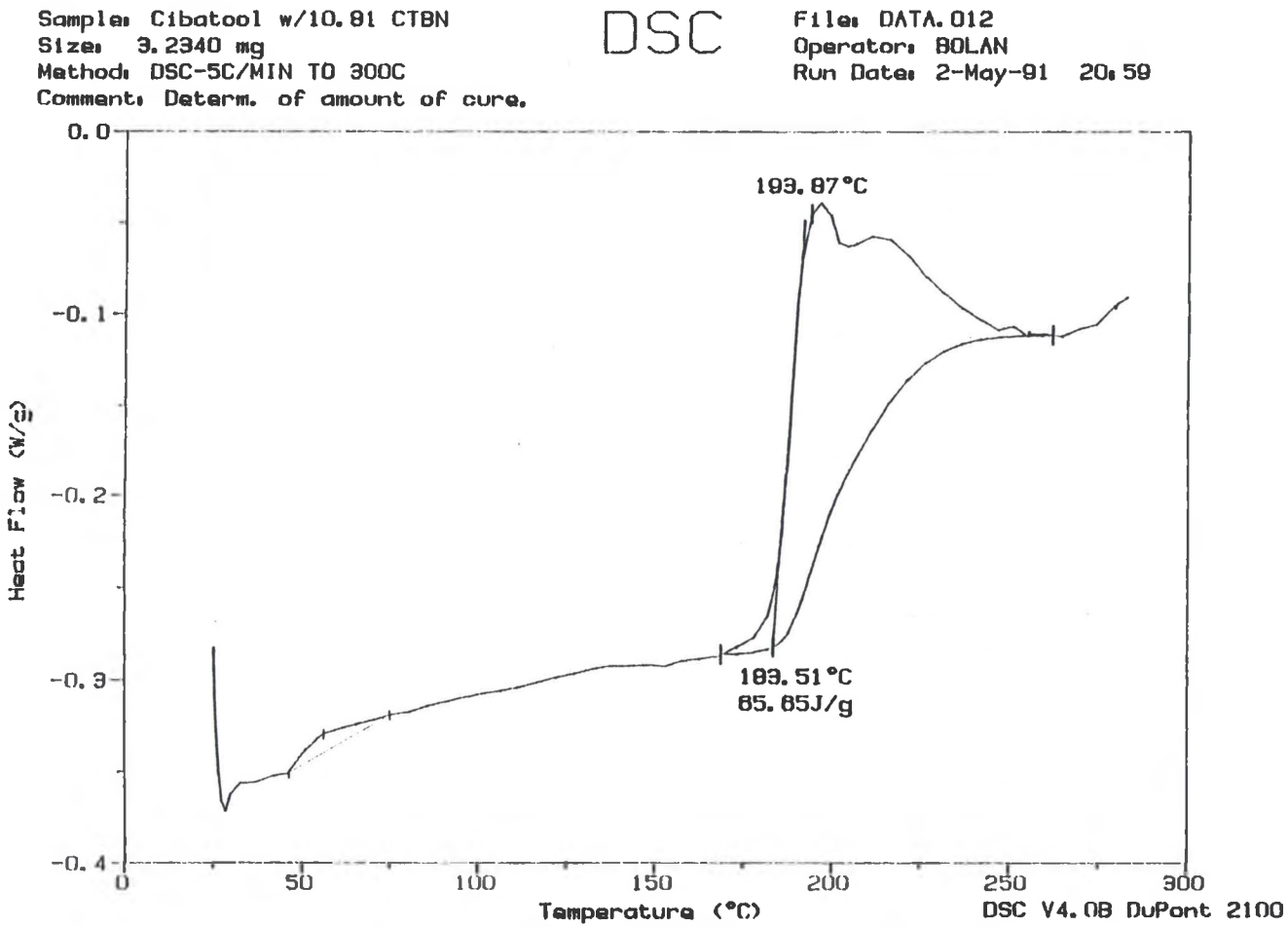

Figure 47. DSC Scan of an Unannealed CTBN Modified XB5081-1 Specimen. Shows Possible Release of Energy Around Previously Determined T_g.

molecular crosslinks (i.e. reducing the crosslink density of the resin and hence increasing the material's ability to react to an applied stress field).

The microstructure of the CTBN modified XB5081-1 resin was investigated to determine if this could account for the change in residual stress levels. Specifically, what was investigated was if the CTBN had phase separated during the rapid polymerization. The uncured liquid resin was examined with an optical microscope at high magnification (i.e. 400X to 1000X) and showed that the system was single phase at this magnification. Cured specimens were exposed to a solution containing 1 percent, by weight, of osmium tetroxide in tetrahydrofuran (THF) for 10 and 20 minute durations. This technique, originally developed by Riew and Smith[27], used the osmium tetroxide containing solution as a stain to find areas which had some chemical reactivity remaining (i.e unsaturation sites). Since CTBN possible has carbon-carbon double bonds remaining after laser polymerization, due to steric hinderence prohibiting crosslinking, it was hoped that if second phase rubbery particles were present in the cured system that the osmium tetroxide solution would make these areas visible to SEM analysis.

Low magnification photographs of both CTBN modified specimens and pure XB5081-1 specimens (as a standard), can be seen in Figures 48 through 51. In these photographs it can be seen that dark edges existed on all the specimens. This can be explained with the idea that the clear areas correspond to that part of the resin which the UV laser energy directly impinged upon, and the dark areas the part of the resin that was exposed to UV energy via the cured material acting as a light guide. The dark edges therefore received a lesser amount of UV energy, were less cured than the clear areas, and consequently more susceptible to staining due to the availability of more unsaturation sites. To support this, the width of the clear area, as defined by the area between the straight lines denoted by

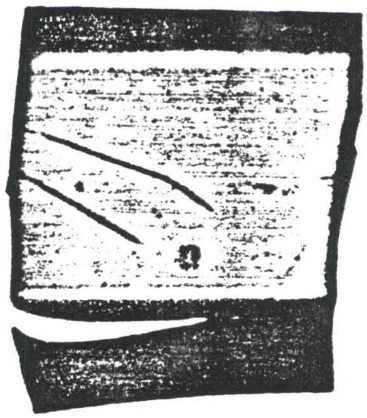

Figure 48. Low Magnification of CTBN Modified XB5081-1 Specimen Stained for 10 Minutes in an OsO_4/THF Solution, 13.5X.

Figure 49. Low Magnification of CTBN Modified XB5081-1 Specimen Stained for 20 Minutes in an OsO_4/THF Solution, 13.5X.

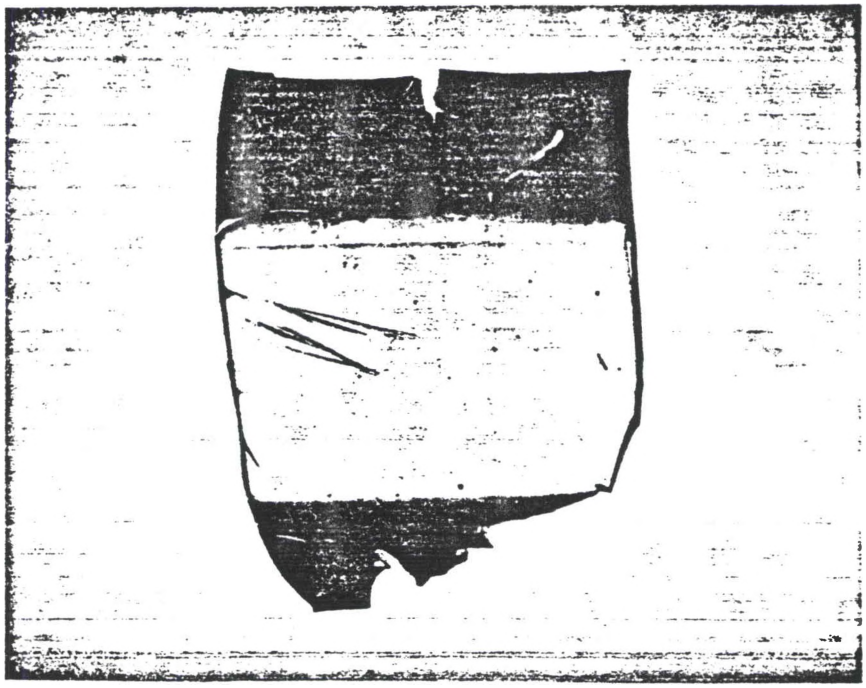

Figure 50. Low Magnification of a XB5081-1 Specimen Stained for 10 Minutes in an OsO_4/THF Solution, 13.5X.

Figure 51. Low Magnification of a XB5081-1 Specimen Stained for 20 Minutes in an OsO_4/THF Solution, 13.5X.

arrows in Figure 50, has been measured to be about 2.4mm which is close to the previously measured width of the beam (i.e. 2.5mm).

Each of the specimens were fractured by bending the specimen around upon itself. This newly created fracture surface was immediately exposed to the osmium tetroxide solution for a specific duration, and then examined with a SEM to determine if second phase rubber particles (domains) were present. Looking at Figures 52 through 57, the fracture surfaces of the CTBN modified specimens appear to have more minute white spots present than due their unmodified counterparts. It is possible that these white spots represent second phase CTBN particles which became visible due to the stain. Microphase separation, which has been demonstrated to exist in other systems[12], could have occurred in this resin as a direct result of the rapid polymerization limiting the amount of diffusion of the resin's different components. This would have resulted in microdomains rich in CTBN which then became visible with the stain. The SEM photographs though, are not absolutely conclusive about second phase CTBN particles being present. This is drawn from the fact that the unstained CTBN specimen shows white spots on its fracture surface (Figure 53) as does the XB5081-1 specimen strained for 20 minutes (Figure 56). It is possible that the white spots could be merely unsaturation sites, which have become visible with the stain. The work of Weissman et al[11] supports this with the idea that two dispersed crosslink densities are present throughout XB5081-1 green specimens. Or it could be that the white spots are both CTBN particles and uncured XB5081-1 resin. More investigation into the microstructure of the CTBN modified specimens should be conducted if this resin proves to be valuable in the manufacture of parts.

Previously it was stated that it had been assumed that the loss of water from the specimens during the annealing cycle did not account for any significant dimensional change in the specimens (i.e

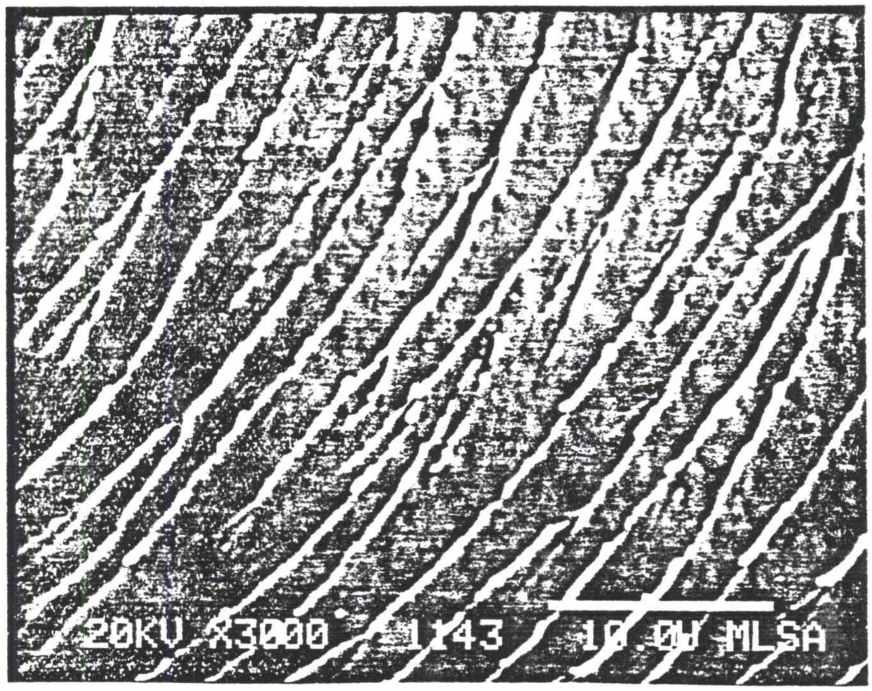

Figure 52. SEM Photograph of a XB5081-1 Specimen's Fracture Surface, Unstained, 3000X.

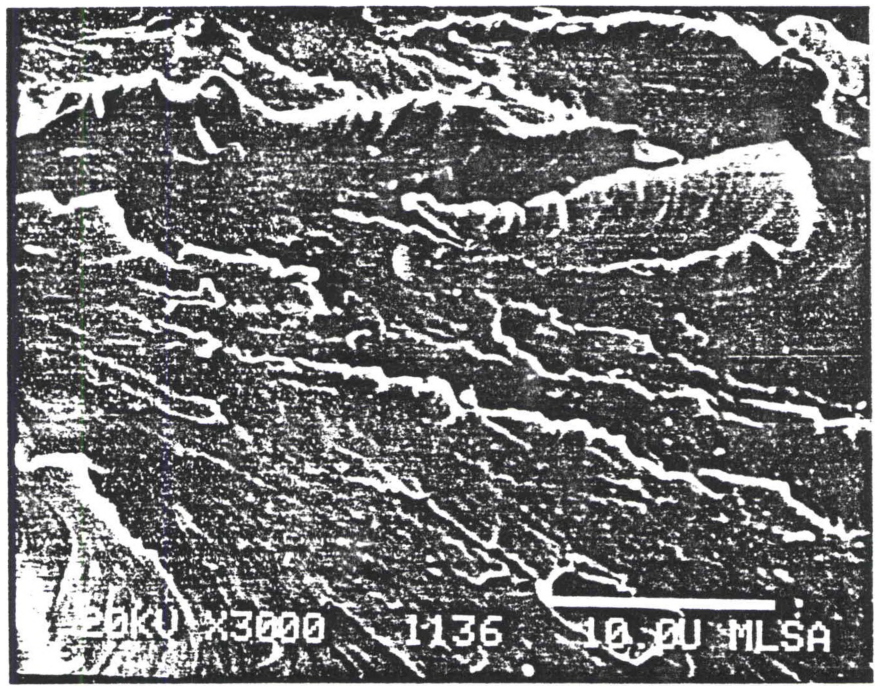

Figure 53. SEM Photograph of a CTBN Modified XB5081-1 Specimen's Fracture Surface, Unstained, 3000X.

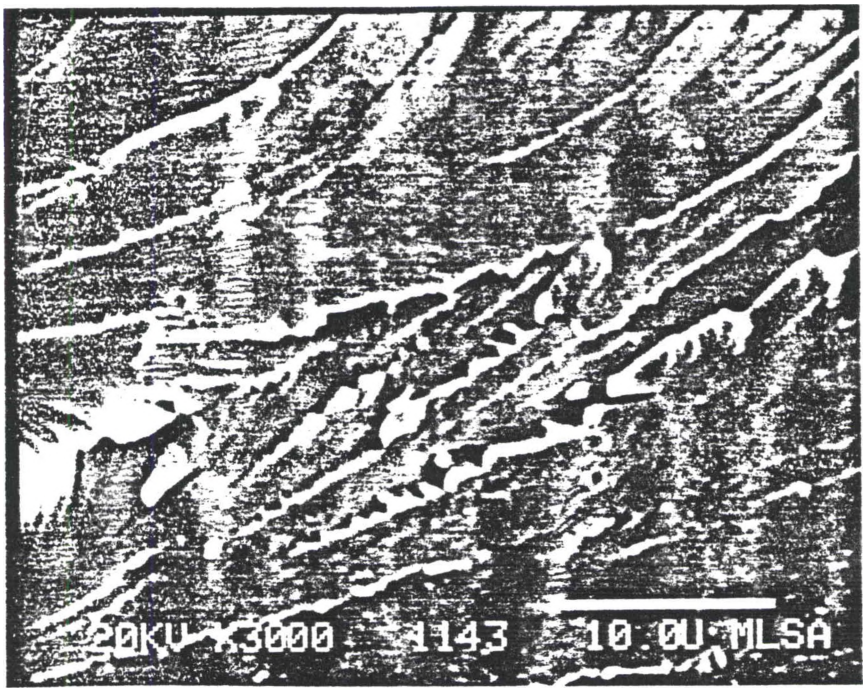

Figure 54. SEM Photograph of a XB5081-1 Specimen's Fracture Surface Stained for 10 Minutes in an OsO_4/THF Solution, 3000X.

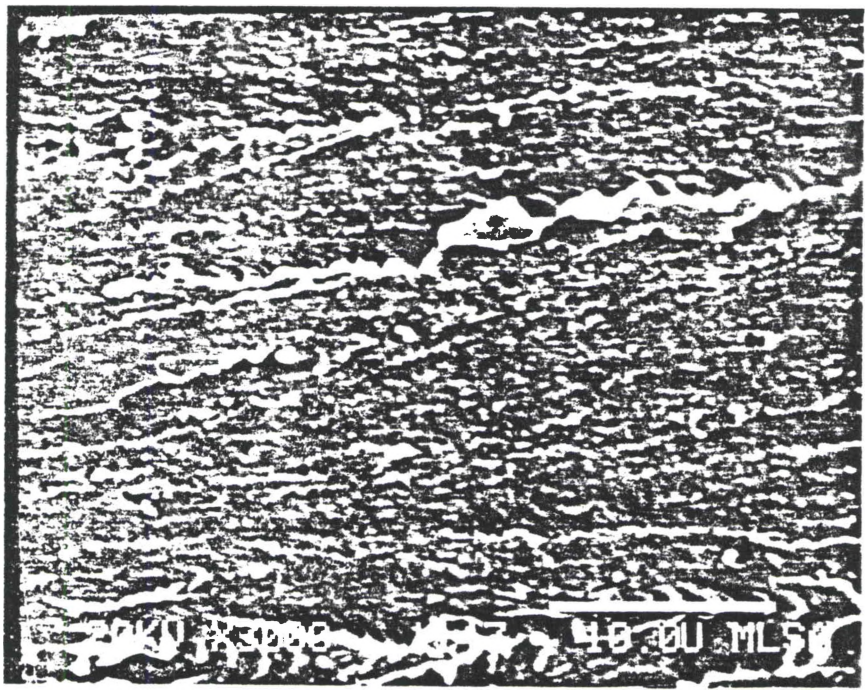

Figure 55. SEM Photograph of a CTBN Modified XB5081-1 Specimen's Fracture Surface Stained for 10 Minutes in an OsO_4/THF Solution, 3000X.

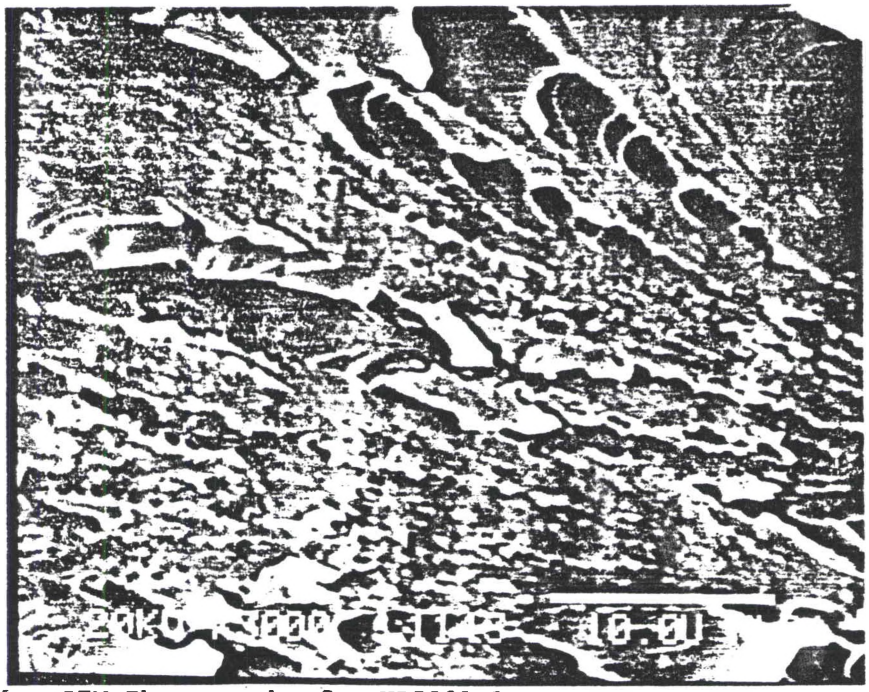

Figure 56. SEM Photograph of a XB5081-1 Specimen's Fracture Surface Stained for 20 Minutes in an OsO_4/THF Solution, 3000X.

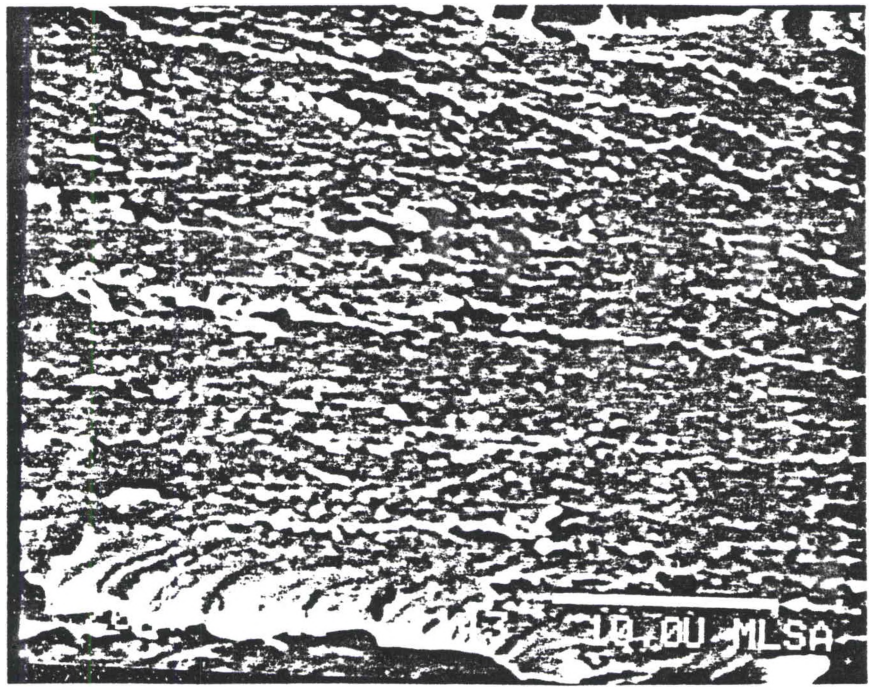

Figure 57. SEM Photograph of a CTBN Modified XB5081-1 Specimen's Fracture Surface Stained for 20 Minutes in an OsO_4/THF Solution, 3000X.

causing a change in strain). This assumption was investigated further by breaking a CTBN modified XB5081-1 specimen in two, measuring the two segments' respective lengths (Table III), then placing one segment in a desiccator and leaving the other exposed to room conditions. After nearly 72 hours, the length of each segment was remeasured (Table III). It was found that the desiccated segment had reduced its length more than the non-desiccated segment. Since the only difference between the two environments was water content, it was concluded that the loss of water from the desiccated segment accounted for the observed length reduction. Because the weight loss which the desiccated segment experienced was not measured, no correlation could be made between its water loss and corresponding effect on length and the water loss and length change experienced by the annealed specimen. It can be concluded though, that the loss of water in the specimens, as a consequence of annealing, does account for some of the length change measured and hence some of the residual stress.

It is also interesting to note that there was some room temperature annealing occurring with the non-desiccated specimen yet none was noted for the XB5081-1 specimens after 14 hours or for the CTBN modified XB5081-1 specimens after 19 hours. It is possible that room temperature annealing was occurring with all the specimens but that it was masked by the specimen's absorption of water which would tend to swell the specimen. At a point in time, greater than the 19 hours after their creation, the water absorption decreased and the room temperature annealing continued resulting in the observed strain. If this was occurring with all the tested specimens, it should have had little effect on the measurement of residual stress as the annealing process would have probably removed the water which was swelling the specimens. The measurements of the amount of strain in the specimens, taken immediately after annealing, would therefore correspond to that due to annealing only.

TABLE III

Moisture Effect on the Length of CTBN Modified XB5081-1 Specimen

Specimen	initial length	length after 71hrs (mm)	strain (mm/mm)	percent strain
Nondesiccated	15.786	15.761	0.025	0.1584
Desiccated	16.655	16.621	0.034	0.2041

The residual stress level present in the specimen's were also calculated by assuming linearly elastic behavior for the resin (valid as long as the time of the test remains short). From Figure 38, the storage modulus at the room temperature of 70°F (22.5°C) was 1.55 x 10^9 Pa. With an average strain value of 0.264 percent for the XB5081-1 resin, the calculated residual stress present equated to 4.09 MPa. This was within 5% of the measured value. Similar results were obtained for the CTBN modified resin system (i.e. 3.14 MPa which was within 10% of the 3.47 MPa value measured). It is therefore concluded that using the storage modulus determined from the DMA of the specimens coupled with the average strain and Hooke's law, allows the ready calculation of the residual stresses which were present in the specimens. This results in simplifying this technique which is crucial to its successful application as a screening mechanism for new resins.

CHAPTER V

CONCLUSIONS

The primary purpose of this study, which was to develop a method to measure the residual stresses in parts created by the Stereolithography process, was finally met with the "Annealing-Straining Analysis" technique. In the process of developing this technique and then utilizing it to study the effect of a chemical modification to the base resin, several conclusions can be made:

(1) Photoelastic analysis of the residual stresses present in specimens created by the stereolithography process was not possible because the specimens were not of a homogenous nature thereby violating the key assumption necessary in evaluating materials photoelasticly. The main contributors to this inhomogeneity are believed to be the laser (e.g. distortions in the coherent beam as a result of lens imperfections and dust in the air), the rapidity of the polymerization reaction caused by the laser and the subsequent void formation, as well as the formation of two discrete phases of different crosslink densities within the specimens.

(2) Two "Constant Strain Analysis" techniques, involving the measurement of the force required to maintain a constant strain on a partially cured specimen when further exposed to UV light, were not capable of measuring the residual stresses which develop in parts upon photopolymerization. In both instances the capabilities and operating principles of the instruments utilized resulted in the failure of the specific technique.

(3) The "Annealing-Straining Analysis" technique demonstrated that in a laser cured single strand of a XB5081-1 material (i.e. green/partially cured), residual stresses on the order of 570 psi (3.93 MPa) can develop. This represents over 12.5% of the green material's Ultimate Tensile Strength (UTS) and about 5% of its fully cured UTS. In an actual part, which is comprised of a multitude of criss-crossing lines of cured material, the amount of residual stress would be expected to be higher. This is due to the multiple laser scans of some of the material creating different crosslink densities within the part and the criss-crossing points pinning the ends of the cured segments thereby limiting their ability to freely shrink.

(4) Modifying the epoxy base resin, XB5081-1, with 10.81 pph CTBN reduced the residual stress levels in a laser cured single strand material to 502 psi (3.47 MPa) which represents a 12% decrease in the residual stress levels over that of the unmodified resin. It is believed that this rubber addition will also increase the impact toughness of a part, a highly desired quality, but to what extent is unknown. A microscopic examination of the morphology of this rubber modified system was inconclusive in determining whether the CTBN had phase separated. Although this rubber addition demonstrated a possible method in which to decrease the residual stress levels in a part, its effect of increasing the resin's viscosity on the part building process and the trade off in strength (i.e reduced crosslink density or percentage of cure) has not been researched.

(5) Using the value of the storage modulus, E', obtained from the DMA plot versus temperature for a specimen, the strain observed as a result of annealing, and Hooke's law, an approximation of the residual stresses that were present within a specimen can be made to within 10 percent of the measured value. This simplifies the Annealing-Straining method and reduces the time required to obtain residual stress values for any given resin.

(6) Water absorption by the specimens and its subsequent loss during the annealing cycle could have accounted for some of the residual stress measured in the specimens. The effect of water loss needs to be investigated further.

In conclusion, it has been demonstrated that the "Annealing-Straining Analysis" technique is a viable method of determining, quantitatively, the residual stress levels in a single strand of material. Although this technique can be used as a comparative method for determining which resin system will develop less residual stresses in a part during the manufacturing process, it is recognized that because it is a time consuming process and requires great attention to detail to obtain good repeatable results, its usefulness as a screening technique for new resins may be limited.

CHAPTER VI

REFERENCES

1. Borman, C.J.; "Beyond Show and Tell", National Conference on Rapid Prototyping, Dayton, Ohio, June 4-5, 1990.

2. Prioleau, F.; "Beyond Prototyping: Using Stereolithography for Production-Quality Parts", National Conference on Rapid Prototyping, Dayton, Ohio, June 4-5, 1990.

3. Hendry, A.W.; Photoelastic Analysis, Pergamon Press, London, 1966.

4. Flach, L.; "Mathematical Modeling of a Laser-Induced Photopolymerization Process, Part III", EMTEC CT-20 Progress Report, Edison Materials Technology Center, Dayton, Ohio, unpublished, Dec 1990.

5. Frocht, M.M.; Selected Papers of M.M. Frocht on Photoelasticity, Pergamon Press, London, 1969.

6. Drucker, D.C.; "Photoelastic Separation of Principal Stresses by Oblique Incidence", J. Appl. Mech., v 101, no. 3, p A156, 1943.

7. Drucker, D.C.; "The Method of Oblique Incidence in Photoelasticity", Proc. SESA, v VIII, no. 1, p 51, 1950.

8. Dally, J.W., and Riley, F.R.; Experimental Stress Analysis, McGraw-Hill Book Company, New York, 1965.

9. Frocht, M.M.; Photoelasticity, vol I and II, John Wiley & Sons, Inc., London, 1962.

10. Product Brochure for Ciba-Geiby's Cibatool XB5081-1 resin formulation, 3D Systems Inc., California.

11. Weissman, P.; Chartoff, R.; and Linden, S.; "Characterizing Physical and Mechanical Properties of a Photopolymer Used in Stereolithography", Proceedings of the North American Thermal Analysis Society (NATAS), 20th NATAS Conference, Minneapolis, MN, September 22, 1991.

12. Liu, C. and Armeniades, C.D.; "Cure Shrinkage Control by Phase Separation in Acrylic Systems", Conference Proceedings ANTEC, Dallas, TX, May 7-11, 1990.

13. Decker, C.; "Laser-Induced Polymerization", Materials for Microlithography, ACS Symposium Series, v 266, p 207, 1984.

14. Kloosterboer, J.G.; Van de Hei, G.M.M.; Grossink, R.G.; Dortant, G.C.M.; "The Effects of Volume Relaxation and Thermal Mobilization of Trapped Radicals on the Final Conversion of Photopolymerized Diacrylates", Polymer Comm., v 25, p 322, 1984.

15. Weissman, P.; unpublished experimental work on stress versus time curves obtained on a single filament of laser cured XB5081 resin upon further exposure to UV light, University of Dayton Research Institute, August 1990.

16. Kloosterboer, J.G.; Lijte, G.F.C.M.; Greidanus, F.J.A.M.; "Structure and Stability of Polyacrylate Radicals Trapped in a Network", Polym. Comm., v 27, p 268, 1986.

17. Decker, C.; Moussa, K.; "Radical Trapping in Photopolymerized Acrylic Networks", J. Polym. Sci., Poly. Chem Ed., v 25, p 739, 1987.

18. DuPont 983 DMA System Product Brochure, DuPont Instruments USA.

19. Lear, J.D. and Gill, P.S.; "Theory of Operation of the DuPont 982 Dynamic Mechanical Analyzer", DuPont Instruments USA.

20. Rheometrics Solid Analyzer II Product Brochure and Principles of Operation, Rheometrics Inc., Piscataway, N.J. 1987.

21. Alkens, D.A.; Bailey, R.A.; Giachino, G.G.; Moore, J.A.; Tomkins, R.P.T.; Integrated Experimental Chemistry, Principles and Techniques, Volume 1, Allyn and Bacon, Inc., Boston, 1978.

22. Emission Data for Cibatool XB5081 resin, 3D Systems Inc., 1989.

23. Weissman, P.; unpublished experimental work on the amount of energy released during full cure of the XB5081 resin via a DSC method, University of Dayton Research Institute, August 1990.

24. Shimbo, M.; Ochi, M.; Shigeta, Y.; "Shrinkage and Internal Stress During Curing of Epoxide Resins", J. of Applied Polymer Sci, v 26, p 2265, 1981.

25. Kamarchik, P. and Jurczak, E.; "Post-UV Cure Phenomena in Radiation Curable Systems", RADTECH Europe Conference, Edinburgh, Scotland, September 29 - October 2, 1991.

26. Weissman, P.; unpublished experimental work on the ultimate tensile strengths of a number of photoreactive resins, University of Dayton Research Institute, May 1991.

27. Riew, C.K. and Smith, R. W.; "Modified Osmium Tetroxide Stain for the Microscopy of Rubber-Toughened Resins", J. of Polymer Sci., Part A-1, Polymer Chem, v 9, p 2739, 1971.

CHAPTER VII

APPENDICES

Appendix A, Theory of Photoelasticity

Birefringence or double refraction, is a phenomenon exhibited in materials which divide an incoming plane polarized light wave into two components normal to each other and traveling at different speeds through the material. Upon emergence from the material one would see two images of the light source and hence the name double refraction. All crystals, strained glass and most strained transparent plastics exhibit this property. This phenomenon is best explained through the use of Figure A1[3] below:

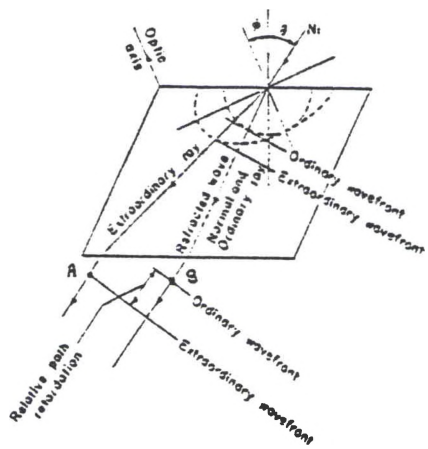

In this figure the optic axis of the crystal is in the plane of the paper and makes an angle of ϕ to the normal to the crystal face. The incident light wave normal makes an angle of θ with the normal to the crystal face. Light will be broken into two components that travel at different paths within the crystal. These are depicted as the ordinary and the extraordinary rays. The ordinary ray has a wavefront which corresponds to the case of light traveling through an isotropic medium and coincides with the wave normal. The

extraordinary ray has a wave front that does not coincide with the wave normal. When looking through the crystal, because of the two emerging wave fronts, two images of the same light source will be observed and hence the name double refraction.

Figure A1 also shows that at points A and B of the ordinary and extraordinary wave fronts respectively, the wave fronts are in phase with each other. The additional distance between these wave fronts represents the relative path retardation of the wavefronts which is a direct consequence of the material transmitting two waves along different paths through the material.

When this same crystal is placed between two polarizing elements which are crossed with respect to each other (i.e. axis of polarizations are at 90 degrees apart so that light transmitted through the first polarizer is not transmitted through the second polarizer) an interference pattern is developed. This is depicted in Figure A2[3].

The light entering the crystal plate is represented by $y = a\sin\phi$ and makes an angle of θ to the direction of polarization of one of the incident waves. The crystal breaks this light wave into two components, the amplitudes of which are represented by:

$$At_1 = ka\sin(\phi + \varepsilon)\cos\theta$$
$$At_2 = ka\sin\phi\sin\theta$$

where k is an absorption factor for the material and $\varepsilon = 2\pi h(n_1 - n_2)/\lambda$ is the relative phase retardation corresponding to a relative path of $(n_1 - n_2)h$. The refractive index of the ordinary and extraordinary waves in the crystal are represented by n_1 and n_2 respectively, for light of wavelength λ and a crystal plate thickness of h.

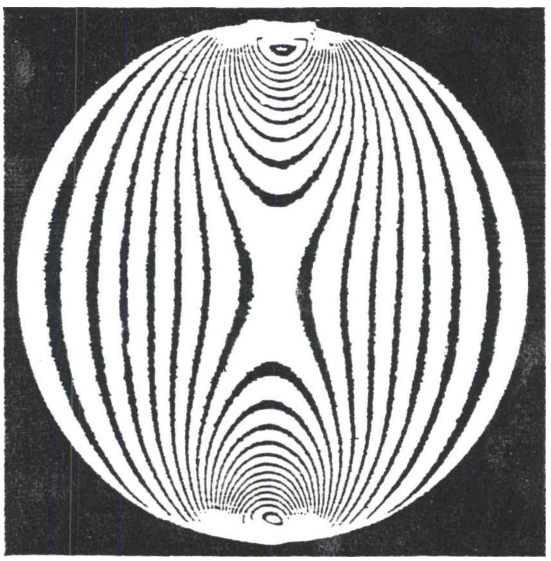

Figure A2. Fringe pattern in a disk under diametral compression.

In passing through the analyzer only the wave components parallel to the analyzer's polarizing axis will be transmitted. The combined transmitted components are:

$$At_2\cos\theta - At_1\sin\theta = ka\sin\phi\sin\theta\cos\theta - ka\sin(\phi+\varepsilon)\cos\theta\sin\theta$$

$$= 0.5a\sin 2\theta\{\sin\phi - \sin(\phi+\varepsilon)$$

$$= ka\sin 2\theta\cos(\phi+\varepsilon/2)\sin\varepsilon/2 \qquad \text{eq (a1)}$$

Examination of the above equations shows that extinction of the light will occur whenever one of the following conditions is met:

- when θ is equal to 0 or $\pi/2$, i.e. when the direction of polarization of the incident beam is in alignment with a polarizing axis in the crystal. The locus of these points are called isoclinics and are observable when a specimen is placed in the field of a crossed plane polariscope.

- when the retardation, ε, is an even multiple of π, i.e. path retardation is an integral number of wavelengths. The locus of these points are called isochromatic fringes, or just fringes, and are observable when a specimen is placed in the field of a crossed circular polariscope which eliminates the isoclinic lines.

It was discovered by Brewster in 1816 that this double refracting phenomenon existed in quasi-crystalline stressed transparent materials as well as crystals. In 1853 Maxwell developed a theory to relate the changes in index of refraction of a material to its stress state. Maxwell found that changes in index of refraction were linearly proportional to the stress level and could be represented by:

$$n_1 - n_0 = C_1\sigma_1 + C_2\sigma_2$$

$$n_2 - n_0 = C_1\sigma_2 + C_2\sigma_1$$

where; n_0 = index of refraction of unstressed material
n_1 = index of refraction along axis 1 associated with 1

n_2 = index of refraction along axis 2 associated with 2

C_1 and C_2 are the stress optic coefficients

$\sigma_3 = 0$, assumed a plane stress state

When the equations are subtracted from each other, n_0 is eliminated leaving:

$$n_1 - n_2 = (C_1 - C_2)(\sigma_1 - \sigma_2) \qquad \text{eq (a2)}$$

The stressed photoelastic model behaves like the crystal with regards to its optical properties, i.e.

$$\varepsilon = 2\pi h(n_1 - n_2)/\lambda$$

or

$$n_1 - n_2 = \varepsilon\lambda/(2\pi h) \qquad \text{eq (a3)}$$

Substituting eq (a2) into eq (a3), one obtains:

$$\varepsilon\lambda/(2\pi h) = (C_1 - C_2)(\sigma_1 - \sigma_2) \qquad \text{eq (a4)}$$

or setting $(C_1 - C_2) = C$ (the relative stress optic coefficient), the relative retardation becomes:

$$\varepsilon = 2\pi hC(\sigma_1 - \sigma_2)/\lambda \qquad \text{eq (a5)}$$

This is the classical description of the stress optic law where the relative retardation is linearly proportional to the difference in the principal stresses. The relative stress optic coefficient is a material property dependent upon the material used in the photoelastic model. This equation also shows that the relative retardation is directly proportional to the thickness, h, of the model and inversely proportional to the wavelength of light employed in analyzing the model.

Equation (a5) is generally rewritten in the following form:

$$\sigma_1 - \sigma_2 = Nf_\sigma/h \qquad \text{eq (a6)}$$

where: $N = \varepsilon/(2\pi)$, the relative retardation in terms of a complete cycle of retardation 2π. It is otherwise called the fringe order (dimensionless quantity)

$f_\sigma = \lambda/C$, the material fringe value (psi-in)

and is termed the stress optic law in two dimensions. This form was utilized throughout this study since the function of a polariscope was to determine the value of N at each point in a model.

Appendix B, Theory of Operation of the Babinet-Soleil Compensator

From the utilization of both light and dark field fringe patterns (see Figure B1[8]) one can at best determine the isochromatic fringe order to the nearest 1/2 order. For greater accuracy in the determination of the fringe order other methods must be employed. The method that will be utilized throughout this research is based upon the Babinet-Soleil compensator.

The Babinet-Soleil compensator, as depicted in Figure B2[8] below, is placed into the field of the polariscope just after the model and between the polarizer and analyzer. The compensator is composed of a quartz plate of uniform thickness and two quartz wedges adjacent to each other. Varying the thickness of the two wedges allows for the adjusting of the birefringence of the compensator. This is accomplished by turning a micrometer screw attached to one of the wedges that allows it to slide past the other stationary wedge effectively changing the thickness of the two wedge plate. The amount of retardation, ε, produced by this compensator is directly dependent upon the thickness of the quartz plates, t_1 and t_2, and the frequency of monochromatic light employed, i.e. $\varepsilon = 2h\pi(n_1 - n_0)/\lambda$. The compensator must be calibrated with the monochromatic light which will be employed in order to obtain a calibration equation. This equation allows for conversion of the screw micrometer reading to a fringe order at the point of the model under study. Only a single point in a model can be studied at any given time due to the fact that a photometer with a detector size of approximately 1 mm was used to aid in determining the fringe order (i.e. local minimums of light intensity).

Optically what is occurring with the compensator in place is best described with the aid of Figure B3[8]. The model produces an

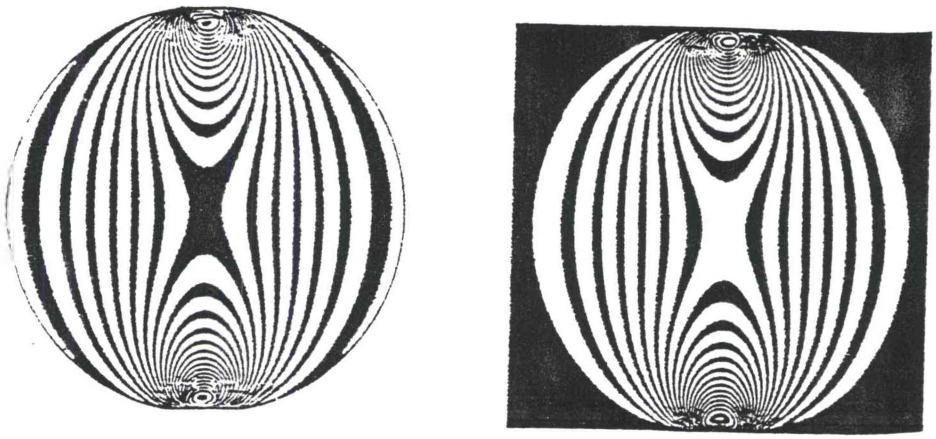

(a) (b)

Figure B1. (a) is a light field (i.e. light background), and (b) is a dark field view of a disk under diametral compression.

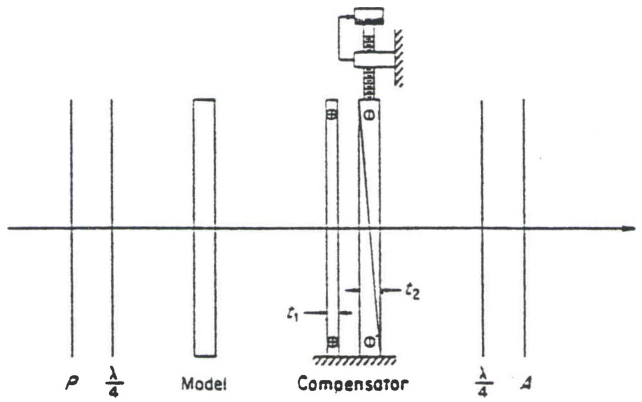

Figure B2. Babinet-Soleil Compensator.

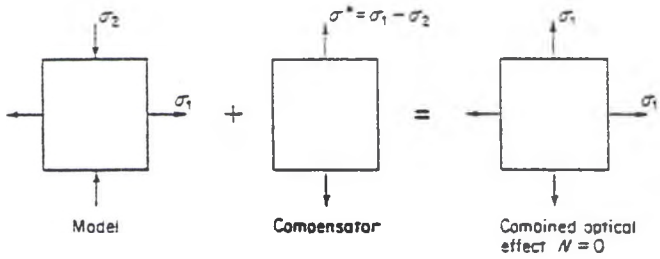

Figure B3. Combined Optical Effect of Model and Compensator.

optical effect (i.e. the fringe order) which is proportional to $\sigma_1 - \sigma_2$. With the compensator in place and its optical axis aligned parallel to the σ_2 direction, the combined response of the system is variable dependent upon the birefringence of the compensator, which is related to its overall thickness. If the thickness of the compensator is adjusted so that its birefringence is equal to the model's, i.e. $\sigma_1 - \sigma_2$, then the resultant fringe order of the system goes to zero since the system has its principle stresses of equal magnitude and therefore no stress difference exists. The micrometer reading on the compensator is then equated to the fringe order in the model via the calibration equation.